# A taxonomic revision of the *Sinopterus* complex (Pterosauria, Tapejaridae) from the Early Cretaceous Jehol Biota, with the new genus *Huaxiadraco* (#78770)

First submission

#### Guidance from your Editor

Please submit by 18 Nov 2022 for the benefit of the authors (and your token reward) .



#### **Structure and Criteria**

Please read the 'Structure and Criteria' page for general guidance.



#### **Custom checks**

Make sure you include the custom checks shown below, in your review.



#### **Author notes**

Have you read the author notes on the guidance page?



#### Raw data check

Review the raw data.



#### Image check

Check that figures and images have not been inappropriately manipulated.

Privacy reminder: If uploading an annotated PDF, remove identifiable information to remain anonymous.

#### **Files**

Download and review all files from the <u>materials page</u>.

- 22 Figure file(s)
- 4 Table file(s)
- 3 Raw data file(s)



#### **New species checks**

- Have you checked our new species policies?
- Do you agree that it is a new species?
- Is it correctly described e.g. meets ICZN standard?

## Structure and Criteria



#### Structure your review

The review form is divided into 5 sections. Please consider these when composing your review:

- 1. BASIC REPORTING
- 2. EXPERIMENTAL DESIGN
- 3. VALIDITY OF THE FINDINGS
- 4. General comments
- 5. Confidential notes to the editor
- You can also annotate this PDF and upload it as part of your review

When ready submit online.

#### **Editorial Criteria**

Use these criteria points to structure your review. The full detailed editorial criteria is on your guidance page.

#### **BASIC REPORTING**

- Clear, unambiguous, professional English language used throughout.
- Intro & background to show context.
  Literature well referenced & relevant.
- Structure conforms to <u>PeerJ standards</u>, discipline norm, or improved for clarity.
- Figures are relevant, high quality, well labelled & described.
- Raw data supplied (see <u>PeerJ policy</u>).

#### **EXPERIMENTAL DESIGN**

- Original primary research within Scope of the journal.
- Research question well defined, relevant & meaningful. It is stated how the research fills an identified knowledge gap.
- Rigorous investigation performed to a high technical & ethical standard.
- Methods described with sufficient detail & information to replicate.

#### **VALIDITY OF THE FINDINGS**

- Impact and novelty not assessed.

  Meaningful replication encouraged where rationale & benefit to literature is clearly stated.
- All underlying data have been provided; they are robust, statistically sound, & controlled.



Conclusions are well stated, linked to original research question & limited to supporting results.



# Standout reviewing tips



The best reviewers use these techniques

Τ	p

# Support criticisms with evidence from the text or from other sources

### Give specific suggestions on how to improve the manuscript

### Comment on language and grammar issues

### Organize by importance of the issues, and number your points

# Please provide constructive criticism, and avoid personal opinions

Comment on strengths (as well as weaknesses) of the manuscript

#### **Example**

Smith et al (J of Methodology, 2005, V3, pp 123) have shown that the analysis you use in Lines 241-250 is not the most appropriate for this situation. Please explain why you used this method.

Your introduction needs more detail. I suggest that you improve the description at lines 57-86 to provide more justification for your study (specifically, you should expand upon the knowledge gap being filled).

The English language should be improved to ensure that an international audience can clearly understand your text. Some examples where the language could be improved include lines 23, 77, 121, 128 – the current phrasing makes comprehension difficult. I suggest you have a colleague who is proficient in English and familiar with the subject matter review your manuscript, or contact a professional editing service.

- 1. Your most important issue
- 2. The next most important item
- 3. ...
- 4. The least important points

I thank you for providing the raw data, however your supplemental files need more descriptive metadata identifiers to be useful to future readers. Although your results are compelling, the data analysis should be improved in the following ways: AA, BB, CC

I commend the authors for their extensive data set, compiled over many years of detailed fieldwork. In addition, the manuscript is clearly written in professional, unambiguous language. If there is a weakness, it is in the statistical analysis (as I have noted above) which should be improved upon before Acceptance.



# A taxonomic revision of the *Sinopterus* complex (Pterosauria, Tapejaridae) from the Early Cretaceous Jehol Biota, with the new genus *Huaxiadraco*

Rodrigo V. Pêgas <sup>1</sup>, Xuanyu Zhou <sup>Corresp., 2, 3, 4</sup>, Xingsheng Jin <sup>5</sup>, Kai Wang <sup>6</sup>, Waisum Ma <sup>7</sup>

Corresponding Author: Xuanyu Zhou Email address: xyzhou@elms.hokudai.ac.jp

The Tapejaridae are edentulous pterosaurs that are relatively common in Cretaceous continental deposits in South America, North Africa, Europe, and China (mostly Early Cretaceous). The Chinese Jiufotang Formation is particularly rich in tapejarid specimens, having yielded over 10 described specimens and dozens of undescribed ones. For the Jiufotang Formation, a total of 7 nominal tapejarid species, and 2 genera, have been proposed. Some debate has existed over how many of those proposed species are valid or, alternatively, sexual or ontogenetic morphs of fewer (or even a single) species. However, detailed revisions of the matter are still lacking. In the present work, we provide a specimen-level survey of anatomical variation in previously described liufotang tapejarid specimens, as well as of 7 new ones. We present qualitative and morphometric comparisons, aiming to provide a basis for a taxonomic reappraisal of the group. Our results lead us to interpret 2 species of Jiufotang tapejarid as valid: Sinopterus dongi and Huaxiadraco corollatus (gen. et comb. nov.). Our primary taxonomic decisions did not rely around cranial crest features, which have typically been regarded as diagnostic for most of these proposed species albeit ever-growing evidence that these structures are highly variable in pterosaurs, due to ontogeny and sexual dimorphism. However, a reassessment of premaxillary crest variation in the Sinopterus complex reveals that while much of the observed variation (crest presence and size) can easily be attributed to intraspecific (ontogenetic and sexual) variation, some of it (crest shape) does seem to represent interspecific variation indeed. A phylogenetic analysis including the species regarded as

valid was also performed.

PeerJ reviewing PDF | (2022:10:78770:0:1:NEW 3 Nov 2022)

<sup>1</sup> Laboratório de Paleontologia de Vertebrados e Comportamento Animal, Universidade Federal do ABC, São Bernardo do Campo, Brazil

<sup>&</sup>lt;sup>2</sup> Department of Natural History Sciences, Hokkaido University, Sapporo, Hokkaido, Japan

<sup>&</sup>lt;sup>3</sup> Hokkaido University Museum, Hokkaido University, Sapporo, Hokkaido, Japan

<sup>&</sup>lt;sup>4</sup> Beipiao Pterosaur Museum of China, Beipiao, Liaoning, China

<sup>&</sup>lt;sup>5</sup> Zhejiang Museum of Natural History, Hangzhou, Zhejiang, China

<sup>&</sup>lt;sup>6</sup> School of Earth Sciences and Resources, China University of Geosciences, Beijing, China

<sup>7</sup> Department of Paleobiology, National Museum of Natural History, Smithsonian Institution, Washington D.C., United States



#### A taxonomic revision of the Sinopterus complex

#### 2 (Pterosauria, Tapejaridae) from the Early Cretaceous

#### Jehol Biota, with the new genus Huaxiadraco

4 Rodrigo V. Pêgas<sup>1</sup>, Xuanyu Zhou<sup>2,3,4\*</sup>, Xingsheng Jin<sup>5</sup>, Kai Wang<sup>6</sup>, Waisum Ma<sup>7</sup>

5

- 6 1. Laboratory of Vertebrate Paleontology and Animal Behavior, Federal University of ABC, São
- 7 Bernardo, Brazil.
- 8 2. Department of Natural History Sciences, Hokkaido University, Sapporo, Japan.
- 9 3. Hokkaido University Museum, Hokkaido University, Sapporo, Japan.
- 10 4. Beipiao Pterosaur Museum of China, Beipiao, Liaoning, China.
- 5. Zhejiang Museum of Natural History, Hangzhou, Zhejiang, China.
- 12 6. School of Earth Sciences and Resources, China University of Geosciences, Beijing, China.
- 7. Department of Paleobiology, National Museum of Natural History, Smithsonian Institution,
- 14 Washington, DC, USA.

15

- 16 Corresponding Author:
- 17 Xuanyu Zhou
- 18 Hokkaido University, Sapporo, Japan
- 19 Email address: xyzhou@elms.hokudai.ac.jp

20

21

#### Abstract

- 22 The Tapejaridae are edentulous pterosaurs that are relatively common in Cretaceous continental
- 23 deposits in South America, North Africa, Europe, and China (mostly Early Cretaceous). The
- 24 Chinese Jiufotang Formation is particularly rich in tapejarid specimens, having yielded over 10
- 25 described specimens and dozens of undescribed ones. For the Jiufotang Formation, a total of seven
- 26 nominal tapejarid species, and two genera, have been proposed. Some debate has existed over how
- 27 many of those proposed species are valid or, alternatively, sexual or ontogenetic morphs of fewer
- 28 (or even a single) species. However, detailed revisions of the matter are still lacking. In the present
- 29 work, we provide a specimen-level survey of anatomical variation in previously described
- 30 Jiufotang tapejarid specimens, as well as of six new ones. We present qualitative and morphometric



32

33

34

35

36

37

38

39

40

comparisons, aiming to provide a basis for a taxonomic reappraisal of the complex. Our results lead us to interpret two Jiufotang tapejarid species as valid: *Sinopterus dongi* and *Huaxiadraco corollatus* (gen. et comb. nov.). Our primary taxonomic decisions did not rely around cranial crest features, which have typically been regarded as diagnostic for most of these proposed species albeit ever-growing evidence that these structures are highly variable in pterosaurs, due to ontogeny and sexual dimorphism. However, a reassessment of premaxillary crest variation in the *Sinopterus* complex reveals that while much of the observed variation (crest presence and size) can easily be attributed to intraspecific (ontogenetic and sexual) variation, some of it (crest shape) does seem to represent interspecific variation indeed. A phylogenetic analysis including the species regarded as valid was also performed.

41

42 43

#### Introduction

- 44 The Tapejaridae (sensu Andres, 2021) are a peculiar clade of Cretaceous edentulous pterosaurs of
- 45 the group Azhdarchoidea (Pterodactyloidea, Eupterodactyloidea), characterized by their short,
- downturned rostra and peculiar premaxillary crests (Kellner & Campos, 2007; Pêgas et al., 2016).
- 47 They comprise over 10 species (up to 14 valid species following Zhang et al., 2019), spanning
- 48 from the Barremian to the Santonian; with records from Brazil, Morocco, Europe, and China
- 49 (Kellner & Campos, 2007; Vullo *et al.*, 2012; Andres *et al.*, 2014; Pêgas *et al.*, 2016).
- 50 In China, tapejarids are a common element of the famous Jehol Biota. From the Yixian Formation,
- a single species, represented by two specimens, has been described: Eopteranodon lii (Lü &
- 52 Zhang, 2005; Lü et al., 2006c). Originally regarded as an undetermined pterodactyloid (Lü &
- Zhang, 2005) or a pteranodontid (Lü *et al.*, 2006c), it was later reinterpreted as a tapejarid (Andres
- & Ji, 2008; Vullo et al., 2012). It is, however, in the Jiufotang Formation that a great abundance
- of tapejarids is found. A total of 15 Jehol tapejarid specimens have been formally described in the
- 56 literature (Wang & Zhou, 2003; Li et al., 2003; Lü & Zhang, 2005; Lü et al., 2005, 2006a,b,c,
- 57 2007, 2016; Liu et al., 2014; Zhang et al., 2019; Shen et al., 2021; Zhou et al., 2022a; 2022b).



81

82

83

Under the accounts of Wu et al. (2017), at least further 9 undescribed specimens are currently 58 deposited in the Paleontological Museum of Liaoning, and further 4 in the Shandong University 59 60 of Science and Technology. According to our observations, further tens of specimens can be found in the collections of other institutions such as the Beipiao Pterosaur Museum of China, the Dalian 61 Natural History Museum, and the Chaoyang National Geopark; bringing the total of recovered 62 specimens to over forty. 63 64 Sinopterus dongi, from the Jiufotang Formation (see Wang & Zhou, 2003), was the first tapejarid to be recovered from China. Subsequently, further six tapejarid species coming from the Jiufotang 65 Fm. have been named: Sinopterus gui, Sinopterus lingvuanensis, Huaxiapterus jii, Huaxiapterus 66 corollatus, Huaxiapterus benxiensis, and Huaxiapterus atavismus (see Wang & Zhou, 2003; Li et 67 68 al., 2003; Lü et al., 2005; 2006; 2007; 2016). The Jiufotang Fm. tapejarids are involved in a complex series of taxonomic controversies, with the genus *Huaxiapterus* having been considered 69 a junior synonym of Sinopterus (Wang & Zhou, 2006; Wang & Dong, 2008; Witton, 2013; Zhang 70 et al., 2019). Thus, the Jiufotang tapejarids will heretofore be referred to as the Sinopterus 71 72 complex. 73 The type species Sinopterus dongi was described by Wang & Zhou (2003) and its validity has never been contested. A second species, Sinopterus gui, was proposed by Li et al. (2003), but its 74 holotype was later reinterpreted as an undiagnostic juvenile specimen, indistinct from S. dongi 75 (Kellner & Campos, 2007; Kellner, 2010). 76 77 Following the description of these two species, the genus *Huaxiapterus* was erected for the typespecies Huaxiapterus jii by Lü et al. (2005). Afterwards, Wang & Zhou (2006) synonymized 78 79 Huaxiapterus jii with Sinopterus dongi, noting that the two holotypic specimens were very similar

to each other. Kellner & Campos (2007) accepted the validity of H. jii at the species level, but

referred it to the genus Sinopterus, as Sinopterus jii. Later, however, Kellner (2010) and Zhang et

al. (2019) regarded S. jii as a synonym of S. dongi, following the proposition by Wang & Zhou

(2006). A consequence of this species-level synonymy is that the genus *Huaxiapterus* would

Peerl reviewing PDF | (2022:10:78770:0:1:NEW 3 Nov 2022)



- 84 become invalid.
- 85 Later, Lü et al. (2006a) attributed a second species to the genus *Huaxiapterus*, *H. corollatus*.
- 86 Kellner & Campos (2007) accepted the species-level validity of *H. corollatus* and suggested that
- it required a new genus name (recognizing the proposed synonymy between *H. jii* and *S. dongi*,
- and considering that *H. corollatus* was sufficiently distinct from *S. dongi* to warrant another genus
- 89 name). Later, another species was proposed for the genus *Huaxiapterus* by Lü et al. (2007):
- 90 Huaxiapterus benxiensis.
- 91 Subsequently, Witton (2013) proposed that the majority of the previously described Jiufotang
- 92 tapejarids could possibly represent a single ontogenetic continuum. Witton (2013) noticed that the
- 93 diagnoses of the proposed species relied heavily on crest size and shape, what is problematic since
- 94 this is most likely strongly influenced by sexual and ontogenetic variation (e.g. Bennett, 1993;
- 95 Wang et al., 2014; Manzig et al., 2014; Pinheiro & Rodrigues, 2017). Though Witton (2013) made
- a case for this possibility, it has never been investigated in detail so far. Andres et al. (2014) did
- 97 not contest the validity of any of the previously proposed species, having coded all the then-
- 98 described species in their phylogenetic analysis: Sinopterus dongi, Huaxiapterus jii, Sinopterus
- 99 gui, Huaxiapterus corollatus and Huaxiapterus benxiensis.
- More recently, Lü et al. (2016) rejected all proposed synonymies and further proposed two new
- 101 species, Sinopterus lingvuanensis and Huaxiapterus atavismus. Subsequently, Zhang et al. (2019)
- sank all species ever attributed to *Huaxipterus* onto *Sinopterus*, and recognized five species as
- valid: Sinopterus dongi, Sinopterus corollatus, Sinopterus benxiensis, Sinopterus lyngyuanensis
- and Sinopterus atavismus. Zhang et al. (2019) regarded Sinopterus gui and Sinopterus jii as junior
- synonyms of Sinopterus dongi. Still, Zhang et al. (2019) did not present detailed discussions
- 106 concerning this taxonomic proposal.
- Subsequently, Naish et al. (2021) preliminarily corroborated the proposition of Witton (2013) that
- all Jiufotang tapejarids represent an ontogenetic continuum of a single species. Still, Naish et al.



109 (2021) noted that at least *Huaxiapterus corollatus* was an apparent outlier regarding limb 110 proportions, thus suggesting that it "may represent a second taxon", pending further testing. More 111 recently, Shen *et al.* (2021) supported the proposition by Naish *et al.* (2021).

In summary, a total of seven tapejarid species have been proposed for the Jiufotang Formation, all eventually attributed to the genus *Sinopterus* and intricated in a series of complex disputes based on preliminary considerations. A detailed review of the *Sinopterus* complex is still lacking, and a critical survey of anatomical variation is thus of the uttermost importance. The present work aims at:

- (1) A specimen-level assessment of morphological variation within the *Sinopterus* complex. For this, we present qualitative anatomical comparisons (specimen by specimen) as well as quantitative analyses (allometric and linear morphometric analyses), englobing previously described specimens as well as six new specimens;
- (2) An interpretation of the surveyed variation (as either intra- or interspecific), in order to interpret the validity and circumscription of each species. Our primary delimitation of species will disregard cranial crest features. After our primary delimitation has been made, we will proceed to map cranial crest variation and interpret it.
  - (3) Inferring the phylogenetic relationships between the established valid species.

With these considerations, we hope to reinterpret the *Sinopterus* complex and provide a taxonomic reassessment, based on which new specimens can be identified. Pivotal to the taxonomic history of the *Sinopterus* complex is the role of cranial crests in pterosaur taxonomy. It is clear that cranial crest features used alone make for dangerous taxonomic decisions (Witton, 2013), as they could rather reflect ontogenetic or sexual variations (Bennett, 1993; Wang *et al.*, 2014; Manzig *et al.*, 2014; Pinheiro & Rodrigues, 2017). However, it is also clear that some closely related species may exhibit disparate cranial crest morphologies (at least when inferred mature males are considered), which can thus contain taxonomic signal (e.g. *Pteranodon longiceps* and



Pteranodon sternbergi; see Bennett, 1994). It is for this reason that, in this work, we aim at revising the taxonomy of the *Sinopterus* complex with extra caution regarding cranial crest variation, by making a primary taxonomic assessment without input from cranial crest data first, and then assessing and interpreting cranial crest variation subsequently; instead of using cranial crest variation as an *a priori* source of taxonomic signal.

139

140

141

134

135

136

137

138

#### **Material & Methods**

#### **Institutional abbreviations**

- 142 **BMNHC**, Beijing Museum of Natural History, Beijing, China; **BPV**, Beijing Natural History
- 143 Museum, Beijing, China; **BXGM**, Benxi Geological Museum, Benxi, China; **D**, Dalian Natural
- history Museum, Dalian, China; GMN, Geological Museum of Nanjing, Nanjing, China; IVPP,
- 145 Institute of Vertebrate Paleontology and Paleoanthropology, Beijing, China; JPM, JZMP, Jinzhou
- 146 Museum of Paleontology, Jinzhou, China; PMOL, Paleontological Museum of Liaoning,
- 147 Liaoning, China; XHPM, Xinghai Museum of Prehistoric Life of Dalian, Dalian, China; ZMNH,
- 148 Zhejiang Museum of Natural History, Hangzhou, China.

149

150

#### **Geological setting**

- 151 The Jiufotang Formation is widely distributed in the terrestrial volcanic sedimentary basins of
- northern Hebei and western Liaoning, which have yielded the diverse Jehol Biota (Xi et al., 2019).
- 153 It represented a lacustrine environment surrounded by temperate forests (Zhou et al., 2003; Benton
- 154 et al., 2008). Although specimens are typically crushed, preservation is nonetheless exceptional
- and soft tissue is often found (Benton *et al.*, 2008).
- 156 The Jiufotang Formation of western Liaoning is distributed within six continental faulted basins,



trending Northeast: Fuxin-Yixian Basin, Beipiao-Chaoyang Basin, Dapingfang-Meileyingzi 157 Basin, Dachengzi-Siguanyingzi Basin, Jianchang Basin, Lingyuan-Sanshijiazi Basin (Su et al., 158 159 2008; Wu et al., 2018; Xi et al., 2019). The rock layers are mainly grey to greyish green in color, interbedded with greyish yellow, greyish 160 white, greyish black and occasionally purple rocks. They consist of calcareous silty shale, shale, 161 and siltstone, interbedded with oil shale, tuff, bentonite, coal seam, marlstone, sandstone, and 162 conglomerates. This sedimentary association is dominated by lake sediments and includes 163 abundant macrofossils of animals and plants. The thickness of Jiufotang Formation varies from 164 ~200-3000 m depending on locality, contacting the underlying Yixian Formation as a parallel 165 unconformity. It is overlaid by formations such as Binggou Formation and Fuxin Formation. 166 Unique fossil-bearing bed (UFBB) refers to a set of Chinese national key protected fossils 167 (classified as level three or above, by National Standard for classification of Paleontological 168 Fossils, China), such as reptiles and birds, which is known from a regionally stable and significant 169 geological formation. A number of unique fossil-bearing beds have been named (e.g., Duan et al., 170 2006; 2010, Wu et al., 2018, Gao et al., 2018), as indicated in Figure 1. 171 Wu et al. (2018) divided Jiufotang Formation into three sections from bottom to top, based on 172 lithology, depositional cycle, basic sequence and fossil assemblage. In general, the base of every 173 174 section consists of yellowish brown-yellowish green, thick-bedded medium to coarse conglomerate. The top layer is made up of yellowish green thin to very thin tuffaceous siltstone 175 and thin silty mudstone. A short-term cycle is formed by conglomerate (containing glutenite), 176 sandstone, siltstone and shale. About seven to nine short-term cycles form a mid-term cycle (three 177 sections of Jiufotang Formation) that exhibits finer grain sizes and thinner beds progressively 178 upward, as shown in a schematic division and correlation diagram of the Jiufotang Formation and 179 the UFBB in western Liaoning (including five basins: Fuxin-Yixian Basin, Beipiao-Chaoyang 180 181 Basin, Dapingfang-Meileyingzi Basin, Dachengzi-Siguanyingzi Basin and Jianchang Basin; Wu et al., 2018). 182



183	Due to the highly fossiliferous nature of the Jehol Group, several fossils are commonly found by
184	local collectors, although without a precise control over their stratigraphic provenance (e.g.
185	Kellner, 2010). A notable exception is the holotype of Sinopterus dongi, known to come from the
186	Lamagou UFBB, of the Second Member of the Jiufotang Formation (Zhang et al., 2007). The
187	holotypes of Sinopterus gui and Huaxiapterus jii come from the mudstone/shale layers of Nanlu,
188	Shengli Town, which correspond to the Yuanjiawa UFBB of the Third Member of the Jiufotang
189	Formation (Zhang et al., 2007). Specimens PMOL-AP00030 and D3072 are known to have come
190	from the Dapingfang locality (Liu et al., 2015; Shen et al., 2021), where the Third Member of the
191	Jiufotang Fm. outcrops (Wu et al., 2018; Fig. 1).
192	The holotype of <i>Sinopterus lingyuanensus</i> and specimen IVPP V 23388 are known to come from
193	Sihedang, Lingyuan, and they are preserved in white-gray shales (Lü et al., 2016; Zhang et al.,
194	2019), what indicates they likely come from the Third Member Sihedang beds (Wu et al., 2018;
195	Fig. 1).
196	The holotype of <i>Huaxiapterus benxiensis</i> is reported to come from Lianhe Town (Lü <i>et al.</i> , 2007),
197	and thus from the Dapingfang Basin, meaning it comes from either the Second or Third Member
198	(Zhang et al., 2007; Wu et al., 2018).
199	For specimens D2525 and the holotype of <i>H. corollatus</i> , the only information available is that they
200	come from Chaoyang City (Lü et al., 2006b; 2007). The same applies to the new specimens
201	reported here (D4019, BPMC 103, BPMC 104, BPMC 105, BPMC 106, and BPMC 107). Within
202	Chaoyang City, two fossiliferous beds of the Jiufotang Formation occur: the Dongpochi Bed of
203	the Second Member, and the Shangheshou Bed of the Third Member (Zhang et al., 2007).
204	
	Unfortunately, it is hard to define from which bed came each of the remaining Jiufotang tapejarid
205	Unfortunately, it is hard to define from which bed came each of the remaining Jiufotang tapejarid specimens, but it can be said that they come from either the Second or the Third Member.

207

#### Morphometric dataset



We have compiled a morphometric dataset for the purposes of our allometric and morphometric 208 clustering analyses. We have coded in our dataset 14 relatively complete Jiufotang tapejarid 209 specimens: the holotypes of Sinopterus dongi (IVPP V 13363, Wang & Zhou, 2003), 210 211 Huaxiapterus jii (GMN-03-11-001, Lü et al., 2005), Huaxiapterus corollatus (ZMNH M813, Lü et al., 2006a), Huaxiapterus benxiensis (BXGM V0011, Lü et al., 2007), Sinopterus 212 lingyuanensis (JPM-2014-005, Lü et al., 2016) and Huaxiapterus atavismus (XHPM 1009, Lü et 213 214 al., 2016), as well as specimens D2525 (Lü et al., 2006b), IVPP V 23388 (Zhang et al., 2019), 215 D3702 (Shen et al., 2021), and five new specimens which are presented here for the first time (D4019, BPMC 103, BPMC 104, BPMC 105, and BPMC 107). The holotype of Sinopterus gui 216 (see Li et al., 2003), specimens PMOL-AP00030 (Liu et al., 2015), SDUST-V1012 (Zhou et al., 217 218 2022a), and SDUST-V1014 (Zhou et al., 2022b), as well the new specimen BPMC 106, were not 219 included in the morphometric dataset due to their high level of incompleteness. 220 For comparative purposes, we have also included in our morphometric analyses other tapejarid species, namely Eopteranodon lii, Tapejara wellnhoferi, Caiuajara dobruskii and Tupandactylus 221 navigans. We have included the two known specimens of Eopteranodon lii, which come from 222 the Yixian Formation: the holotype BPV-078 (Lü & Zhang, 2005), and the referred specimen 223 D2526 (Lü et al., 2006c). Our entry for Tapejara wellnhoferi is based on specimens SMNK PAL 224 225 1137 (Eck et al., 2011) and AMNH 24445 (Vila Nova et al., 2015). Tupandactylus navigans is based on specimen GP/2E 9266 (Beccari et al., 2021), and Caiuajara dobruskii is based on a 226 combination of specimens CP.V 872a, CP.V 1006, and CP.V 1001b (Manzig et al., 2014). Data 227 for Caiuajara specimens was taken from Manzig et al. (2014). Data for all other specimens was 228 taken first-hand. 229 We compiled a morphometric dataset of 21 skeletal measurements, among six skull measurements 230 and 15 postcranial elements. The analyzed skull measurements comprise rostral index, rostral 231 value, rostrum deflection angle, length/height ratio of the nasoantorbital fenestra, orbit ventral 232 angle, and quadrate reclination angle. The postcranial bone measurements comprise the length of 233





the fourth cervical, fifth cervical, humerus, ulna, metacarpal I, metacarpal IV, wing phalanges 1– 4, femur, tibia, metatarsal I, and metatarsal II. A spreadsheet containing our morphometric dataset

is available as Supplemental File 1 (Sheet 1).

237

238

247

248

249

250

251

252

253

254

255

256

257

258

#### Allometric correlation analysis

The dataset for the correlation and allometric analyses was restricted to specimens of the 239 Sinopterinae, more specifically the Jehol tapejarids (Jiufotang tapejarids plus Eopteranodon lii 240 from the Yixian Fm.), which are deemed as a complex of closely related and rather conservative 241 242 species, and thus similar ontogenetic trends were assumed. The same assumption cannot be made 243 for more distantly related tapejarid taxa, which were thus left aside from these analyses in order to avoid potential noise). A spreadsheet containing our dataset for the allometric correlations (log-244 transformed morphometric values for the Sinopterinae only) is available within our Supplemental 245 File 1 (Sheet 2). 246

Bivariate allometric analyses were performed to test for correlation to size variation and potential allometric relationships when correlation is present. We utilized the standardized major axis (SMA) line-fitting method to determine the allometric equation (Warton *et al.*, 2006), largely following the protocol of Yang *et al.* (2022). We utilized humeral length as the common independent variable (*i.e.* as a proxy for body size), that is, using it as the common parameter for assessing morphometric variables in different specimens, and thus aiming at testing potential correlations and allometric relationships between morphometric variables and body size. All values were log-transformed for the SMA analyses.

We thus performed the SMA analyses between log-transformed values of humeral length and each of the analyzed proportions: rostral index, rostral value, rostrum deflection angle, length/height ratio of the nasoantorbital fenestra, orbit ventral angle, quadrate reclination angle, fourth cervical length, fifth cervical length, ulna length, metacarpal I length, metacarpal IV length, wing phalanges



1–4 lengths, femur length, tibia length, metatarsal I length, and metatarsal II length. The p-value was calculated in order to test for correlation between body size variation (as indicate by humeral length as a proxy) and each analyzed variable. For each variable, if the correlation was statistically significant (p < 0.05), then the allometric correlation was performed for this variable. If the correlation was not statistically significant (*i.e.* a certain variable does not correlate to body size), then the variable in question can be interpreted as not ontogenetically variable, and thus allometry is not calculated for this variable. The SMA analyses were undertaken using the software PAST (Hammer *et al.*, 2001). Isometry is considered as the null hypothesis.

Typically, a correlation is deemed as isometric when, in the line fitting equation, slope equals (or is insignificantly different from) 1 (see Warton *et al.*, 2006; Yang *et al.*, 2022). In contrast, the correlation is deemed as negatively allometric and positively allometric when slope is, respectively, significantly lower and higher than 1. To determine this, 95% confident intervals (with 1000 iterations) were calculated for the slope for each SMA analysis. The null hypothesis (isometry) is rejected if the slope's 95% confidence interval (CI) lays entirely above or below 1, indicating, respectively, positive or negative allometry. If the CI is comprised between a lower value below 1 and an upper value above 1 (*i.e.* 1 is comprised within the CI), then isometry is assumed.

#### Linear morphometric multivariate analyses

After our SMA analyses, we constructed a morphometric dataset of skeletal proportions (all log-transformed) based on skeletal elements devoid of allometric signal, as per the results of the previous SMA analyses. Thus, aiming at excluding noise from data that is allometrically correlated to size variation, our morphometric dataset aims to be based on two types of morphometric data: (1) data that is not correlated to size variation and (2) data that is isometrically correlated to size variation. Afterwards, our preened tapejarid morphometric dataset (including all tapejarid taxa)





was subjected to an unweighted pair-group average (UPGMA) cluster analysis (using Euclidean distance) as well as a Principle Component Analysis (PCA). Two different PCA analyses were performed, each differing in the treatment of missing data: one using mean values imputation, and one using iterative imputation. These analyses were executed using the software PAST (Hammer *et al.*, 2001). A spreadsheet containing our dataset for the multivariate analyses (preened skeletal angles and proportions for all analyzed tapejarids) is available within our Supplemental File 1 (Sheet 3).

#### **Ontogenetic assessment**

For the purpose of assessing the ontogenetic stages of the studied specimens, we follow here the many criteria put forward by workers such as Bennett (1993), Kellner & Tomida (2000), and Kellner (2015). However, we do not strictly follow the "5 ontogenetic stages" model based on bone fusion sequence (Kellner, 2015), since not all pterosaur clades exhibited similar sequences of ontogenetic bone fusion (Dalla Vecchia, 2018). For the purpose of a relative assessment of ontogenetic development within the *Sinopterus* complex, the specimens are here compared to each other only (based on bone fusion), and thus put in a restricted, in-clade context (Supplemental File 1, Sheet 5).

#### Phylogenetic analysis

Subsequent to our reassessment of the species-level taxonomy of the *Sinopterus* complex, we proceeded to perform a phylogenetic analysis, which is the last step of the present work. After obtaining the results from our taxonomic reassessments (see below for our taxonomic proposals and species circumscriptions), we included and coded all Chinese tapejarid species (those that were considered as valid here) in an updated version of the data matrix from Pêgas *et al.* (2021). For





808	this reason, in the present paper, a separate Phylogenetic Analysis section is presented only after
309	the main Discussion section.
310	We performed a cladistic analysis using the software TNT 1.5 (Goloboff et al. 2008), which was
311	divided in two steps. The first search was performed using New Technology Search (using
312	Sectorial Search, Ratchet, Drift and Tree fusing, default parameters), with random seed = 0.
313	Subsequently, using trees from RAM, we performed a Traditional Search swapping (using TBR,
314	10000 replications, collapsing trees after search). All characters were treated with equal weights.
315	A Mesquite file (Nexus format) containing the data matrix is available as Supplemental File 02. A
316	TNT file, ready for analysis execution in TNT, is available as Supplemental File 3.
317	Coding for Bakonydraco galaczi is restricted to jaw elements (Ősi et al., 2005; 2011). Coding for
318	Afrotapejara zouhri is based on the holotype and the three referred specimens (Martill et al.,
319	2022a). Coding for Aerotitan sudamericanus follows the interpretation of the holotype as a lower
320	jaw (Pêgas et al., 2021; contra Andres, 2021). The holotype of Alanqa saharica is also coded here
321	as a lower jaw (Pêgas et al., 2021; contra Ibrahim et al., 2020); however, its coding is corrected
322	here based on an anatomical reinterpretation after further preparation of the holotype, as follows.
323	The purported dentary occlusal eminence of the holotype material (Ibrahim et al., 2010; Pêgas et
324	al., 2021) was in fact made up of sediments, which were covering a groove bordered by a pair of
325	raised ridges (R. Smith & D. Martill, pers. comm.; Smith et al., in press), similar to that seen in
326	specimen FSAC KK 4000 (Martill & Ibrahim, 2015).
327	
328	Nomenclatural acts
329	The electronic version of this article in Portable Document Format (PDF) will represent a
330	published work according to the International Commission on Zoological Nomenclature (ICZN),
331	and hence the new names contained in the electronic version are effectively published under that
332	Code from the electronic edition alone. This published work and the nomenclatural acts it





- contains have been registered in ZooBank, the online registration system for the ICZN. The
- ZooBank LSIDs (Life Science Identifiers) can be resolved and the associated information viewed
- through any standard web browser by appending the LSID to the prefix http://zoobank.org/. The
- LSID for this publication is: urn:lsid:zoobank.org:pub:E836D564-B986-497A-9E3C-
- 337 8277EF8EF50E. LSID for the new genus: urn:lsid:zoobank.org:act:39AA06E5-6882-4041-9585-
- 338 8F2106424C81.

340

#### Phylogenetic nomenclature

- 341 The present work favors the recent propositions of the PhyloCode (de Queiroz et al., 2020) as a
- means of standardizing and stabilizing phylogenetic nomenclature. We thus primarily follow the
- phylogenetic definitions given and registered by Andres (2021) and Pêgas et al. (2021) concerning
- 344 azhdarchoids, though with a few unrestricted emendations. The phylogenetic nomenclatural
- scheme employed here, following recommendations of the PhyloCode, is presented in Table 1.
- 346 Of particular note concerning phylogenetic nomenclature in azhdarchoids is the conflicting usages
- of the terms Tapejaridae, Tapejarinae, and Thalassodrominae. Originally, the family Tapejaridae
- 348 was erected in order to encompass *Tapejara wellnhoferi* and *Tupuxuara longicristatus* (Kellner,
- 1989), and later defined as the least inclusive clade containing these two taxa (Kellner, 2003).
- 350 Tapejaridae was later divided into Tapejarinae and Thalassodrominae, which can be roughly
- described, respectively, as a "Tapejara-Sinopterus group" and a "Thalassodromeus-Tupuxuara
- group" (Kellner & Campos, 2007). Disagreement over the sister-group relationship between the
- 353 "Tapejara-Sinopterus group" and the "Thalassodromeus-Tupuxuara group" led to a restrictive
- redefinition of the Tapejaridae by some workers, as the least inclusive clade containing *Tapejara*
- wellnhoferi and Sinopterus dongi, with the "Thalassodromeus-Tupuxuara group" thus elevated to
- a family-level Thalassodromidae (Lü et al., 2005; Andres, 2021). A consequence of this problem
- is: even though the existence of both a "Tapejara-Sinopterus group" and of a "Thalassodromeus-



362

363

364

365

366

367

368

369

370

371

372

373

374

375

376

377

378

379

380

381

382

383

Tupuxuara group" has been remarkably consensual, the same clades have received different names
 according to preferred phylogeny. Albeit valid under the ICZN, this situation is conflictive with
 the principles of phylogenetic nomenclature.

Under the light of phylogenetic nomenclature, it is undesirable that two equivalent clades should bear inconsistent names across distinct phylogenies. If distinct phylogenies agree on recovering a given clade (which is a great feat in pterosaur systematics), then this clade should have a consistent name, for the sake of stability. Different clade names should only exist when de facto distinct clade proposals exist. For example, a clade that includes *Thalassodromeus* and *Azhdarcho* but excludes Tapejara does not exist in certain propositions (e.g. Kellner, 2003). However, this clade exists in others (Unwin, 2003; Andres, 2021), under which such a proposed clade does need a name ("Neoazhdarchia"). Thus, Neoazhdarchia is a name that only exists (or is valid) within the context of a certain phylogenetic proposal (Unwin, 2003; Andres, 2021). In contrast, a clade that includes Sinopterus and Tapejara and excludes Thalassodromeus and Azhdarcho is universally accepted among pterosaur researchers. It is unfortunate that such welcome phylogenetic consensus is not accompanied by nomenclatural stability, as it should. It is for this reason that we adopt here the restrictive usage of Tapejaridae sensu Andres (2021), which has already been proposed and registered under the PhyloCode. This definition can be utilized in any phylogenetic proposal, and its adoption will prevent different workers from referring to different clades by, confoundingly, using the same names – as well as from referring to a same clade by different names.

Arguments for the restrictive usage of Tapejaridae *sensu* Andres (2021) need not come exclusively from the point of view of the PhyloCode, but could also be argued for under the ICZN. In the same way that the expansive Pteranodontidae *sensu* Bennett (1989; 1994) was elevated to the Pteranodontoidea of Kellner (2003), turning Pteranodontidae more restricted, then one might also regard that the original Tapejaridae *sensu* Kellner (1989; 2003) should be elevated to the Tapejaromorpha, with Tapejaridae becoming more restricted. We emphasize that the usage of these definitions as explored here do not imply, in any way, which phylogeny is preferred, and can



stably be employed onto any presently existent phylogenetic proposal. In fact, the preferred proposal employed here is based on Pêgas *et al.* (2021), which is ultimately derived from Kellner (2003) – we corroborate the sister-group relationship between Tapejaridae and Thalassodromidae.

#### Results

#### **Specimen-level variation survey**

The generalized osteological pattern of *Sinopterus* complex specimens has already been described elsewhere (Zhang *et al.*, 2019; Shen *et al.*, 2021; Zhou *et al.*, 2022a). This section is not intended as a monographical account of the morphology of each specimen, but as a report of their most striking features, with particular focus on the anatomical variations we surveyed. Monographical descriptions are beyond the scope of the present paper and will be provided elsewhere. Specimens PMOL-AP00030 (Liu *et al.*, 2015), SDUST-V1012 (Zhou *et al.*, 2022a) and SDUST-V1014 (Zhou *et al.*, 2022b) are not included in the present reassessment due to their rather incomplete nature. The holotype of *Nemicolopterus crypticus*, which may be a hatchling tapejarid (Witton, 2013; Naish *et al.*, 2021), is also not included due to its very immature nature and disputed identification, and is thus discussed separately further below in the Discussion section.

Despite the relative completeness of several specimens, observation of anatomical details is rather limited due to preservational issues. As all specimens are crushed, bones are usually visible from a single side, sometimes obscured by overlaying bones, and sometimes too damaged, thus highly limiting comparisons. Osteological details are given below as possible. However, in most circumstances, details do not go further than gross shape seen from a single view (as demonstrated in our plates) and measurements. All specimens were measured first-hand, and raw measurements are presented in Supplemental File 01 (Sheet 1). Specimens are presented below in chronological order of publication, from the oldest reported one to the most recently reported ones, and then finally with the ones reported here for the first time (D4019, BPMC 103, BPMC 104, BPMC 105, BPMC 106, and BPMC 107).



411

435

#### IVPP V 13363 (holotype of *Sinopterus dongi*)

Morphological survey. This specimen (Fig. 2) was originally described by Wang & Zhou (2003). 412 It exhibits a relatively slender rostrum (~36% of jaw length), with a very low, incipient 413 premaxillary crest and a low dentary crest. The rostrum is gently downturned at about 14° relative 414 415 to the posterior occlusal line. The premaxillary crest is parabolical in outline. The nasoantorbital fenestra length/height ratio is not readily clear due to a slight anteroventral displacement of the 416 orbitotemporal region. Still, it can be restored as somewhere between 2.8 and 3.2 (by restoring the 417 position of the orbitotemporal region based on the inferred location of the quadratomandibular 418 419 joint as indicated by the proportions of the mandible). The orbit has been described as subcircular (e.g. Andres et al., 2014), since its height and length are subequal. However, it may be described 420 as subquadrangular due to the angular corners. This differs from the typical elongated piriform 421 422 condition (higher than long, with a round dorsal margin and tapered ventral margin) of tapejarids and azhdarchoids in general (e.g. Kellner & Campos, 2007). Still, a tapered shape of the lower 423 orbital margin is still present (in the jugal). The lacrimal process of the jugal is subvertical (only 424 slightly anterodorsally oriented). A pair of slender, anteroventrally directed, and medially placed 425 descending nasal processes is present. The posterior cranial crest processes (the posterior process 426 of the premaxillae, and the frontoparietal crests) curve upwards. The quadrate is posteriorly 427 reclined at  $\sim 160^{\circ}$  relative to the palatal plane. The observable cervical formula is III < IV > V > 428 VI > VII. The scapula is about 1.30 the length of the coracoid. The coracoid exhibits a clear ventral 429 430 flange. The humeral deltopectoral crest is tongue-like and its long axis is sub-perpendicular relative to the long axis of the humeral shaft. The pteroid accounts for 43% of ulnar length. 431 Metacarpal I is elongate, reaching the carpal region, while metacarpals II and III are reduced and 432 restricted distally. Metatarsal I is the longest of the metatarsals (Wang & Zhou, 2003; Zhang et al., 433 2019). 434

**Ontogenetic assessment.** This specimen has already been regarded before as a juvenile (Kellner,



2010; Zhang et al., 2019). A large number of skeletal elements remain unfused in this specimen: scapulacoracoid, humeral epiphysis, carpal series, extensor tendon process of the first wing phalanx, and tibiotarsus. Several skull elements also remain unfused. It is clear that this specimen is a juvenile indeed, if compared to more ontogenetically advanced specimens in which the abovementioned elements are fused, such as in the postcranial skeleton of D2525 (Supplemental File 1, Sheet 5). At a wingspan of 1.2 m, it would be conceivable that it was an advanced juvenile, older than smaller specimens such as the holotypes of S. gui (0.8 m), S. lingyuanensis (~0.85 m) and H. atavismus (0.85 mm, see further below), and younger than larger specimens such as the holotype of *S. jii* (1.6 m) and D2525 (2 m). 

**Remarks.** This specimen is the holotype of *Sinopterus dongi* – the first genus and species of tapejarid to be described for the Jiufotang Fm. and Jehol Group as a whole. The validity of this genus and species has never been questioned.

#### BPV-077 (holotype of Sinopterus gui)

Morphological survey. The specimen (Fig. 3) is unfortunately badly preserved, with quite damaged and crushed bone surfaces (Li *et al.*, 2003). Still, general outlines of some of the skull and appendicular bones can be discerned. The skull is exposed mostly in left lateral view, except for the posterior region which seems to be broken and exposed in a slightly dorsolateral view. The rostrum accounts for ~39% of total jaw length. It is very slender (RI = 0.33) and crestless, while the dentary symphysis bears a very shallow crest. The nasoantorbital fenestra is very elongate (length/height ratio ~3.2). Quadrate inclination is unclear due to the bad preservation of the posterior region of the skull. Details of the cervical series are unclear due to bad preservation. The coracoid ventral margin bears a flange, similar to other *Sinopterus* complex specimens (see below). The deltopectoral crest of the humerus is rectangular, proximally placed, and bears a long axis roughly perpendicular relative to the main humeral shaft. The relative length of metacarpals I-III



465

466

467

468

469

470

471

472

473

474

475

476

477

478

479

480

481

482

483

484

485

486

cannot be assessed. Of the wing fingers, only a first phalanx is preserved, thus obscuring wing phalanges proportions. Unfortunately, not much further details can be assessed due to the very limited preservational quality of the specimen.

**Ontogenetic assessment.** Unfused elements: palatal and posterior skull bones, dorsal centra and neural arches, scapula and coracoid, pelvic elements, tibia and fibula (entirely unfused). Other ontogenetic correlates cannot be assessed. This specimen is clearly a very young juvenile. It is also the second smallest of all Jehol tapejarid specimens (second to the holotype of *Nemicolopterus crypticus*), with an estimated wingspan of only 64 cm (Kellner & Campos, 2007).

**Remarks.** This specimen is the holotype of *Sinopterus gui* – the second species of tapejarid to be described for the Jiufotang Fm. and Jehol Group as a whole (Li et al., 2003). It was subsequently recognized as a very young juvenile (Kellner & Campos, 2007). The validity of this species has been questioned several times, in all such cases being regarded as a junior synonym of S. dongi even when multiple Jiufotang tapejarid species were accepted, on the basis that it could not be distinguished from S. dongi (Kellner & Campos, 2007; Kellner, 2010; Zhang et al., 2019). This is problematic because recent publications have simply repeated the interpretation of S. gui being indistinguishable from S. dongi while not comparing S. gui to other more recently named species considered as valid, thus not justifying why it is indistinguishable from S. dongi only and not from any further species (e.g. Zhang et al., 2019). First described by Li et al. (2003), these authors recognized it as distinct from Sinopterus dongi at a species-level, yet sufficiently similar to be placed in the same genus. Originally, Li et al. (2003) proposed the following diagnosis for the new species: "[e]leven dorsal vertebrae fused into notarium, and they are nearly equal in length. At least four sacral vertebrae, humerus longer than scapula, wing metacarpal slightly shorter than the first wing phalange, the distal end of the deltopectoral process not expanded, ratio of the femur to the tibia is approximately 0.49" (Liu et al., 2003: p. 445). Later, Kellner & Campos (2007) observed that this specimen does not present a notarium (which is an advanced ontogenetic feature). Instead, it represents a very young, juvenile specimen (Kellner & Campos, 2007; Kellner,



2010). Most authors have, since then, been unable to distinguish *S. gui* from *S. dongi*, and thus interpreted the holotype of *Sinopterus gui* as a juvenile specimen of *Sinopterus dongi* (e.g. Kellner & Campos, 2007; Zhang *et al.*, 2019), although Kellner (2010) noticed that it could represent a juvenile of some other Jiufotang tapejarid instead, such as *Huaxiapterus corollatus* (therein referred to as *Sinopterus corollatus*). The interpretation of the holotype of *S. gui* as a juvenile of *S. dongi* (and not any other Jiufotang tapejarid species) has been maintained by Zhang *et al.* (2019) without further justifications, even though these authors accept the validity of several other *Sinopterus* species (*S. lingyuanensis*, *S. corollatus*, *S. benxiensis*, and *S. atavismus*). We maintain here that *S. gui* is indeed indistinguishable from *S. dongi* except for the complete absence of a premaxillary crest in the former, which is easily attributed to ontogeny (Witton, 2013; Zhang *et al.*, 2019).

#### GMN-03-11-001 (holotype of *Huaxiapterus jii*)

Morphological survey. This almost complete specimen includes a partial skull, although the posterior region is disarticulated and damaged (Fig. 4). The rostrum is ventrally deflected at 14° relative to the posterior palatal plane. The rostrum exhibits a premaxillary crest. It is similar in shape to that of *S. dongi* (parabolical in outline), despite being larger. It is distinct from the premaxillary crest condition of other proposed species, such as the pointed premaxillary crests of *Huaxiapterus atavismus* (both specimens, the holotype XHPM 1009 and the referred specimen IVPP V 22338) or the trapezoidal crests of *Huaxiapterus corollatus* and *Huaxiapterus benxiensis*, or the crestless conditions seen in *Sinopterus gui* and *Sinopterus lingyuanensis*. Most of the posterior region of the skull is badly damaged, except for the left jugal which is partially preserved. The jugal is triradiate, unlike the tetraradiate condition seen in *Tapejara wellnhoferi* (Wellnhofer & Kellner, 1991), *Caiuajara dobruskii* (Manzig *et al.*, 2014) and *Tupandactylus navigans* (Beccari *et al.*, 2021). The lacrimal and postorbital processes of the jugal describe a roughly perpendicular angle. The proportions of the nasoantorbital fenestra cannot be readily measured due to the



damaged nature of the posterior region of the skull, but an estimate can still be given based on the 513 location of the lacrimal process of the jugal (about three times as long as high). As with the 514 515 premaxillary crest, the dentary crest is also larger than in S. dongi. Only two disarticulated cervical 516 vertebrae can be seen, so that the cervical formula cannot be assessed. Pteroid length is equivalent 517 to about 44% of the ulna length. Metacarpal I is elongate, extending for at least 90% the length of metacarpal IV. Wing proportions are closest to the holotype of S. dongi (Fig. 4; Supplemental File 518 519 01, Sheets 1, 3). Pedal elements are entirely disarticulated, so that the metatarsal formula cannot 520 be assessed. **Ontogenetic assessment.** The holotype of S. jii has been regarded as a juvenile compatible with 521 the holotype of S. dongi, given their similarity in lacking bone fusion between posterior skull 522 523 elements, scapulocoracoid, humeral epiphyses, carpals, extensor tendon process of the first wing phalanx, and tibiotarsus (Kellner, 2010). However, it is worth noticing that the dorsal centra and 524 arches of GMN-03-11-001 are partially fused (they bear a visible suture, but are not found 525 disassociated), unlike some entirely unfused and disassociated dorsal centra and arches seen in the 526 holotype of S. dongi. This suggests that GMN-03-11-001 is slightly more ontogenetically 527 developed than the holotype of S. dongi, both as juveniles. 528 Remarks. This specimen was originally described as representing a new genus and species, 529 Huaxiapterus jii (Lü & Yuan, 2005). Subsequent publications have considered it either as a species 530 of Sinopterus, as S. jii (Kellner & Campos, 2007; Pinheiro et al., 2011; Kellner, 2013), or as a 531 junior synonym of Sinopterus dongi (Wang & Zhou, 2006; Witton, 2013; Zhang et al., 2019), thus 532 invalidating the genus *Huaxiapterus*. Still, other researchers still considered *H. jii* as valid and as 533 a distinct taxon, with the genus *Huaxiapterus* being valid (Andres et al., 2014; Lü et al., 2016). 534 This taxon was originally diagnosed based on cranial crest development: premaxillary and dentary 535 crests deeper than in Sinopterus dongi and shallower than in Tapejara wellnhoferi (see Lü & Yuan, 536 537 2005). Later, this species has been regarded as a junior synonym of Sinopterus dongi: Wang & 538 Zhou (2006) were unable to find differences between the holotypes of the two species, and thus



540

541

542

543

544

synonymized them. At the time, these two species (together with *Sinopterus gui*) were the only named species within the *Sinopterus* complex. We maintain that the holotypes of *S. gui* and *S. jii* are indistinguishable from *S. dongi*, and further add that *S. jii* shares with *S. dongi* the following features: metacarpal I articulating with the carpus, and wing phalanx 4/phalanx 1 length ratio about ~0.30, which distinguish these proposed taxa from other proposed taxa such as *H. corollatus* and *H. benxiensis* (see below). Sadly, these features are uncertain in the holotype of *S. gui*.

545

546

547

548

549

550

551

552

553

554

555

556

557

558

559

560

561

562

563

#### ZMNH M813 (holotype of *Huaxiapterus corollatus*)

**Morphological survey.** This specimen is almost complete, although some skeletal regions are badly damaged and anatomical details are obliterated, particularly the posterior region of the skull, post-cervical vertebrae, and the pedes (Fig. 5). The skull exhibits a trapezoidal premaxillary crest and a shallow dentary crest. The rostrum is relatively robust, akin to that of the holotype of Huaxiapterus jii and unlike the holotypes of S. dongi or S. gui. The rostrum is ventrally deflected by 21° (contra 14° in the holotypes of S. dongi and H. jii). The nasoantorbital fenestra is relatively short, with an estimated length/height ratio of about 2.2 (based on its length as inferred from the location of the quadratomandibular joint, as indicated by the preserved mandible, as it roughly correlated to the posterior margin of the nasoantorbital fenestra in sinopterines and tapejarids overall). A clear occlusal gap is present between the dentary and the rostrum (as originally indicated, see Lü et al., 2006), unlike what has been represented in some reconstructions (e.g. Witton, 2013). The cervical series is partially obscured by the radius and ulna, which lay over cervicals IV-V, hindering assessment of their relative lengths. Metacarpals I-III are reduced, and it can be seen that metacarpals I and II do not contact the carpus, reaching only about a third of the length of metacarpal IV. Wing proportions deviate from previously reported specimens in that the fourth wing phalanx is relatively shorter, accounting for only ~20% of the first phalanx (contra  $\sim$ 30% in the holotypes of S. dongi and S. jii).



Ontogenetic assessment. In this specimen, unfused skeletal elements include the posterior skull 564 bones, scapulocoracoid, and extensor tendon process of the first wing phalanx. Unfortunately, 565 fusion of humeral epiphyses cannot be assessed due to poor preservation. The tarsals are fused to 566 567 the tibia, forming a tibiotarsus, as can be seen from the right hindlimb. The carpals also seem to 568 be fused into distal and proximal syncarpals. Thus, this specimen seems to be relatively more mature than the holotypes of S. dongi, S. gui and S. jii, as a subadult. 569 570 **Remarks.** This specimen was designated as the holotype of *Huaxiapterus corollatus* by Lü *et al.* (2006). The species-level validity of this species (irrespective of its generic status) has been mostly 571 accepted (Pêgas et al., 2016; Lü et al., 2016; Zhang et al., 2019; Andres, 2021), except for Witton 572 (2013) who preliminarily proposed that all Jiufotang tapejarids were synonymous with S. dongi. It 573 is interesting to note that, although Naish et al. (2021) preliminarily corroborated Witton's (2013) 574 view, they highlighted that at least the holotype of *H. corollatus* could potentially represent a new 575 taxon (based on its limb proportions), pending further study. 576 The taxon *Huaxiapterus corollatus* was originally diagnosed on the basis of cranial crest features, 577 namely crest shape ("hatchet-shaped"), position (level with the anterior margin of the 578 nasoantorbital fenestra), and orientation ("short axis perpendicular to the anterodorsal margin of 579 the nasoantorbital fenestra"; see Lü et al., 2006). These conditions differ starkly from what is seen 580 in the holotypes of S. dongi, S. gui and H. jii. However, as noticed by Witton (2013) and Naish et 581 al. (2021), cranial crest features used alone make for dangerous taxonomic decisions, as they could 582 rather reflect ontogenetic or sexual variations. Still, the holotype of H. corollatus also differs from 583 the holotypes of S. dongi and S. jii in exhibiting a reduced metacarpal I, and in wing proportions 584 (Supplemental File 01, Sheet 1). H. corollatus exhibits a reduced wing phalanx 4, which accounts 585 for ~20% of the length of the first wing phalanx, contra ~30% in the previously named S. dongi 586 and H. jii. Naish et al. (2021) noticed that the holotype of H. corollatus was an apparent outlier 587 within the Sinopterus complex regarding limb proportions, leading them to propose that it could 588 be a potentially valid taxon pending further study. 589

591

592

593

594

595

596

597

598

599

600

601

602

603

604

605

606

607

608

609

610

611

612

613

614

615

D2525

**Morphological survey.** D2525 is an almost complete postcranial skeleton, lacking the skull, part of the anterior cervical series, part of the posterior dorsal series, and the sacral and caudal series (Fig. 6). The preserved cervical vertebrae, as well as shoulder girdle and right humerus, are badly damaged. Although previously unreported, the ?fourth cervical (exposed in ventral view, retaining some tridimensionality) clearly exhibits a pneumatic foramen piercing its lateral surface. The sternum is approximately square, with the posterior margin convex. The left coracoid bears a welldeveloped ventral flange. The left humerus is exposed in dorsal view, and no dorsal proximal pneumatic foramen can be seen in this specimen, as in IVPP V 23388 (Zhang et al., 2019). The ulnar crest is rounded. The humeral shaft is mostly straight, except for the distal portion which is slightly anteriorly recurved. Metacarpals I-III are tightly appressed to metacarpal IV on the distal metacarpal region on both sides. Metacarpal I extends for only about 40% of the length of metacarpal IV (Fig. 6). Wing proportions are very similar to the holotypes of *H. corollatus* and *H.* benziensis, with the fourth wing phalanx corresponding to ~20% the length of the first wing phalanx (contra ~30% in S. dongi and S. jii). Wing phalanges are exposed in ventral view, and a longitudinal ridge can be seen in phalanges 2 and 3, similarly to H. atavismus (Lü et al., 2016) and IVPP V 23388 (Zhang et al., 2019). In the pedes, metatarsal I is distinctively shorter than metatarsal II, which is the longest.

**Ontogenetic assessment.** Specimen D2525 is the second largest of all known Jiufotang tapejarids, with a 2-meter wingspan (Lü *et al.*, 2005), and also appears to be one of the most osteologically mature ones. Observable fused elements include dorsal neural arches and centra, the scapulocoracoid, the syncarpals, and the extensor tendon process of the first wing phalanx. Partial fusion (almost complete fusion, with faint indications of sutures) can also be seen in the pelvis, tibiotarsus, and tarsal elements. The presence of a notarium cannot be assessed due to preservational limitations, since the anterior dorsal series is preserved in ventral view and badly



616 crushed.

Remarks. This specimen was originally described as a new specimen of *Sinopterus dongi*, based on the assertion that the limb proportions of D2525 were most similar to *S. dongi* than to *S. gui*, *H. jii* or *H. corollatus*, which were the four existing nominal species at the time (Lü *et al.*, 2006). Such referral has never been contested in the literature. Contrary to previous reports (Lü *et al.*, 2006), the limb proportions of D2525 are most similar to the holotype of *H. corollatus*, and not *S. dongi* (see Supplemental File 01, Sheets 1, 3). In fact, D2525 is herein considered as indistinguishable from *H. corollatus*, with which it shares a shortened metacarpal I (about 40% the length of metacarpal IV, *contra* >90% in *S. dongi* and *S. jii*) and a shortened fourth wing phalanx (~20% of first phalanx length, *contra* ~30% in *S. dongi* and *S. jii*). It differs from the holotypes of *S. dongi* and *H. jii* in wing proportions and in metatarsals I-II relative length (metatarsal II is the longest one in D2525, instead of metatarsal I as in *S. dongi*).

#### BXGM V0011 (holotype of *Huaxiapterus benxiensis*)

Morphological survey. This specimen consists on a virtually complete specimen (Fig. 7). However, some anatomical regions are damaged and/or partially obscured, mainly the torso region (with the post-cervical vertebral series, sternum, ribs, and scapulocoracoid). The rostrum is built similarly to the holotype of *H. corollatus*, with a downward deflection of 20°. The premaxillary crest is slightly larger than in the holotype of *H. corollatus*, but it is similar in being distinctively anterodorsally protrusive with abrupt limits, unlike the smoothly-transitioning borders of the parabolical crests of the holotypes of *S. dongi* and *S. jii*. Despite broken, the premaxillary crests seems to have been trapezoidal in shape, as in the holotype of *H. corollatus*. The posterior process of the premaxillae is steeply dorsally recurved. An elongate posterior spine (posterior process of the premaxillae + frontoparietal crest) is present, much larger than in the holotype of *S. dongi*. The nasoantorbital fenestra is approximately as elongate as in *S. dongi*, with a length/height ratio of



642

643

644

645

646

647

648

649

650

651

652

653

654

655

656

657

658

659

660

661

662

663

664

665

666

about 2.4. The long axis of the nasal process is very deflected anteriorly, unlike the almost verticalized nasal process seen in the holotype of S. dongi. The shape of the jugal (as seen from the lacrimal and postorbital processes) demonstrates that the orbit was piriform, with a tapered ventral margin, and quite higher than wide, unlike the subquadrangular orbit of S. dongi. The quadrate is posteriorly inclined at about 153°. Not much further detail can be seen due to extensive superficial damage. The observable cervical formula is III < IV < V > VI. Both humeri are badly damaged, with only a section being exposed. The original description reported on an oddly short humerus only 55% the length of the femur (Lü et al., 2007), but this seems to have been based on the fairly incomplete right humerus. We reidentify here the damaged proximal and distal limits of the left humerus, which indicate it was comparable to that of other Jiufotang tapejarids (about 80%) of femur length) instead of oddly short (Fig. 7A, D). The extension of the pteroid is unclear. Metacarpal I confidently extends for only ~40% the length of metacarpal IV. The proximal extension of metacarpals II and III is unfortunately unclear, since it is unclear if the proximal tips are broken or not. Wing proportions closely match H. corollatus, with relatively short fourth wing phalanges (20% the length of the first phalanx). The relative length of metatarsals I-III overall cannot be assessed due to poor preservation.

Ontogenetic assessment. In this specimen, fused skeletal elements include the humeral epiphyses, syncarpals, the extensor tendon process of the first wing phalanx, and the tibiotarsus. Scapulocoracoid cannot be observed due to damage. Only the posterior skull bones are still unfused to the rest of the skull. Indeed, posterior skull bones are known to be among the last skeletal elements to fuse in pterosaurs (e.g. Kellner, 2015). This specimen thus exhibits a relatively advanced level of skeletal fusion, fitting well with the concept of an advanced subadult among pterosaurs (e.g. Kellner & Tomida, 2000). This specimen is clearly one of the most mature ones in the present sample, along with D2525 (see above), since all of the previously described specimens lack fusion of the extensor tendon process of the first wing phalanx.

**Remarks.** The species *H. benxiensis* was erected on the basis of BXGM V0011 and attributed to



the genus *Huaxiapterus*, following *H. jii* and *H. corollatus*. The validity of this species has been mostly accepted without further comments (Pinheiro *et al.*, 2011; Kellner, 2013; Pêgas *et al.*, 2016; Zhang *et al.*, 2019; Andres, 2021), except for works that argued for the "restrictive taxonomic scheme" of the *Sinopterus* complex, which regarded it as most likely a junior synonym of *S. dongi* along with all other nominal species of Jiufotang tapejarids (Witton, 2013; Naish *et al.*, 2021).

Huaxiapterus benxiensis has been regarded as distinct from H. corollatus on the basis of an "elongate parietal spine", "well-developed premaxillary crest", and a "shallow groove" on the occlusal surface of the dentary symphysis (Lü et al., 2007). Witton (2013) noticed that crest-related features could be influenced by ontogeny rather than interspecific variation. We further note that the "shallow groove" on the anterior end of the symphysis corresponds to the anterior occlusal depression (ubiquitous to tapejarids), interrupted posteriorly by a transverse ridge (similar to the condition seen in  $Bakonydraco\ galaczi$ ; see Ösi  $et\ al.$ , 2005). This condition can also not set H. benxiensis apart from any other proposed Jehol tapejarid species, since preservation precludes the verification of this feature in other type specimens. H. benxiensis is here considered as indistinguishable from H. corollatus, with which it shares a rostrum deflection of ~20°, a reduced metacarpal I, and a reduced fourth wing phalanx (~20% of first wing phalanx length). Both H. benxiensis and H. corollatus further differ from S. dongi and S. gui in exhibiting a relatively shorter nasoantorbital fenestra (only 2.2–2.4 in height/length ration,  $contra \sim 3$  in S. dongi and S. gui).

#### JPM-2014-005 (holotype of *Sinopterus lingyuanensis*)

**Morphological survey.** The holotype of *S. lingyuanensis* exhibits a relatively fine preservation, comprising an almost complete skeleton lacking only some distal wing phalanges and the tail. Some anterior trunk and appendicular elements, such as posterior cervical vertebrae, some dorsal vertebrae, ribs, sternum, and pectoral girdle, are severely crushed against each other and cannot be discerned (Fig. 8). Other than that, most other skeletal elements are discernible, with decent surface



717

718

preservation despite crushing. The skull is exposed mainly in left lateral view, and the occipital 692 region is laterally displaced towards the left, thus being visible in a somewhat posterolateral view. 693 The rostrum is entirely crestless and slender, accounting for 44% of total jaw length. The rostrum 694 is gently deflected at 12° relative to the palatal plane. Beneath the anterior level of the 695 nasoantorbital fenestra, a bulge is present on the jaw margin, indicating the presence of a slight 696 lateral palatal expansion similar to what is seen in *Tapejara* and *Caiuajara* (Wellnhofer & Kellner, 697 1991; Manzig et al., 2014). The nasoantorbital fenestra is quite elongate, being 3.25 times longer 698 699 than high. The nasals exhibit a pair of descending nasal processes, which are subvertical and elongate, similar to S. dongi and unlike the anteriorly directed, short condition seen in H. 700 701 benxiensis. The orbit is roughly subquadrangular, about as wide as high, similarly to S. dongi. The divergence angle between the lacrimal and postorbital processes of the jugal is about ~90°, similar 702 to S. dongi and H. jii but unlike H. benxiensis (~68°), which exhibits a piriform orbit. The quadrate 703 is reclined at about 160°. A small, short frontoparietal crest is present, extending beyond the 704 occiput. The mandible is exposed in dorsal view. Sadly, the occlusal surface is not well-preserved. 705 706 Still, it can be seen that a slight lateral expansion occurs at the posterior region of the symphysis, as in Tapejara and Caiuajara (Wellnhofer & Kellner, 1991; Manzig et al., 2014), matching the 707 slight lateral palatal expansion beneath the anterior margin of the nasoantorbital fenestra. The 708 dentary symphysis and the retroarticular process account for, respectively, 53% and 4% of total 709 710 mandibular length. Atlas and axis cannot be observed. The observable cervical formula is III < IV > V > VI, similar to S. dongi and unlike H. benxiensis in which the fifth cervical is the longest. 711 The mid-cervicals clearly exhibit at least one pneumatic foramen piercing their lateral sides. The 712 pteroid accounts for 47% of ulnar length. Sadly, the distal extensions of metacarpals I-III are 713 714 obscured by metacarpal IV. The relative length of the fourth wing phalanx is also unknown. In the pedes, the metatarsal formula is I < II > III > IV, similar to D2525 but unlike S. dongi. 715

**Ontogenetic assessment.** JPM-2014-005 is small-sized, with a skull length of 112 mm and an estimated totalized wingspan of ~850 mm. Skull elements are mostly unfused, to the exception of the premaxillomaxillae and dentaries. Postcranial unfused elements include the humeral epiphyses,



carpals, extensor tendon process of the first wing phalanx, pelvic elements, and tibiotarsus. Fusion 719 (or lack thereof) of further elements cannot be assessed. The available information suggests JPM-720 2014-005 is a young juvenile, as the holotypes of S. gui and S. dongi. 721 **Remarks.** This specimen was originally designated as the holotype of a new species. S. 722 lingvuanensis, by Lü et al. (2016). This was subsequent to Witton's (2013) proposition that all 723 Jiufotang tapejarids formed an ontogenetic continuum of S. dongi, which was not accepted by Lü 724 725 et al. (2016). Later, Zhang et al. (2019) expressed their approval over the validity of S. lingvuanensis, without further comments. Later, Naish et al. (2021) echoed the proposition of 726 Witton (2013) that all proposed Jiufotang tapejarids most likely represented a single species (to 727 the potential exclusion of *H. corollatus*), including *S. lingyuanensis*. 728 The species Sinopterus lingvuanensis was proposed based on the following features: nasoantorbital 729 fenestra length/height ratio 3.2, rostral index 3.03, femur/tibia length ratio 0.66, and wing phalanx 730 731 2/wing phalanx 1 length ratio 0.85 (Lü et al., 2016). However, all of these values fit well within the spectrum seen in the *Sinopterus* complex (Supplemental File 01, Sheet 1) and cannot set S. 732 lingyuanensis apart from other species, particularly from S. dongi, S. gui and H. jii which also 733 exhibit nasoantorbital fenestra about three times as long as high (distinct in this regard from the 734 holotypes of H. corollatus and H. benxiensis). Still, S. lingyuanensis does differ from S. dongi in 735 metatarsal configuration (I  $\approx$  II, rather than I > II), and also differs from H. benxiensis in orbit 736 shape (subcircular rather than piriform), nasal descending process configuration (subvertical and 737 elongate, rather than anteriorly directed and short), and cervical formula (IV > V, rather than IV < 738 V). It also differs from both H. corollatus and H. benxiensis in exhibiting a gentler rostrum 739 deflection (12° rather than 20°). The significance of these variations will be discussed further 740

742

743

741

#### XHPM 1009 (holotype of *Huaxiapterus atavismus*)

below, in the Discussion section.



- **Morphological survey.** Despite virtually complete, many skeletal remains of this specimen are quite jumbled together, preventing the observation of much anatomical data (Fig. 9). The rostrum exhibits a very small, triangular-shaped premaxillary crest, whose apex is anterodorsally oriented and located posterior to the anterior margin of the nasoantorbital fenestra (this configuration is distinct from any other tapejarid specimen previously published, but similar to specimens IVPP V 23388 and D4019). The rostrum is slender, ventrally deflected by  $14^{\circ}$ , and with a deflection point anteriorly located, similarly to *S. lingyuanensis*. A small, yet clearly perceivable, occlusal gap is present. The dentary bears a slight dorsal eminence, as well as a low dentary crest. The observable cervical formula is  $III < IV > V \cong VI > VII > VIII$ . Not much can be discerned from the remaining of the axial skeleton, and the same is true for the pectoral girdle. The pteroid accounts for 40% of ulnar length. Unfortunately, the relative lengths of the metacarpals cannot be assessed. Wing phalanx proportions are a close match for *S. dongi* and *S. jii* (Supplemental File 01, Sheet 1), and distinct from *H. corollatus*, *H. benxiensis* and D2525 which exhibit a comparatively reduced fourth wing phalanx about 20% the length of the first wing phalanx (Supplemental File 01, Sheet 1). Metatarsal I is shorter than metatarsal II, which is the longest, unlike *S. dongi*.
- Ontogenetic assessment. XHPM 1009 is a small-sized specimen, with an estimated skull length of ~120 mm and total wingspan of ~850 mm. Unfused skeletal elements include the carpals, extensor tendon process of the first wing phalanx, and tibiotarsus. Sadly, not much else can be discerned. Still, this specimen is compatible with a young juvenile, not much more advanced than the holotype of *S. gui*.
- Remarks. This specimen was originally designated as the holotype of a new species, *H. atavismus*, by Lü *et al.* (2016). This was subsequent to Witton's (2013) proposition that all Jiufotang tapejarids formed an ontogenetic continuum of *S. dongi*. Still, Zhang *et al.* (2019) accepted the validity of this species, which they assigned to the genus *Sinopterus*, as *Sinopterus atavismus*. Later, Naish *et al.* (2021) echoed the proposition of Witton (2013), to the inclusion of *S. atavismus*.
- 769 The species H. atavismus was originally diagnosed based on the presence of a "squared



premaxillary crest" and of a ventral groove on the second wing phalanx. As noticed by Zhang *et al.* (2019), the crest is actually not squared (Fig. 9), and cranial crest morphology should be viewed with caution when discussing pterosaur diagnoses; while the ventral groove on the second wing phalanx is probably common within tapejarids (see Zhang *et al.*, 2019), although admittedly hard to ascertain in any other *Sinopterus* complex specimens due to heavy crushing. *H. atavismus* shares with *S. dongi* and *S. lingyuanensis* a fourth cervical vertebra longer than the fifth, distinct from *H. benxiensis* and other tapejarids. *H. atavismus* differs from the holotype of *S. dongi* in pedal morphology, showing the typical condition (metatarsal II the longest), and not the unique condition seen in *S. dongi* (metatarsal I the longest). *H. atavismus* differs from *H. corollatus* and *H. benxiensis* in exhibiting a gentler rostrum deflection and a more elongate fourth wing phalanx (Supplemental File 01, Sheet 1), and from D2525 in the latter aspect as well.

#### IVPP V 23388

**Morphological survey.** This specimen has been described and figured in detail by Zhang *et al.* (2019). The rostrum is elongate and slender, with a gentle ventral deflection of 14°. The rostrum deflection point lies anterior to the anterior margin of the nasoantorbital fenestra, as in S. *lingyuanensis* and *H. atavismus*. The premaxilla produces a small, subtriangular crest, as noted by Zhang et al. (2019), similar to that seen in the holotype of H. atavismus. Despite the incomplete, disarticulated nature of the skull remains, the nasoantorbital fenestra is notoriously elongate, and was confidently over three times as elongate as high (Zhang et al., 2019). The jugal is triradiate, and the angle formed between the lacrimal and postorbital processes is very wide (~90°, similar to S. dongi and S. lingvuanensis), indicating the orbit was probably subquadrangular in shape, and not ventrally tapered (piriform) as in *H. benxiensis*. The postoccipital extension of the premaxillae VIII > IX (contra Zhang et al., 2019). The coracoid exhibits a deep ventral flange proximally. Metacarpals II and III are reduced, while the preserved metacarpal I extends for about 85% the

#### **PeerJ**

- length of metacarpal IV. The proximalmost tip of metacarpal I is missing due to a crack in the slab.
- Sadly, pteroid and wing phalanges 4 are missing. Metatarsal I is shorter than metatarsal II, which
- is the longest.
- 799 **Ontogenetic assessment.** With a wingspan of ~1600 mm, this specimen is similar in size to the
- 800 holotype of H. benxiensis, and amongst the largest specimens in the Sinopterus complex. Partially
- fused elements include the carpals, pubis and ischium, ilium and pubosichiadic plate, notarium
- 802 and synsacrum, and tibiotarsus these elements are tightly bound, though with faint, visible
- 803 sutures. Unfused elements include the scapulocoracoid, humeral epiphysis extensor tendon
- process, and orbitotemporal bones. Despite not an adult, this specimen is clearly more mature than
- 805 the juvenile holotypes of S. gui, S. dongi, S. lingyuanensis and H. atavismus, and could be
- 806 considered a subadult.
- 807 **Remarks.** This specimen has been attributed to *Sinopterus atavismus* (= *Huaxiapterus atavismus*)
- by Zhang et al. (2019). No alternative attributions have been given by any other workers, except
- for Naish et al. (2021) who preliminarily considered that all Jiufotang tapejarids were most likely
- conspecific with S. dongi (to the potential exception of H. corollatus only).
- This fairly complete specimen was described recently by Zhang et al. (2019), who were unable to
- 812 distinguish it from *Huaxiapterus atavismus* and thus referred the new specimen to this species
- 813 (using the combination *Sinopterus atavismus*). Zhang et al. (2019) considered that 3 features
- allowed IVPP V 23388 to be identified as *H. atavismus*: the shape of the premaxillary crest, the
- shape of the anterodorsal margin of the premaxilla, and the proportions between metatarsals I and
- 816 II (Zhang et al., 2019). However, the first two features are influenced by the development of the
- premaxillary crest, which, as discussed above, is prone to sexual and ontogenetic variation, and
- should be viewed with caution before being utilized in diagnoses, as will be discussed further
- below in this work.
- Furthermore, proportions between metatarsals I and II in IVPP V 23388 (metatarsals I/II =  $\sim 0.90$ )



and the holotype of *H. atavismus* are rather close to those of other specimens such as *S. lingyuanensis* (Supplemental File 01, Sheets 1, 3), and thus this condition should be seen with caution. These three specimens also match well in the configuration of the nasoantorbital fenestra (over 3 times as long and high) and rostrum deflection angle (12°–14°), also matching *S. dongi* and *H. jii* in these regards, being all distinct from *H. corollatus* and *H. benxiensis* (with nasoantorbital fenestrae about 2.3 times as long as high, and rostrum deflections of 20°–21°). We regard that IVPP V 23388, along with the holotype of *H. atavismus*, are both indistinguishable from *S. lingyuanensis*. They are all also undistinguishable from *S. dongi* except for the metatarsi proportions.

#### D3072

Morphological survey. This specimen has been recently described and figured in detail by Shen et al. (2021). It consists of a partial postcranial skeleton, comprising most of the cervical and dorsal series, the forelimbs, and partial hindlimbs. The observable cervical formula is III < IV > V > VI > VII > VIII > IX. Single pneumatic foramina can be seen piercing the lateral sides of some cervical vertebrae (at least III, IV and V; unclear in others). Metacarpal I is elongate, with a preserved portion accounting for about 90% of metacarpal IV length; the proximal tip is missing and it may have been longer. The first wing phalanx exhibits two pneumatic foramina piercing the ventral side of the proximal region, similar to Keresdrakon vilsoni (see Kellner et al., 2019). The fourth phalanx is relatively large, accounting for 36% the length of the first wing phalanx, approaching more closely the value seen in the holotype of S. dongi and in IVPP V 23388 (30%). In the pedes, metatarsal I is the longest one.

**Ontogenetic assessment.** As originally indicated by Shen *et al.* (2021), this specimen is clearly a juvenile as indicated by the lack of fusion between many skeletal elements: the humeral epiphyses, scapulocoracoid, the extensor tendon process of the first wing phalanx, the carpal elements, tibia



and fibula, tibia and proximal tarsals, and neural arches and centra of most dorsal vertebrae. Only the neural arches and centra of cervical vertebrae and anterior dorsal vertebrae are fused. With a humerus of 55 mm in length, this specimen is similar in size to the holotype of *S. dongi* (humerus 58 mm in length), which is also interpreted as a juvenile.

**Remarks.** This specimen has been referred to *S. dongi* by Shen *et al.* (2021), as accepted by Zhou *et al.* (2022b) and not commented on the literature any further so far. Shen *et al.* (2021) noticed that D3072 shares with the holotype of *S. dongi* similar limb proportions as well as a reduced metatarsal I (shorter than metatarsals II and III), which has been considered a diagnostic apomorphy for *S. dongi* within the expansive taxonomic scheme of the *Sinopterus* complex (Zhang *et al.*, 2019).

## D4019 (new specimen)

Morphological survey. This specimen comprises an almost complete skeleton, although not very well-preserved. Many of the elements are articulated, except for most skull and manual elements (Fig. 10). The rostrum is slender and gently decurved (by 13°) and bears a well-developed, heaped crest. The dorsal margin of the premaxilla is slightly jagged. The jugal-quadratojugal-quadrate complex indicates the quadrate was strongly reclined (by 162°). Unfortunately, the jugal is incompletely preserved and lacks a lacrimal process. A well-developed and posterodorsally inclined frontoparietal crest is present. The cervical vertebrae not very well-preserved and not much can be observed beyond their lengths. The fourth cervical is the longest. The trunk region is very crushed and not much can be observed. Limb elements bear slightly abraded surfaces, precluding observation of much detail. Scapulocoracoid, humeral epiphyses, and carpal elements are unfused. As preserved, metacarpal I reaches 82% the length of metacarpal IV, but its proximal end is unclear and it may have been longer. Both pedes are badly preserved and not much can be discerned.



**Ontogenetic assessment.** The new specimen D4019 is small-sized, with a humerus length of 64 mm (only slightly larger than the holotype of *S. dongi*, with a 58 mm humerus). Based on the lack of ossification between scapulocoracoid elements, humeral epiphyses, and carpal elements, this individual is inferred as a juvenile.

875

876

877

878

879

880

881

882

883

884

885

886

887

888

889

890

891

892

893

894

895

871

872

873

874

#### **BPMC 103 (new specimen)**

Morphological summary. This specimen includes an almost complete skull (exposed in left lateral view), incomplete cervical series (exposed in dorsal view), incomplete forelimbs, and incomplete hindlimbs (Fig. 11). The rostrum is slender and deflected ventrally at an angle of 20°. A slight ventrolateral tilt of the plane of exposure of the rostrum reveals that the occlusal surface is sulcate, sporting thick tomial edges that emarginate an elongate sagittal excavation. Slit-like neurovascular foramina pierce the lateral surface of the rostrum close to the tomial edge (unclear in the occlusal surface). The premaxillary crest is large and protrusive. The anterior margin is roughly perpendicular to the main dorsal margin of the rostrum, anterodorsally oriented, similar to H. benxiensis and H. corollatus, and thus seems to have been originally trapezoidal in shape. The posterodorsal edge of the premaxillary crest is damaged, but it seems to have been anteroposteriorly longer than dorsoventrally high. The proportions of the nasoantorbital fenestra are not directly clear due to the disarticulation of the posterodorsal margin (nasal and lacrimal), but can be estimated at around 2.5 based on its length and mid-height. The dentary symphysis accounts for roughly 55% of total mandibular length, and sports a dorsal eminence as well as a low ventral crest. The anterior symphyseal region is pierced by slit-like foramina close to the occlusal line. Although the forelimbs are incompletely preserved, a partial humerus and both wing fingers are completely preserved. Metacarpal I preserves a clear proximal end and extends for only about 40% the length of metacarpal IV. The fourth wing phalanx accounts only for 20% of the first wing phalanx length. Metatarsal II is the longest one.



**Ontogenetic assessment.** This specimen lacks fusion of the posterior skull elements, humeral epiphyses, carpals, extensor tendon process of the first wing phalanx, and tarsal elements. Unfortunately, neither pectoral nor pelvic girdles are preserved. This specimen may be a juvenile or a an early subadult.

900

901

902

903

904

905

906

907

908

909

910

911

912

913

914

915

916

917

918

919

920

921

896

897

898

899

# **BPMC 104 (new specimen)**

Morphological summary. This specimen includes most of the skeleton, including a premaxillomaxilla, an almost complete mandible, incomplete cervical and dorsal series, and almost complete fore and hindlimb elements (Fig. 12). The rostrum is relatively robustly built and ventrally deflected at an angle of 20°. The rostrum deflection point is located roughly beneath the anterior margin of the nasoantorbital fenestra, where a bulge also seems to indicate the presence of a slight lateral palatal expansion. The premaxillary crest is unfortunately incompletely preserved, but it extends anterior to the anterior margin of the nasoantorbital fenestra and its broad base suggests it was relatively large. Despite the incompleteness of the skull, the length of the nasoantorbital fenestra can be assessed based on the location of the remains of the base of the lacrimal process of the jugal. The height of the nasoantorbital fenestra was measured at its midlength, to account for the typical position of its maximum height limit as seen in more complete specimens. In this way, the length/height ratio of the nasoantorbital fenestra of BPMC SC02 can be estimated at roughly 2.3 The lacrimal process of the jugal is not preserved. The jagged dorsal skull margin is reminiscent of the conditions seen in *Tupandactylus* (Campos & Kellner, 1997; Frey et al., 2003), suggesting it sported a soft tissue crest. The dentary exhibits a dorsal eminence as well as a low ventral crest. Cervical formula cannot be assessed. The sacral vertebrae (number unclear) are partially fused and bear intersacral fenestrae. The coracoid bears a large ventral flange. The extension of metacarpal I can be assessed due to the good preservation of its proximal tip, despite the loss of some of the diaphysis (Fig. 12G). It extends for 41% the length of metacarpal IV, similar to H, benxiensis. The first wing phalanx exhibits a single pneumatic foramen on its



ventral surface. The fourth wing phalanx is relatively reduced, corresponding to 20% of first wing phalanx length. In the pelvic girdle, the medial margin of the postacetabular process is excavated by a fossa, similar to *Tapejara wellnhoferi* and *Vectidraco daisymorrisae* (Eck *et al.*, 2011; Naish *et al.*, 2013). The neck of the postacetabular process is relatively thick and elongate, similar to *Vectidraco daisymorrisae* (Naish *et al.*, 2013) and unlike the rather constricted condition seen in *Tapejara wellnhoferi* (Eck *et al.*, 2011) or short condition seen in *Tupandactylus navigans* (Beccari *et al.*, 2021). The femoral head exhibits a thick neck, with no visible constriction from the posterior view. The greater trochanter is well-developed, and a large pneumatic foramen is present near its base. The distal end of the femur is expanded. In lateral view, the femur bows posteriorly. Two (?femoral) unfused epiphyses are present near the proximal end of the tibia. In the pedes, metatarsal II is the longest one.

**Ontogenetic assessment.** This specimen exhibits fusion of the scapulacoracoid, pelvic girdle (with closed, but still faintly visible, sutures), and distal tarsals. The extensor tendon process of the wing phalanx is still unfused, as are the posterior skull elements, ?femoral epiphyses, and proximal tarsals. The specimen is thus interpreted as a subadult.

#### **BPMC 105 (new specimen)**

Morphological summary. Despite relatively complete, this specimen is badly preserved – most bones are jumbled together, and most bone surfaces are badly weathered or cracked beyond the point of bearing relevant anatomical details (Fig. 13). Still, the outlines of some bones and structures still reveal some interesting data. The skull, exposed in left lateral view, exhibits a trapezoidal premaxillary crest that is conspicuously protrusive, higher than anteroposteriorly long. The shape of the rostrum and the configuration of its ventral deflection are unclear. The nasoantorbital fenestra is about 2.2 times as long as high. The orbit seems to have been piriform. The dentary symphysis bears a dorsal eminence and a low ventral crest. Measurements for visible



limb bones are given in Supplemental File 01 (Sheet 1), but not much further comparative information can be retrieved. Wing proportions closely match those of *H. corollatus* and *H. benxiensis*, with the fourth wing phalanx accounts for roughly 20% the length of the first wing phalanx. The second metatarsal is the longest. Not much further information can be assessed.

**Ontogenetic assessment.** Unfused elements include posterior skull bones and humeral epiphyses, carpals, the extensor tendon process of the first wing phalanx, and the tibiotarsus. It is, in this way, compatible with the holotype of *S. dongi* in both ontogenetic correlates and body size (Supplemental File 1, Sheet 5). This specimen may thus be regarded as a juvenile.

## **BPMC 106 (new specimen)**

**Morphological summary.** This small specimen preserves mainly a partial skull (missing the rostrum) and partial forelimbs other than partial cervical and dorsal series, although not much can be observed (Fig. 14). A triangular, dorsally oriented premaxillary crest is present, located anterior to the inferred anterior limit of the nasoantorbital fenestra, similarly to the holotype of *H. atavismus* and specimens IVPP V 23388 and 4019. The dorsal edge of the premaxillary crest, and of the posterior process of the premaxilla as well, is jagged (as in *Tupandactylus* spp.; see Frey *et al.*, 2003), indicating the potential presence of soft tissue extension. The proportions of the nasoantorbital fenestra are unclear due to the incompleteness of the rostrum and disarticulation between the premaxillomaxilla and the posterior skull region. The shape of the jugal indicates the base of the orbit was broad, implying the orbit was probably subquadrangular/subcircular in shape. The first metacarpal is quite elongate, reaching at least 95% the length of the wing metacarpal.

**Ontogenetic assessment.** Unfused elements include the posterior skull elements, humeral epiphyses and the carpals. In terms of size, this specimen is relatively small in the Jiufotang tapejarid sample, with a humerus length of 69 (similar to specimen D4019, and intermediate between the holotypes of *S. dongi* and *H. jii*; Supplemental File 01, Sheets 1, 5). The specimen is



972 interpreted as a juvenile.

973

974

975

976

977

978

979

980

981

982

983

984

985

986

987

988

989

990

991

992

993

994

995

996

### **BPMC 107 (new specimen)**

Morphological summary. This specimen comprises an almost complete skeleton, despite exhibiting badly preserved bone surfaces (Fig. 15). The rostrum is relatively slender and exhibits only a faint, incipient premaxillary crest, very similar to the holotype of S. dongi. The nasoantorbital fenestra is very elongate, with an estimated length/height ratio of about 3. The orbital region is not preserved. The posterodorsal region of the skull exhibits a short frontoparietal crest. The dentary symphysis is exposed in ventral view. It exhibits a dentary crest, which is dorsoventrally crushed and thus appears as a crushed keel. The dentary symphysis accounts for about half of mandibular length. The posterior region of the symphysis is damaged. The left mandibular ramus is complete, including the articular region and the retroarticular process, allowing for estimation of the location of the quadratomandibular articulation in the skull despite the absence of a preserved quadrate (and hence allowing for a rough estimation of the proportions of the nasoantorbital fenestra). The cervical series is incompletely preserved, and the longest cervical vertebra cannot be assessed. The preserved wings exhibit morphology and proportions comparable to the holotype of Sinopterus dongi, although metacarpals I-III cannot be assessed (Supplemental File 01, Sheet 3). The sternum exhibits a rounded posterior margin. Metatarsal I is slightly longer than metatarsal II.

Ontogenetic assessment. Specimen BPMC 107 is the largest Jiufotang tapejarid specimen within the sample analyzed here, with a humerus length of 111 mm and a totalized wingspan of ~2.18 m (only slightly larger than D2525). It bears several signs of an advanced ontogenetic stage, inclusion complete fusion of the scapulacoracoid, humeral epiphyses, syncarpals, extensor tendon process, tibiotarsus, and almost complete fusion of the pelvic elements. Only the posterior skull elements were probably not completely fused, given their absence (presumably derived from disarticulation,



implying lack of complete fusion). This specimen thus may be an advanced subadult close to skeletal maturity.

### SMA – correlations and allometry

Of our 21 tested variables, six turned out to be unrelated to absolute humeral length (proxy for body size), and are thus interpreted as independent of body size and not explainable by ontogenetic variation (rostrum deflection, nasoantorbital fenestra length/height ratio, orbit ventral angle, quadrate inclination, metacarpal I length, and wing phalanx 4 length). Of the 15 variables that were recovered as correlated to absolute humerus length, two are positively allometric (femur and tibia length, though both are near-isometric) and two are negatively allometric (rostral value and rostrum index). These are thus interpreted as size-dependent, and thus easily explainable by ontogenetic variation. The remaining 11 traits were recovered as isometrically related to humerus length (Table 2).

#### Linear morphometric multivariate analyses

As mentioned above (see Materials and Methods), our multivariate analyses only include skeletal proportions based on features which are interpreted as devoid of ontogenetic bias, *i.e.* features that are either uncorrelated to body size variation, or features that develop isometrically, as per the results of our SMA analyses. These features were rostrum deflection angle, nasoantorbital length/height ratio, ventral orbital angle, quadrate reclination angle, cervicals IV/V ratio, and the ratios between humerus and the following limb elements: ulna, pteroid, metacarpal I, metacarpal IV, wing phalanges 1–4, femur, metatarsal I, and metatarsal II (see Supplemental File 01, Sheet 2, for the dataset). Skeletal proportions based on elements influenced by allometric development (rostrum index, rostral value, and tibia/humerus ratio) were not included. All analyzed taxa were



included (i.e. sinopterines, *Tapejara*, *Caiuajara*, and *Tupandactylus*).

Under the results of our UPGMA analysis, members of the *Sinopterus* complex are segregated, distributed within two separate groups (Fig. 16). The first group, hereby termed Morphotype I, includes eight specimens: the holotypes of *Sinopterus dongi*, *Huaxiapterus jii*, *Sinopterus lingyuanensis*, and *Huaxiapterus atavismus*, as well as specimens IVPP V 23388, D4019, D7302, and BPMC 107. Morphotype I is the sister-cluster of *Eopteranodon lii*. The second morphotype, hereby termed Morphotype II, comprehends the remaining six analyzed specimens of the *Sinopterus* complex: the holotypes of *H. corollatus* and *H. benxiensis*, along with specimens D2525, BPMC 103, BPMC 104, and BPMC 105. Morphotype II is the sister-cluster to *Tupandactylus navigans*. Another cluster includes *Tapejara wellnhoferi* and *Caiuajara dobruskii*, as the sister-cluster to the whole remaining sample.

Subsequent to our clustering analysis, PCA analyses were also carried out (Fig. 17). When groups corresponding to the UPGMA's Morphotypes I and II are plotted onto the results of both of our PCA analyses, the resulting graphs reveal that there is no intersection between their convex hulls or 95% confidence ellipses. In the first PCA (using mean value imputation for missing data), there is an overlap between *Eopteranodon lii* and the 95% confidence ellipse of Morphotype I. *Tapejara wellnhoferi*, *Caiuajara dobruskii* and *Tupandactylus navigans* all fall outside of either morphotype's morphospace. In the second PCA (using iterative imputation for missing data), a similar pattern is observed, except that *Tupandactylus navigans* falls within the 95% confidence ellipse of Morphotype II.

## **Discussion**

### Anatomical variations and their interpretations (excluding cranial crests)

Based on the specimen-level remarks presented above, we discuss below the anatomical variations surveyed here for the *Sinopterus* complex. Our aim is to (1) identify and contextualize variation at



specimen and morphotype levels, and (2) interpret these variations as potentially: sexual, ontogenetic, individual, or interspecific in nature. Of particular interest in this discussion are the features that, according to the results of our SMA analyses, are not correlated to body size and thus interpreted as not ontogenetic in nature. For now, cranial crest variation will be set aside, and addressed only further below, in order to circumvent the fact that these cannot be regarded *a priori* as a reliable source of either intra or interspecific variation.

It is worth highlighting that the amount of anatomical variation we were able to compilate here is, in a certain way, rather low if one considers that our sample includes several skeletons with high degrees of completeness. However, it must be observed that, unfortunately, such completeness is deceptive. The amount of information retrievable from these specimens is highly limited due to preservational issues. All the specimens are crushed and preserved in two-dimensions, so that in each specimen every bone is only visible from a single view. Some bones are further obliterated by other bones overlying them. Plus, some of these specimens also exhibit highly worn bone surface, precluding observation of many details (*e.g.* metatarsal lengths in D4019).

Rostrum, proportions (RI and RV). Some variation in rostrum proportions in the *Sinopterus* complex had already been noted by Zhang *et al.* (2019). RI values vary from 2.85 (*Sinopterus lingyuanensis*) to 1.33 (BPMC 104), and RV values range from 6.53 (*Huaxiapterus atavismus*) to 3.5 (BPMC 104). It is clear that smaller, younger specimens tend to exhibit slenderer rostra, while larger, more mature specimens exhibit stouter rostra. In the present work, our SMA analysis indicates that both RI and RV are positively allometric relative to body size. Since the measurement of RI is directly influenced by the presence and development of premaxillary crests, this result indicates that premaxillary crests grow with ontogeny in the *Sinopterus* complex. This result was to be expected, as cranial crest development is already well-known as an ontogenetic feature in pterosaurs, as demonstrated by taxa such as *Caiuajara dobruskii* (Manzig *et al.*, 2014), *Anhanguera* spp. (Pinheiro & Rodrigues, 2017), and *Pteranodon* spp. (Bennett, 1993).

It is clear, as already noted by Witton (2013) and Naish et al. (2021), that cranial crest development



(and by extension, RI) should not be utilized as a tool for diagnosing potential *Sinopterus* complex 1072 species. Furthermore, we add here that the same is true for rostrum measurements that disregard 1073 crest development (i.e. RV), which show that the rostrum itself (exclusive of cranial crests) also 1074 1075 develop to be stouter with ontogeny in the *Sinopterus* complex. **Rostrum, deflection angle.** The ventral deflection of the rostrum is one of the most conspicuous 1076 cranial features of tapejarids, as seen in Caupedactylus, Tapejara, Tupandactylus, Caiuajara, 1077 1078 Afrotapejara, Wightia, Eopteranodon, and in the Sinopterus complex. In the Sinopterus complex, Morphotype I exhibits a deflection angle range of 12°-15°, whereas the range is 20°-21° in 1079 1080 Morphotype II (Supplemental File 01, Sheet 4). Our SMA analysis indicates that this variation is not correlated to body size, and is thus interpreted as not ontogenetic in nature. 1081 Martill et al. (2020a) had already reported on the intra- and interspecific variation of this feature 1082 within tapejarids. According to our own observations, deflection angles (as measured between the 1083 long axis of the deflected rostrum and the long axis of the maxilojugal bar) vary between 21°-25° 1084 in Tupandactylus imperator, 23°-25° in Tup. navigans, 25°-28° in Tapejara wellnhoferi, and 32°-1085 1086 37° in Caiuajara dobruskii (Supplemental File 01, Sheet 4). We were unable to reproduce the measurements given by Martill et al. (2020a) for Caiuajara dobruskii, which produced a 1087 remarkably larger variation spectrum. This is probably explained by the variation in the shape of 1088 1089 the palatal expansion bulge in Caiuajara dobruskii, which hampers the accurate measurement of 1090 the deflection angle if the maxillojugal bar posterior to it is not preserved (L. Piazentin, pers. 1091 comm.), and thus measurements of deflection angles in Caiuajara should be restricted to specimens with relatively complete maxillojugal bars. Anyway, intraspecific variation in rostrum 1092 deflection in tapejarids does not seem to surpass a  $\sim 5^{\circ}$  range. 1093 Given the patterns of variation in other tapejarid species (Supplemental File 01, Sheet 4), as well 1094 as the pattern that, within the Jiufotang sample, angles of 20°-21° are exclusive to Morphotype II 1095 1096 while the other morphotypes are restricted to angles of 12°–15°, and that this variation is not related 1097 to body size, we regard this as a potential taxonomic signal for the *Sinopterus* complex.



Nasoantorbital fenestra, length/height ratio. Within the Jehol tapejarid sample, Morphotype I stands out due to its relatively elongate nasoantorbital fenestra, which is typically ~3 times as long as high (Supplemental File 01, Sheet 1), as seen in the holotypes of *S. dongi*, *S. jii*, *S. gui* and *S. lingyuanensis*, and as can be roughly inferred from the holotype of *S. atavismus* as well as specimen IVPP 23388V. This contrasts with Morphotype II, in which the range for the nasoantorbital fenestra length/height ratio is 2.1–2.5. This seems to be roughly the typical condition for tapejarids, as seen in *Eopteranodon lii* (~2.1), *Caupedactylus ybaka* (~2.1), and *Tupandactylus navigans* (2.1–2.2). *Caiuajara* and *Tapejara* stand out in exhibiting a relatively low ratio (~1.3; see Supplemental File 01, Sheet 1). In this way, the particularly elongate nasoantorbital fenestra in Morphotype I is highly distinctive. Our SMA analysis indicates that nasoantorbital fenestra length/height ratio is not correlated to body size, and is thus interpreted as not ontogenetic in nature. It is worth highlighting that the elongate nasoantorbital fenestra of Morphotype I can be found in all skulls attributed to this morphotype, irrespective of ontogenetic stages – from the small juvenile holotype of *S. gui* to the large, subadult holotype of *S. jii*. This feature could thus suggest a taxonomic distinction between Morphotype I and other tapejarids.

Nasal process, shape. In the holotypes of *S. dongi* and *S. lingyuanensis* (Morphotype I), the descending nasal processes are long, subvertically oriented, and extremely thin. This condition is also present in *Tupandactylus navigans* (Frey *et al.*, 2003). In *Thalassodromeus sethi*, the nasal process is also subvertical, although it is extremely reduced instead of elongated (Pêgas *et al.*, 2018). In the holotype of *H. benxiensis* (Morphotype II), however, the nasal process is anteriorly oriented, as already pointed out before in the data matrix of Andres *et al.* (2014), although this feature was not explicitly reported in the original description of the specimen (Lü *et al.*, 2007). Despite the substandard preservation of the nasal bones in the holotype of *H. benxiensis* (BXGM V0011), it can be seen upon close inspection that the right nasal, seen in medial view and partially overlayed by the incomplete left nasal, displays a preserved nasal process that is anteriorly inclined. Thus, we corroborate the coding provided by Andres *et al.* (2014) and regard this very unusual condition as unique and possibly of taxonomic value for Morphotype II.



1126

1127

1128

1129

1130

1131

1132

1133

1134

1135

1136

1137

1138

1139

1140

1141

1142

1143

1144

1145

1146

1147

1148

1149

1150

1151

**Orbit shape.** Within the *Sinopterus* complex, variation exists concerning orbit shape, with the orbit being piriform in some specimens and subquadrangular/subcircular in others. This variation can be translated into the measurement of the angle between the lacrimal and postorbital processes of the jugal (ventral orbit angle), whereby subquadrangular orbits exhibit an angle close to 90° while piriform orbits exhibit a lower, acute angle. This difference in orbit shape distinguishes Morphotypes I and II. Morphotype I exhibits orbit angles of  $\sim 90^{\circ}$ , as seen in the holotypes of S. dongi and S. lingvuanensis, as well as in IVPP 23388 V and BPMC SC04. Morphotype II exhibits lower values, with angles of 68° in the holotype of H. benxiensis and 65° in BPMC SC003. Within tapejarids, the peculiar subquadrangular orbit shape seen in Morphotype I is unique to this morphotype and to *Eopteranodon lii* (see below), with the piriform condition being the typical one, as seen in Morphotype II, Tapejara wellnhoferi, Tupandactylus navigans, Tupandactylus imperator, Caiuajara dobruskii, and Caupedactylus ybaka, as well as in thalassodromids (e.g. Pêgas et al., 2018) and chaoyangopterids (e.g. Wu et al., 2017). Our SMA analysis indicates that this feature is not correlated to body size. In effect, in Morphotype I, a perpendicular orbit angle can be found in both juveniles (holotypes of S. dongi and S. lingyuanensis, and specimen BPMC 106) and advanced subadults (IVPP 23388 V and holotype of H. jii). In this way, we regard that the distinctive orbit shape of Morphotype I most likely indicates distinctiveness between Morphotypes I and II. Quadrate reclination. Within tapejarids, quadrate reclination usually surrounds 140°-150°, as seen in Tapejara wellnhoferi (145°), Caiuajara dobruskii (147°), Tupandactylus navigans (145°), and Caupedactylus ybaka (150°). The holotype of Huaxiapterus benxiensis falls within this pattern, with a quadrate reclination of 147°. However, Morphotype I specimens exhibit a stronger quadrate reclination of 160°-162°, as seen in the holotypes of S. dongi and S. lingyuanensis, and specimens D4019 and BPMC 104 (Supplemental File 01, Sheet 1). According to our SMA analysis, this variation is uncorrelated to body size. Quadrate reclination has been regarded as of taxonomic importance for *Pteranodon* (Bennett, 1994), tapejarids (Kellner, 2013), *Nurhachius* (Zhou et al., 2019), and wukongopterids (Zhou et al., 2021). Based on pterosaur species known



from multiple specimens, intraspecific variation in quadrate reclination seems to surround 3°-6°. 1152 as seen in Pterodactylus antiquus, Aerodactylus scolopaciceps, Hamipterus tianshanensis, 1153 Pteranodon longiceps, and Pteranodon sternbergii (see Zhou et al., 2019). We regard this 1154 1155 variation in the *Sinopterus* complex as of potential taxonomic value. Cervical formula. Concerning the relative lengths of cervical vertebrae, the typical pterodactyloid 1156 condition is that the fifth is the longest one. This can be observed in chaoyangopterids (Leal et al., 1157 1158 2017; Wu et al., 2017), azhdarchids (Naish & Witton, 2017), and Tupuxuara (Shen et al., 2021). However, some variation exists within tapejarids. In *Tapejara wellnhoferi*, cervicals four and five 1159 are roughly the same size (Vila Nova et al., 2015). In contrast, in Tupandactylus navigans the four 1160 cervical is longer than the fifth (Beccari et al., 2021). The same is true for Eopteranodon lii (Lü et 1161 1162 al., 2006c) and for Morphotype I of the Sinopterus complex, as seen in the holotypes of S. dongi, S. lingyuanensis, specimen IVPP V 23388, and D3072. In contrast, the fourth cervical is shorter 1163 than the fifth in Morphotype II, as seen in the holotype of H. benxiensis (Lü et al., 2007). Our 1164 SMA analysis indicates that variation in cervical IV length is uncorrelated to body size in the 1165 Sinopterus complex. We thus regard this feature as of potential taxonomic value, distinguishing 1166 Morphotypes I and II. 1167 Metacarpal I, length relative to metacarpal IV. An elongate metacarpal I that reaches the carpus 1168 is the plesiomorphic condition for azhdarchoids, as seen in Tapejara wellnhoferi, Eopteranodon 1169 1170 lii, Tupuxuara leonardii, chaoyangopterids and azhdarchids (e.g. Kellner & Campos, 2007; Wu et al., 2017). An interesting amount of variation regarding this feature has already been reported 1171 before for the Jiufotang tapejarids, with some specimens reportedly bearing either elongate 1172 metacarpals I that were subequal to (~90%–100% the length of) metacarpal IV (e.g. Wang & Zhou, 1173 2003) or reduced metacarpals I (e.g. Lü et al., 2005). 1174 Recently, Shen et al. (2021) expressed concern and recommended caution regarding this variation 1175 1176 in the Sinopterus complex, since broken/obscured metacarpals could be mistaken for reduced 1177 metacarpals in some specimens. In the present work, our close inspection corroborates the presence



of reduced metacarpals I (about 30%–40% of the length of metacarpal IV) in specimen D2525 and 1178 in the holotypes of "H." benxiensis and "H." corollatus, along with the new specimens BPMC 1179 103 and BPMC 104. Similarly, elongate metacarpals I (about 90%–100% the length of metacarpal 1180 1181 IV) are confirmed for the holotypes of S. dongi and H. jii, as well as specimens IVPP V 23388 and 1182 D3072, and the new specimen BPMC 106. The condition is unclear in the holotypes of S. lingyuanensis and "H." atavismus. 1183 1184 Our SMA analysis indicates that this feature is uncorrelated to body size. This large amount of variation is unreported for pterosaur species and is highly suggestive that more than one species is 1185 present in this sample. Thus, we conclude that Morphotype II can be characterized by a short 1186 metacarpal I (about 30%-40% of metacarpal I length), which does not reach the carpus. Such 1187 1188 condition is unique for Morphotype II and *Tupandactylus* within all known tapejarids. Wing digit, fourth phalanx length. Similar to what has been found for *Rhamphorhynchus* (Hone 1189 1190 et al., 2020) and anurognathids (Yang et al., 2022), our SMA analyses indicate that most wing elements exhibit isometric growth within the Sinopterus complex. The sole exception to this 1191 1192 pattern concerns fourth wing phalanx length, as our SMA analysis shows that its variation is not correlated to body size. 1193 1194 In fact, a noticeable variation occurs in this feature between Morphotypes I and II, irrespective of 1195 ontogenetic stage. The length ratio between wing phalanges 4 and 1 is about 0.30-0.40 in Morphotype I, as seen in the holotypes of S. dongi, S. jii, and "H." atavismus, and specimen 1196 D3702. This is similar to Tapejara wellnhoferi and Caiuajara dobruskii, while in Eopteranodon 1197 1198 lii the ratio is 0.45. In contrast, this ratio is no higher than 0.20 in Morphotype II, as seen in the holotypes of "H." corollatus and "H." benxiensis, as well as specimens D2525, BPMC SC001, 1199 BPMC SC002, and BPMC SC003. This is similar to *Tupandactylus navigans*, for which the same 1200 ratio is about 0.13 (Beccari et al., 2021). We thus regard that the short wing phalanx 4 (under 20% 1201 1202 the length of wing phalanx 1, or under 50% the length of the humerus) of Morphotype II suggests 1203 taxonomic distinction from Morphotype I (and all other tapejarids, representing a potential



1204 diagnostic apomorphy).

Metatarsal I, relative length. The relative proportions of the metatarsals have already been deemed of taxonomic importance before (Zhang *et al.*, 2019). The general tapejaroid condition is that metatarsal I is shorter than metatarsals II-III, and subequal to metatarsal IV; as found in *Tapejara* (Eck *et al.*, 2011), *Eopteranodon* (Lü *et al.*, 2006c), chaoyangopterids (Wu *et al.*, 2017), and dsungaripterids (Hone *et al.*, 2017). This general condition can be seen in Morphotype II specimen D2525, although unclear in the holotypes of "H." *corollatus* and "H." *benxiensis*. On the other hand, the holotype of *Sinopterus dongi* and specimens D3702 and BPMC 106 are unique within tapejaroids in exhibiting an elongate metatarsal I (longer than metatarsal II). However, metatarsal I is subequal to metatarsal II (90%–95% of its length) in other Morphotype I specimens, as seen in IVPP V 23388 (Zhang *et al.*, 2019), and the holotypes of *S. lingyuanensis* (Fig. 8) and *H. atavismus* (Fig. 9), what is not significantly different from Morphotype II. Our SMA analysis indicates that metatarsals I and II grow isometrically relative to humeral length.

It is noticeable that an unusually long metatarsal I is exclusive to a subset of the Morphotype I within the whole known tapejaroid sample, but, considering the data as a whole, it is difficult to set this subset of Morphotype I from the remainder of the morphotype, and thus this feature may only represent a polymorphism. We also note that this feature can be found elsewhere within pterosaurs, such as in *Anurognathus ammoni* (Bennett, 2007) and *Anhanguera piscator* (RVP, pers. obs.).

#### **Species-level taxonomic interpretations**

The primary taxonomic assessment presented in this subsection is based on the interpretation of the variations explored above (that is, excluding cranial crest variation). Each morphotype exhibits notorious, unique features, even when cranial crests are set aside. These particular features are summarized in Table 3 and Figure 18.



Morphotypes I and II are quite distinguishable from each other. Within the Jiufotang tapejarid 1229 sample, Morphotype I is characterized by a subquadrangular orbit, a gentle rostrum deflection of 1230 12°-15°, an elongate nasoantorbital fenestra (over 3 times as long as high), a subvertical nasal 1231 1232 process, a quadrate reclination of ~160°, a fourth cervical longer than the fifth, and an elongate wing phalanx 4 (about 30%–40% the length of the first wing phalanx). Morphotype II differs from 1233 Morphotype I in exhibiting a piriform orbit, a stronger rostrum deflection of 20°-22°, a stouter 1234 nasoantorbital fenestra (about 2.2–2.5 times as long as high), a nasal descending process anteriorly 1235 oriented, a quadrate reclination of ~150°, a fourth cervical shorter than the fifth, a reduced 1236 metacarpal I far from contacting the carpus (30%–40% the length of metacarpal IV), and a short 1237 wing phalanx 4 (about 20% the length of the first wing phalanx). 1238 1239 We regard that these different combinations of features cannot be attributed to ontogenetic variation, as indicated by our SMA analyses – all of the characteristics mentioned above are 1240 uncorrelated to body size (see above). These features also fail to match what (little) is known about 1241 sexual dimorphism in pterosaurs (see Bennett, 1993; 1995; Wang et al., 2014). This great amount 1242 of variation also surpasses the level of individual variation that is seen in the few known 1243 monospecific pterosaur bonebeds (see Manzig et al., 2014; Wang et al., 2014; Andres & Langston, 1244 2021). Furthermore, it is notorious that these variations are consistently co-occurrent, effectively 1245 1246 allowing us to segregate two morphotypes without overlap (each with their own unique features), what is suggestive of heterobatmy. We thus regard that these features are best interpreted as 1247 interspecific in nature. Based on the weight of these combined features, we regard that each 1248 morphotype is, indeed, distinct from each other at the species-level, meaning the Jiufotang 1249 tapejarid sample would comprise at least two species. 1250 1251 As we are unable to satisfactorily distinguish proposed species within each morphotype, we interpret that a single species is present in each morphotype. In this way, Morphotype I would 1252 represent Sinopterus dongi, with S. gui, H. jii, S. lingyuanensis, and H. atavismus as junior 1253 synonyms. From heretofore, 'Huaxiapterus' will thus be referred to between single quotation 1254



1255	marks to indicate its status as invalid (as a subjective junior synonym of <i>Sinopterus</i> ). Morphotype
1256	II would represent 'H.' corollatus, with 'H.' benxiensis as a junior synonym. A reinterpretation of
1257	the taxonomic attribution of Jiufotang tapejarid specimens, based on the aforementioned remarks,
1258	is presented in Table 4.
1250	We agree with Witton (2013) and Naish et al. (2021) that, at the time of their writings, evidence
1259	
1260	for multiple Jiufotang tapejarid species was insufficient due to the lack of detailed data on their
1261	anatomical variation. Still, the present work provides new anatomical and comparative data which
1262	we interpret as compelling evidence for the existence of two tapejarid species in the Jiufotang
1263	Formation.
1064	
1264	Overlap in the stratigraphic distributions of <i>S. dongi</i> and <i>'H.' corollatus</i> suggests that these two
1265	proposed species have coexisted in time. We emphasize that the occurrence of a few sympatric,
1266	closely related pterosaur species should not be viewed, by default, as unlikely. As observed by
1267	Longrich et al. (2018), sympatry of closely related species is not uncommon for seabirds (e.g.
1268	species of <i>Fregata</i> , <i>Larus</i> ), and we add here that the same is true for continental birds ( <i>e.g.</i> species
1269	of Cathartes, Accipiter, Ramphastos, Ara, Amazona; e.g. Sigrist, 2004). Despite stratigraphic
1270	overlap, Sinopterus dongi and 'H.' corollatus are not yet known from the exact same localities.
1271	Thus, the possibility remains that these two species took part in some sort of niche partitioning, as
1272	has been proposed for the two species of Quetzalcoatlus that co-occur in the layers of the Javelina
1273	Formation: while the giant Q. northropi has been recovered from stream channel facies, the
1274	remains of the smaller Q. lawsoni stem from abandoned channel-lake facies (Andres & Langston,
1275	2021; Brown et al., 2021; Lehman, 2021). Further work on the lithology and depositional
1276	environments of Jiufotang localities may shed light on this possibility for Jiufotang tapejarids as

1279

# Cranial crest variation: mapping and interpretation



**Premaxillary crest, development and size.** Within the entire sample of Jiufotang tapejarids here 1280 analyzed, only two specimens lack premaxillary crests: the holotypes of Sinopterus gui and S. 1281 lingyuanensis. These are the two smallest specimens analyzed here, and are both interpreted as 1282 1283 juveniles. The holotype of *Nemicolopterus crypticus*, which is a near-hatchling, may represent a third specimen of crestless Jiufotang tapejarid (see Witton, 2013; Naish et al., 2021). Thus, it can 1284 be said that premaxillary-crestless Jiufotang tapejarids are restricted to very young individuals. 1285 1286 All remaining Jiufotang tapejarid specimens exhibit premaxillary crests, but of differing sizes. Within our Morphotype I (= Sinopterus dongi), the holotype of Sinopterus dongi exhibits but a 1287 very discrete crest; that is, it only discretely disrupts the skull margin (by protruding 1288 anterodorsally). This specimen is interpreted as a juvenile (see above). Specimen BPMC 107 1289 1290 exhibits a similarly incipient premaxillary crest, despite being regarded as close to skeletal maturity. In contrast, the holotype of 'H.' atavismus, which is regarded as a juvenile and is smaller 1291 in size than the holotype of S. dongi, bears a more conspicuous premaxillary crest than the latter 1292 specimen. 1293 1294 Because premaxillary-crestlessness is restricted to the smallest juvenile specimens, it seems clear that premaxillary crest absence/presence is an ontogenetic feature. Ontogenetic variation in the 1295 presence and development of premaxillary crests is corroborated by our SMA analysis, which 1296 indicates positive allometry between rostrum index and body size. The positively allometric 1297 1298 growth of rostrum index can easily be explained by the ontogenetic development of the 1299 premaxillary crest, which is a feature that augments the value of the rostrum index. 1300 Still, because premaxillary crest size still varies between larger juveniles and subadults of each 1301 species, it also seems likely that variation in premaxillary crest size is influenced also by individual and/or sexual variation, and not only to growth. These variations concerning premaxillary crest 1302 presence and size are clearly affected by intraspecific (ontogenetic, individual, and sexual) 1303 1304 variations and seem to apply to the Sinopterus complex as a whole. Thus, these variations 1305 (concerning crest presence and size) should not be regarded as taxonomic informative for the





1306	Sinopterus complex. On the other hand, stating that crest presence/size cannot differentiate
1307	between species within our analyzed sample does not imply that a single species exists. Rather, it
1308	suggests that sexual and ontogenetic variation (expressed in premaxillary crest size/development)
1309	is present in all potentially valid species, whether a single one or more (two as we propose here).
1310	Premaxillary crest, shape. Apart from premaxillary crest presence and size, variation in crest
1311	shape can also be seen in Jiufotang tapejarids. Crested specimens exhibit crests of roughly two
1312	shapes: heaped and trapezoidal.
1313	Morphotype I is characterized by heaped crests, as seen in the holotypes of S. dongi, 'H.' jii, 'H.'
1314	atavismus, and specimens IVPP 23388 V, D4019, BPMC 106, and BPMC 107. In contrast,
1315	Morphotype II is characterized by trapezoidal crests, as seen in the holotypes of 'H.' corollatus
1316	and 'H.' benxiensis, as well as specimens BPMC 103 and BPMC 105.
1317	It is important to highlight that we do not mean to imply that these proposed shape categories are
1318	homogenous. Some degree of variation is evidently present within each of them and no two crests
1319	are the same, as should be expected given the intraspecific variation in cranial ornamentation that
1320	is seen in extant vertebrates, such as in the casques of Numida (Angst et al., 2020) and Casuarius
1321	(Naish & Perron, 2016; Green et al., 2022).
1322	It is notorious that these two shape categories match the two recognized morphotypes/species,
1323	apparently without overlap or relation to ontogeny. Consequently, the favored explanation under
1324	this scenario is that each shape is characteristic of each morphotype/species.
1325	
1326	Comments on the usage of cranial crests in pterosaur taxonomy
1327	The two Jiufotang tapejarid species interpreted as valid here can be set apart from each other even
1328	when cranial crest variation is unconsidered. As explored above, it is clear, beyond any reasonable

doubt, that crest development and size are attributable to sexual and ontogenetic variations in these

1329



species. However, when only crested morphs are considered, then each of these three recognized 1330 species do coincide with two distinct crest shapes: heaped in Sinopterus dongi, and trapezoidal in 1331 'H.' corollatus. 1332 We thus interpret that, within Jiufotang tapeiarids, (1) variation in crest presence is linked to 1333 ontogeny, (2) variation in crest size is linked to individual/sexual variation, and (3) crest shape is 1334 linked to interspecific variation. As an example of a similar case, we can mention the *Pteranodon* 1335 1336 complex. By following the most restrictive taxonomic interpretation of this species complex (Bennett, 1994, Martin-Silverstone et al., 2017), it can be said that crest shape (as seen in proposed 1337 mature males) is diagnostic for the two valid *Pteranodon* species: elongate and posteriorly oriented 1338 in Pteranodon longiceps, and "bulbous" and upright in Pteranodon sternbergi (Bennett, 1994). In 1339 1340 contrast to that, juveniles and females of these two *Pteranodon* species cannot be set apart by cranial crest morphology, since these morphs would bear underdeveloped crest morphologies 1341 (Bennett, 1994; Martin-Silverstone et al., 2017). 1342 We thus propose here that a similar reasoning applies to the *Sinopterus* complex: while crest shape 1343 may be useful to distinguish between the crested morphs of these species (or at least relatively 1344 mature ones), incipiently-crested morphs of these species can simply not be set apart by crest 1345 morphology. It is important to highlight that this proposition is made here a posteriori, only after 1346 diagnosing the herein recognized species on other grounds, and after identifying potential 1347 1348 ontogenetic and sexual trends in crest development and size – crest variation was not interpreted a priori as a case of interspecific variation here, nor as a primary tool for delimiting species 1349 1350 circumscriptions in the first place. We regard that we should expect for pterosaurs the same amount of complexity we seen in extant birds: species with and without sexual dimorphism in ornaments; 1351 closely related species with distinct (and diagnostic) ornaments; and closely related species with 1352 similar ornaments. We regard here that each case will need its own assessment, and that no general 1353 pattern should be expected for pterosaurs as a whole – a very diverse group that radiated for over 1354 165 million years. 1355



### Short comments on Nemicolopterus crypticus

As observed by Witton (2013) and Naish et al. (2021), the holotype specimen of Nemicolopterus crypticus clearly represents a young juvenile, as indicated by its "small size, proportionally enormous orbit, rounded and unfused pelvic bones, poorly defined limb articulations with unfused epiphyses, unfused skull bones, unfused scapulocoracoid, and lack of fusion between the tibia and tarsus" (Naish et al., 2021). Furthermore, it resembles tapejarids due to a combination of several features, most importantly edentulousness, a downturned rostrum, a slender and subvertical lacrimal process of the jugal, a jaw joint ventral to the anterior half of the orbit, and relatively elongate hindlimbs (Naish et al., 2021). We further note that one of the proposed diagnostic features of Nemicolopterus crypticus, a penultimate phalanx of pedal digit 4 longer than the first (Wang et al., 2005), is a feature it shares with Jiufotang tapejarids (e.g. Shen et al., 2020).

Here, we highlight that *Nemicolopterus crypticus* exhibits a morphology that is far distinct from any other Jiufotang tapejarid specimen, what can be attributed to its very young stage – this is expressed by the entire lack of cranial crests, a relatively large orbit, a relatively diminutive nasoantorbital fenestra, a not much reclined quadrate, and a "knife-shaped" humeral deltopectoral crest (Wang *et al.*, 2005). Absence of cranial crests and large orbits are well-known indicators of young ontogenetic stages (e.g. Bennett, 1993). It is interesting to note that the distinctive shape of the humeral deltopectoral crest of the holotype of *N. crypticus* could easily be explained by an incipient ossification of the structure – in fact, neonate specimens of *Hamipterus tianshanensis* seem to be characterized by incipiently ossified humeral deltopectoral crests (Wang *et al.*, 2017).

Concerning the holotype of *N. crypticus*, we regard that its very early juvenile status (near-hatchling; Naish *et al.*, 2021) is insufficient for a satisfactory diagnosis and prevents a confident identification as conspecific with either *S. dongi* or *'H.' corollatus* (or yet a distinct species). Thus, we consider that the holotype of *Nemicolopterus crypticus* should be regarded as an indeterminate



1381 Sinopterinae (Table 4).

1382

1383

# Short comments on Eopteranodon lii

1384	As discussed above, Eopteranodon lii is a tapejarid species that comes from the Yixian Formation,
1385	which is slightly older than and underlies the Jiufotang Formation (from which the Sinopterus
1386	complex comes from). Eopteranodon lii has been regarded as a close relative of the genus
1387	Sinopterus in several phylogenetic analyses (Vullo et al., 2012; Andres et al., 2014; Pêgas et al.,
1388	2021), a result that is corroborated here (see below). However, the tapejarid nature of
1389	Eopteranodon lii has not been consensual. This taxon has been, at times, interpreted as a
1390	chaoyangopterid (e.g. Lü et al., 2008). Furthermore, Martill et al. (2022b) noted that a tapejarid-
1391	like downturned rostrum could not be verified in the holotype of Eopteranodon lii due to the lack
1392	of detailed illustrations, and that a re-study of the holotype would be desirable. Close analysis of
1393	the type specimen reveals clear tapejarid features (Figs. 19-20), including a downturned rostrum
1394	with a premaxillary crest (note that the original identifications of skull and mandibular remains
1395	were mistakenly switched).
1396	Eopteranodon lii exhibits striking similarities to Sinopterus dongi, especially in orbit shape
1397	(subquadrangular), quadrate reclination (about 160°), and in cervical IV being the longest one.
1398	Still, Eopteranodon lii differs from Sinopterus dongi in exhibiting a stouter nasoantorbital fenestra
1399	(about 2.5 times as long as high), a fairly elongate pteroid (pteroid/ulna length ratio about 0.56),
1400	an elongate wing phalanx 4 (wing phalanx 4/phalanx 1 length ratio about 0.45), and a metatarsal I
1401	shorter than metatarsal II. Thus, we corroborate the distinction between Eopteranodon lii and
1402	Sinopterus dongi, as well as 'H.' corollatus.
1403	We further note that, due to the close proximity between Eopteranodon lii and Sinopterus dongi,
1404	and to the fact that the former is chronologically older than the latter, it is possible that
1405	Eopteranodon lii and Sinopterus dongi could be linked in an anagenetic continuum and thus



represent chronospecies. This is similar to what has been proposed for other closely related pterosaur species that are stratigraphically successive: *Pteranodon sternbergi* and *P. longiceps* (Bennett, 1994), and *Nurhachius luei* and *N. ignaciobritoi* (Zhou *et al.*, 2019).

1409

1410

1406

1407

1408

# Phylogenetic analysis

1411 Our search produced 3 minimum-length trees, with 551 steps, consistency index of 0.593 and retention index of 0.860. In our strict consensus tree (Fig. 21), we recovered a clade of Jehol 1412 tapejarids, in which the clade Eopteranodon lii + Sinopterus dongi is the sister-group of 'H.' 1413 1414 corollatus. This Jehol clade (comprising Eopteranodon lii, Sinopterus dongi, and 'H.' corollatus) is supported by the following unambiguous synapomorphies: char. 109(1), dentary symphysis, 1415 dorsal eminence apex, position: posteriorly shifted (located posterior to the anterior third of 1416 mandibular length); char. 127(2), mandibular ramus, dorsal margin; concave; and char. 131(2), 1417 retroarticular process, shape: elongate (char. 161 of Wu et al., 2017). 1418 The node joining Eopteranodon lii and Sinopterus dongi was supported by the following four 1419 synapomorphies: char. 8(1), orbit shape: subquadrangular; char. 30(0), skull height (from 1420 1421 squamosal to premaxilla, exclusive of cranial crests) relative to jaw length: under 25% of jaw length (modified from Witton, 2012; Andres et al., 2014); char. 70(4) quadrate, reclination: about 1422 160° (ambiguous synapomorphy); and char. 178(1) mid-cervicals, fourth longer than the fifth: 1423 1424 present. 1425 Based on the compelling anatomical differences between S. dongi and 'Huaxiapterus' corollatus, along with the fact that S. dongi is recovered here as closer to E. lii than to 'Huaxiapterus' 1426 corollatus, we regard that 'Huaxiapterus' corollatus requires a new generic name – agreeing with 1427 previous suggestions (Kellner & Campos, 2007) and phylogenetic analyses (Andres et al., 2014). 1428 1429 We thus erect *Huaxiadraco* gen. nov. to accommodate *Huaxiadraco corollatus* comb. nov. (Fig.



1 120	22).
1430	//\
17.70	441.

It is interesting to note that the relationships between the Jehol tapejarid species as recovered by our phylogenetic analysis is different from the distance-based relationships between the morphotypes in our morphometric analysis. Particularly, *Tupandactylus navigans* is recovered closer to Morphotype II than to *Tapejara wellnhoferi* and *Caiuajara dobruskii*. It is important to bear in mind that the cluster analysis is based on similarity (which are measured by distance, and can reflect homoplasy), and not shared traits (as is the case of the phylogenetic analysis). This kind of analysis may produce useful information on a species-level taxonomy (granted the analyzed traits are not sexual or ontogenetic in nature, as discussed here), but it has no bearing on the phylogenetic relationships between the analyzed species. While our species circumscriptions are based on morphological and morphometric variation (thus the utility of a specimen-level phenogram in order to cluster specimens), our generic attributions must be guided by our phylogenetic results.

# **Systematic Paleontology**

- 1445 Pterosauria Owen, 1842
- 1446 Pterodactyloidea Plieninger, 1901
- 1447 Azhdarchoidea Unwin, 1995 (sensu Kellner, 2003)
- 1448 Tapejaridae Kellner, 1989 (sensu Andres, 2021)
- 1449 Sinopterinae Lü et al., 2016 (sensu Andres, 2021)

#### Sinopterus dongi Wang & Zhou, 2003



- 1452 **Holotype.** IVPP V 13363.
- 1453 **Referred material.** BPV-077, GMN-03-11-001, JPM-2014-005, XHPM 1009, IVPP V 23388,
- 1454 D3072, D4019, BPMC 106, BPMC 107.
- 1455 **Synonymy.** Sinopterus gui Li et al. (2003), Huaxiapterus jii Lü & Yuan (2005), Sinopterus
- 1456 lingyuanensis Lü et al. (2016), and Huaxiapterus atavismus Lü et al. (2016).
- 1457 **Type locality and horizon.** Chaoyang City of Liaoning Province. Jiufotang Formation.
- 1458 **Diagnostic apomorphies.** Sinopterinae with the following unique features (autapomorphies):
- nasoantorbital fenestra relatively elongate (over three times as long as high); pteroid shorter than
- half of ulna length; metatarsal I subequal to or longer than metatarsal II (longer than metatarsal
- 1461 III).
- 1462 **Differential diagnosis.** Sinopterinae species with the following combination of features:
- premaxillary crest heaped in outline, in the crested morph (= Eopteranodon,  $\neq Huaxiadraco$ );
- 1464 rostrum deflection of  $12^{\circ}-15^{\circ}$  (= Eopteranodon,  $\neq$  Huaxiadraco); nasoantorbital fenestra
- relatively elongate, over three times as long as high (autapomorphy); nasal process subvertical and
- 1466 elongate (= Eopteranodon, \neq Huaxiadraco); subquadrangular orbit (= Eopteranodon, \neq Eopteranodon)
- 1467 Huaxiadraco); quadrate reclination of  $\sim 160^{\circ}$  (= Eopteranodon,  $\neq$  Huaxiadraco); fourth cervical
- vertebrae the longest (= Eopteranodon,  $\neq Huaxiadraco$ ); pteroid shorter than half of ulna length
- (autapomorphy); metacarpal I subequal to metacarpal IV (= Eopteranodon,  $\neq$  Huaxiadraco); wing
- phalanx 4/phalanx 1 length ratio about 0.30 (\(\neq Eopteranodon\), \(\neq Huaxiadraco\); metatarsal I
- subequal to or longer than metatarsal II, and longer than metatarsal III (autapomorphy).
- 1473 Eopteranodon lii Lü & Zhang, 2005
- 1474 **Holotype.** BPV-078.

- 1475 **Referred material.** D2526.
- 1476 **Type locality and horizon.** Beipiao, Liaoning Provice. Yixian Formation.
- 1477 Diagnostic apomorphies. Tapejarid with the following autapomorphies: elongate pteroid
- 1478 (pteroid/ulna length ratio about 0.56); elongate wing phalanx 4 (subequal to phalanx 3 and about
- 1479 45% the length of phalanx 1).
- 1480 **Differential diagnosis.** Sinopterinae with following combination of features: premaxillary crest
- heaped in outline, in the crested morph (= Sinopterus,  $\neq$  Huaxiadraco); rostrum deflection of 15°
- 1482 (= Sinopterus,  $\neq$  Huaxiadraco); nasoantorbital fenestra relatively stout, about 2.5 times as long as
- high ( $\neq$  Sinopterus, = Huaxiadraco); nasal process subvertical and elongate (= Sinopterus,  $\neq$
- 1484 *Huaxiadraco*); subquadrangular orbit (= Sinopterus, \neq Huaxiadraco); quadrate reclination of
- 1485 ~160° (= Sinopterus, \neq Huaxiadraco); fourth cervical vertebrae the longest (= Sinopterus, \neq
- 1486 Huaxiadraco); pteroid over half of ulna length (autapomorphy); metacarpal I subequal to
- metacarpal IV (= Sinopterus,  $\neq Huaxiadraco$ ); elongate wing phalanx 4, subequal to phalanx 3 and
- about 45% the length of phalanx 1 (autapomorphy); metatarsal I shorter than metatarsal II (\neq
- 1489 Sinopterus, = Huaxiadraco).
- 1490
- 1491 Huaxiadraco gen. nov.
- 1492 **Etymology.** After *Huaxia*, an ancient, pre-imperial name for the Chinese civilization (literal
- meaning: beautiful grandeur), and *draco*, Latin for dragon.
- 1494 **Type species.** *Huaxiadraco corollatus* (Lü *et al.* 2005), new combination.
- 1495 **Diagnosis.** As for type and only species.
- 1496



1497	Huaxiadraco corollatus (Lü et al. 2006) comb. nov.
1498	Holotype. ZMNH M813.
1499	Referred material. BXGM V0011, D2525, BPMC 103, BPMC 104, BPMC 105.
1500	Synonymy. Huaxiapterus benxiensis Lü et al. 2005.
1501	Type locality and horizon. Chaoyang City of Liaoning Province. Jiufotang Formation.
1502	Diagnostic apomorphies. Sinopterinae with the following unique features (autapomorphies):
1503	premaxillary crest trapezoidal in shape and slanting anterodorsally (in the crested morph); nasal
1504	descending process anteriorly oriented; short metacarpal I (30%-40% the length of metacarpal
1505	IV); and short wing phalanx 4 ( $\sim$ 20% the length of wing phalanx 1).
1506	Differential diagnosis. Sinopterinae species with premaxillary crest trapezoidal in shape and
1507	slanting anterodorsally, in the crested morph (autapomorphy); orbit piriform in shape ( $\neq$
1508	Sinopterus, ≠ Eopteranodon); rostrum deflection of ~20° (≠ Sinopterus, ≠ Eopteranodon);
1509	nasoantorbital fenestra relatively stout, 2.2–2.5 times as long as high (≠ Sinopterus, =
1510	Eopteranodon); quadrate reclination of ~150° (\( \neq \) Sinopterus, \( \neq \) Eopteranodon); fifth cervical
1511	vertebrae the longest ( $\neq$ Sinopterus, $\neq$ Eopteranodon); short metacarpal I, 30%–40% the length of
1512	metacarpal IV (autapomorphy); short wing phalanx 4, ~20% the length of wing phalanx 1
1513	(autapomorphy); and metatarsal I shorter than metatarsal II ( $\neq$ Sinopterus, = Eopteranodon).
1514	
1515	Conclusions
1516	Jiufotang tapejarids were originally divided into seven nominal species, all entangled in a series
1517	of disputed interpretations. Our qualitative and quantitative reassessments lead us to recognize 2
1518	morphotypes of Jiufotang tapejarids, and to conclude that each of these morphotypes represents a



distinct species. These are: Morphotype I, corresponding to *Sinopterus dongi* (with *S. gui*, *H. jii*, *S. lingyuanensis*, and *H. atavismus* as junior synonyms), and Morphotype II, corresponding to *Huaxiadraco corollatus* gen. et comb. nov. (with *Huaxiapterus benxiensis* as a junior synonym). We diagnose each species by compelling and unique combinations of features (including autapomorphies) that are unlikely to be explained by intraspecific variation, as indicated by our qualitative and quantitative analyses. In addition, we regard that premaxillary crest morphology in sinopterines seems to be explained by multiple sources of variation: ontogenetic variation regarding crest presence (with young juveniles being crestless), individual/sexual variation regarding crest development (with mature, crested morphs expressing varying levels of crest size), and interspecific variation regarding crest shape (with a heaped shape in *S. dongi* and a trapezoidal shape in *H. corollatus*). We corroborate the view of *Sinopterus* as being more closely related to the Yixian tapejarid *Eopteranodon lii* than to *Huaxiadraco corollatus*, and regard *Nemicolopterus crypticus* as a very young, undiagnostic, indeterminate sinopterine.

# **Acknowledgements**

We thank the Willi Hennig Society for making TNT freely available. For access to specimens under their care, we thank Cunyu Liu (BPMC), Xuefang Wei (CC-CGS), Caizhi Shen (DNHM), Qiannan Zhang (BMNH), Shaowen Zhang (CAGS), Fangfang Teng (XHPM), Jun Zhang and Honggang Huo (BXGM), Deyu Sun (JPM), Junjie Yao (CDM), Shunxin Jiang and Xiaolin Wang (IVPP), Alexander Kellner, Luciana Carvalho and Uiara Cabral (MN/UFRJ), Dieter Schreiber and Eberhard Frey (SMNK), and Carl Mehling and Mark Norell (AMNH). RVP thanks FAPESP for their Ph.D. scholarship (#2019/10231-6), Tainá Constância (UFABC) and Kamila Bandeira (MN/UFRJ) for help with image software, and Lucas Piazentin (USP), Borja Holgado (URCA) and Arthur Brum (MN/UFRJ) for fruitful discussions. XZ thanks the Hokkaido University DX Doctoral Fellowship (#JPMJSP2119). WM thanks the National Museum of Natural History, Smithsonian Institution for the Deep Time Peter Buck Postdoctoral Fellowship. XZ and WM were 



1545	supported by the Fund from the Key Laboratory of Stratigraphy and Paleontology, Ministry of
1546	Natural Resources (#KLSP2101). Special thanks to Cunyu Liu (BPMC) for his great efforts in
1547	advancing Liaoning paleontology.
1548	
1549	References
1550	Andres B. 2021. Phylogenetic systematics of Quetzalcoatlus Lawson 1975 (Pterodactyloidea:
1551	Azhdarchoidea). Journal of Vertebrate Paleontology, 41(sup1): 203–217.
1552	Andres B, Ji Q. 2008. A new pterosaur from the Liaoning Province of China, the phylogeny of
1553	the Pterodactyloidea, and the convergence in their cervical vertebrae. Palaeontology, 51: 453–
1554	469.
1555	Andres B, Langston Jr W. 2021. Morphology and taxonomy of Quetzalcoatlus Lawson 1975
1556	(Pterodactyloidea: Azhdarchoidea). <i>Journal of Vertebrate Paleontology</i> , <b>41(sup1)</b> : 46–202.
1557	Andres B, Clark JM, Xu X. 2014. The earliest pterodactyloid and the origin of the group. Current
1558	Biology, <b>24(9)</b> : 1011-1016.
1559	Angst D, Barnoud J, Cornette R, Chinsamy A. 2020. Sex and ontogenetic variation in the crest
1560	of Numida meleagris: implications for crested vertebrates. The Anatomical Record, 303(4):
1561	1018-1034.
1562	Beccari V, Pinheiro FL, Nunes I, Anelli LE, Mateus O, Costa, FR. 2021. Osteology of an
1563	exceptionally well-preserved tapejarid skeleton from Brazil: Revealing the anatomy of a
1564	curious pterodactyloid clade. PloS one, 16(8): e0254789.
1565	Bennett SC. 1993. The ontogeny of <i>Pteranodon</i> and other pterosaurs. <i>Paleobiology</i> , 19(1): 92–
1566	106.
1567	Bennett SC. 1994. Taxonomy and systematics of the Late Cretaceous pterosaur Pteranodon
1568	(Pterosauria, Pterodactyloidea). Occasional papers of the Natural Natural History
1569	Museum/The University of Kansas, 169: 1–70.
1570	Bennett, S. C. 2007. A second specimen of the pterosaur Anurognathus



- 1571 ammoni. Paläontologische Zeitschrift, **81(4):** 376.
- 1572 **Benton MJ, Zhonghe Z, Orr PJ, Fucheng Z, Kearns SL. 2008.** The remarkable fossils from the
- 1573 Early Cretaceous Jehol Biota of China and how they have changed our knowledge of Mesozoic
- life. *Proceedings of the Geologists' Association*, **119(3-4):** 209-228.
- 1575 **Brown MA, Sagebiel JC, Andres B. 2021.** The discovery, local distribution, and curation of the
- giant azhdarchid pterosaurs from Big Bend National Park. Journal of Vertebrate
- 1577 *Paleontology*, **41(sup1)**: 2–20.
- 1578 Campos D, Kellner AWA. 1997. Short note on the first occurrence of Tapejaridae in the Crato
- 1579 Member (Aptian), Santana Formation, Araripe Basin, Northeast Brazil. Anais da Academia
- 1580 Brasileira de Ciências, **69**: 83–87.
- 1581 Dalla Vecchia FM. 2018. Comments on Triassic pterosaurs with a commentary on the"
- ontogenetic stages" of Kellner (2015) and the validity of Bergamodactylus wildi. Rivista
- 1583 Italiana di Paleontologia e Stratigrafia, **124(2)**.
- de Queiroz K, Cantino PD, Gauthier JA. 2020. Phylonyms: a Companion to the PhyloCode.
- 1585 CRC Press.
- 1586 **Duan Y, Zhang LJ, Li L, Cheng SL. 2006.** Division and correlation of unique fossil-bearing beds
- of Jiufotang Formation in Dapingfang-Meileyingzi Basin of western Liaoning (in Chinese with
- English abstract). *Global Geology*, **25(2)**: 113-119.
- 1589 **Duan Y, Zhang LJ, Zhang LJ, Hu DY. 2010.** Division and correlation of unique fossil-bearing
- beds of Jiufotang Formation in Jianchang Basin of western Liaoning (in Chinese). Chinese
- 1591 *Journal of Geology*, **45(2)**: 606-613.
- 1592 Eck K, Elgin RA, Frey E. 2011. On the osteology of *Tapejara wellnhoferi* Kellner 1989 and the
- first occurrence of a multiple specimen assemblage from the Santana Formation, Araripe
- Basin, NE-Brazil. Swiss *Journal of Palaeontology*, **130(2)**: 277.
- 1595 Frey E, Martill DM, Buchy MC. 2003. A new species of tapejarid pterosaur with soft-tissue head
- 1596 crest. Geological Society, London, Special Publications, 217(1): 65-72.
- 1597 Gao FL, Jiang Y, Pan YQ, Wang X, Wu ZJ, Fan S, Dai DY. 2018. Division and significance



1598	of the precious fossil-bearing beds of Jiufotang Formation in Sihedang area, Liaoning
1599	Province. Geology and Resource (in Chinese with English abstract). Geology and
1600	Resources, 27(6): 503-507.
1601	Goloboff PA, Farris JS, Nixon KC. 2008. TNT, a free program for phylogenetic
1602	analysis. Cladistics, 24(5): 774–786.
1603	Hammer Ø, Harper DA, Ryan PD. 2001. PAST: Paleontological statistics software package for
1604	education and data analysis. Palaeontologia electronica, 4(1): 9.
1605	Hone DWE, Jiang S, Xu X. 2018. A taxonomic revision of Noripterus complicidens (Young,
1606	1973) and Asian members of the Dsungaripteridae. Geological Society, London, Special
1607	Publications, <b>455(1)</b> : 149–157.
1608	Hone DW, Ratcliffe JM, Riskin DK, Hermanson JW, Reisz RR. 2021. Unique near isometric
1609	ontogeny in the pterosaur Rhamphorhynchus suggests hatchlings could fly. Lethaia, 54(1):
1610	106–112.
1611	Kellner AWA. 1989. A new edentate pterosaur of the Lower Cretaceous from the Araripe Basin,
1612	Northeast Brazil. Anais da Academia Brasileira de Ciências, 61: 439-446.
1613	Kellner AWA. 2003. Pterosaur phylogeny and comments on the evolutionary history of the
1614	group. Geological Society, London, Special Publications, 217(1): 105–137.
1615	Kellner AWA. 2010. Comments on the Pteranodontidae (Pterosauria, Pterodactyloidea) with the
1616	description of two new species. <i>Anais da Academia Brasileira de Ciências</i> , <b>82</b> , 1063–1084.
1617	Kellner AWA. 2013. A new unusual tapejarid (Pterosauria, Pterodactyloidea) from the Early
1618	Cretaceous Romualdo Formation, Araripe Basin, Brazil. Earth and Environmental Science
1619	Transactions of the Royal Society of Edinburgh, 103(3-4): 409–421.
1620	Kellner AWA. 2015. Comments on Triassic pterosaurs with discussion about ontogeny and
1621	description of new taxa. Anais da Academia Brasileira de Ciências, 87: 669-689.
1622	Kellner AWA, Campos DA. 2007. Short note on the ingroup relationships of the Tapejaridae
1623	(Pterosauria, Pterodactyloidea). Boletim do Museu Nacional, Nova Série, Rio de Janeiro-
1624	Brasil. <i>Geologia</i> , <b>75</b> : 1–14.



1625	Kellner AWA, Tomida Y. 2000. Description of a new species of Anhangueridae
1626	(Pterodactyloidea) with comments on the pterosaur fauna from the Santana Formation
1627	(Aptian-Albian), Northeastern Brazil. National Science Museum, Tokyo, Monographs, 17:
1628	1–135.
1629	Kellner AWA, Weinschütz LC, Holgado B, Bantim RA, Sayao JM. 2019. A new toothless
1630	pterosaur (Pterodactyloidea) from Southern Brazil with insights into the paleoecology of a
1631	Cretaceous desert. Anais da Academia Brasileira de Ciências, 91.
1632	Leal MEC, Pêgas RV, Bonde N, Kellner AWA. 2018. Cervical vertebrae of an enigmatic
1633	pterosaur from the Crato Formation (Lower Cretaceous, Araripe Basin, NE
1634	Brazil). Geological Society, London, Special Publications, 455(1): 195–208.
1635	<b>Lehman TM. 2021.</b> Habitat of the giant pterosaur <i>Quetzalcoatlus</i> Lawson 1975 (Pterodactyloidea:
1636	Azhdarchoidea): a paleoenvironmental reconstruction of the Javelina Formation (Upper
1637	Cretaceous), Big Bend National Park, Texas. Journal of Vertebrate
1638	Paleontology, 41(sup1): 21–45.
1639	Li JJ, Lü JC, Zhang BK. 2003. A new lower Cretaceous sinopterid pterosaur from Western
1640	Liaoning, China. Acta Palaeontologica Sinica, 42: 442–447.
1641	Liu DX, Zhou CF, Wang JQ, Li WG, Wei QW. 2014. New data on the cervical morphology of
1642	the Chinese tapejarine. <i>Historical Biology</i> , <b>27(6)</b> : 638-645.
1643	Longrich NR, Martill DM, Andres B. 2018. Late Maastrichtian pterosaurs from North Africa
1644	and mass extinction of Pterosauria at the Cretaceous-Paleogene boundary. PLoS
1645	biology, <b>16(3)</b> : e2001663.
1646	Lü JC, Gao CL, Liu JY, Meng QJ, Ji Q. 2006c. New material of the pterosaur Eopteranodon
1647	from the Early Cretaceous Yixian Formation, western Liaoning, China. Geological Bulletin
1648	of China, <b>25</b> : 555–571.
1649	Lü JC, Gao YB, Xing LD, Li ZX, Sun ZY. 2007. A new species of Huaxiapterus from the Early
1650	Cretaceous of western Liaoning, China. Acta Geologica Sinica, 81(5): 683–687.
1651	Lü JC, Jin XS, Unwin DM, Zhao LJ, Azuma Y, Ji Q. 2006a. A new species of Huaxiapterus



1652	(Pterosauria: Pterodactyloidea) from the Lower Cretaceous of western Liaoning, China
1653	with comments on the systematics of tapejarid pterosaurs. Acta Geologica Sinica, 80(3):
1654	315–326.
1655	Lü JC, Liu JY, Wang XR, Gao CL, Meng QJ, Ji Q. 2006b. New material of the pterosaur
1656	Sinopterus (Reptilia: Pterosauria) from the Early Cretaceous Jiufotang Formation, Western
1657	Liaoning, China. Acta Geologica Sinica, 80: 783–789.
1658	Lü JC, Teng FF, Sun DY, Shen CZ, Li GQ, Gao X, Liu HF. 2016. The toothless pterosaurs
1659	from China. Acta Geologica Sinica, 90(9): 2513–2525.
1660	Lü J, Unwin DM, Xu L, Zhang X. 2008. A new azhdarchoid pterosaur from the Lower
1661	Cretaceous of China and its implications for pterosaur phylogeny and
1662	evolution. Naturwissenschaften, 95(9): 891–897.
1663	Lü JC, Yuan CX. 2005. New tapejarid pterosaur from western Liaoning, china. Acta Geologica
1664	Sinica, <b>79(4)</b> : 453-458.
1665	Lü J, Zhang BK. 2005. New pterodactyloid pterosaur from the Yixian Formation of western
1666	Liaoning. Geological Review, 51: 458–462.
1667	Manzig PC, Kellner AWA, Weinschütz LC, Fragoso CE, Vega CS, Guimarães GB, Godoy
1668	LC, Liccardo A, Ricetti JHZ, de Moura CC. 2014. Discovery of a rare pterosaur bone
1669	bed in a Cretaceous desert with insights on ontogeny and behavior of flying reptiles. PloS
1670	one, <b>9(8)</b> : e100005.
1671	Martill DM, Ibrahim N. 2015. An unusual modification of the jaws in cf. Alanqa, a mid-
1672	Cretaceous azhdarchid pterosaur from the Kem Kem beds of Morocco. Cretaceous
1673	Research, <b>53:</b> 59–67.
1674	Martill DM, Smith R, Unwin DM, Kao A, McPhee J, Ibrahim N. 2020. A new tapejarid
1675	(Pterosauria, Azhdarchoidea) from the mid-Cretaceous Kem Kem beds of Takmout,
1676	southern Morocco. Cretaceous Research, 112: 104424.
1677	Martill DM, Green M, Smith RE, Jacobs ML, Winch J. 2020. First tapejarid pterosaur from
1678	the Wessex Formation (Wealden Group: Lower Cretaceous, Barremian) of the United



1679	Kingdom. Cretaceous Research, 113: 104487.
1680	Martin-Silverstone E, Glasier JRN, John H. Acorn JH, Mohr S, Currie PJ. 2017.
1681	Redescription of Dawndraco kanzai Kellner, 2010 and reassignment of the type specimen to
1682	Pteranodon sternbergi Harksen, 1966. Vertebrate Anatomy Morphology Palaeontology 3:
1683	47-59.
1684	Naish D, Perron R. 2016. Structure and function of the cassowary's casque and its implications
1685	for cassowary history, biology and evolution. Historical Biology, 28(4): 507-518.
1686	Naish D, Witton MP. 2017. Neck biomechanics indicate that giant Transylvanian azhdarchid
1687	pterosaurs were short-necked arch predators. PeerJ, 5: e2908.
1688	Naish D, Witton MP, Martin-Silverstone E. 2021. Powered flight in hatchling pterosaurs:
1689	evidence from wing form and bone strength. Scientific Reports, 11(1): 1-15.
1690	Ősi A, Weishampel DB, Jianu CM. 2005. First evidence of azhdarchid pterosaurus from the Late
1691	Cretaceous of Hungary. Acta Palaeontologica Polonica, 50(4), 777-787.
1692	Ősi A, Buffetaut E, Prondvai E. (2011). New pterosaurian remains from the Late Cretaceous
1693	(Santonian) of Hungary (Iharkút, Csehbánya Formation). Cretaceous Research, 32(4),
1694	456-463.
1695	Pêgas RV, Leal MEC, Kellner AWA. 2016. A basal tapejarine (Pterosauria; Pterodactyloidea;
1696	Tapejaridae) from the crato formation, Early Cretaceous of Brazil. PLoS One, 11(9):
1697	e0162692.
1698	Pêgas RV, Costa FR, Kellner AWA. 2018. New information on the osteology and a taxonomic
1699	revision of the genus <i>Thalassodromeus</i> (Pterodactyloidea, Tapejaridae,
1700	Thalassodrominae). Journal of Vertebrate Paleontology, 38(2): e1443273.
1701	Pêgas RV, Holgado B, David LDO, Baiano MA, Costa FR. 2021. On the pterosaur Aerotitan
1702	sudamericanus (Neuquén Basin, Upper Cretaceous of Argentina), with comments on
1703	azhdarchoid phylogeny and jaw anatomy. Cretaceous Research: e104998.
1704	Pinheiro FL, Rodrigues T. 2017. Anhanguera taxonomy revisited: is our understanding of
1705	Santana Group pterosaur diversity biased by poor biological and stratigraphic



control? PeerJ 5: e3285. 1706 Shen C, Pêgas RV, Gao C, Kundrát M, Zhang L, Wei X, Zhou X. 2021. A new specimen of 1707 Sinopterus dongi (Pterosauria, Tapejaridae) from the Jiufotang Formation (Early Cretaceous, 1708 China). *PeerJ*, **9**: e12360. 1709 **Sigrist T. 2004.** Aves do Brasil: uma visão artística. Avis Brasilis. 1710 Su YS, Gao JH, Li SG, Bu CP, Zhu CQ. 2008. The Basin Growth Characteristic and 1711 Hydrocarbon Assesment of the Mesozoic in Songnan-Liaoxi Area (in Chinese with English 1712 abstract). Geosciences, 22(4): 505-519. 1713 1714 **Unwin DM. 2003.** On the phylogeny and evolutionary history of pterosaurs. *Geological Society*, London, Special Publications, 217(1): 139-190. 1715 Vila Nova BC, Sayão JM, Langer MC, Kellner AWA. 2015. Comments on the cervical 1716 vertebrae of the Tapejaridae (Pterosauria, Pterodactyloidea) with description of new 1717 1718 specimens. *Historical Biology*, **27(6)**: 771-781. 1719 Vullo R, Marugán-Lobónm J, Kellner AWA, Buscalioni A, Fuente M, Moratalla JJ. 2012. A 1720 new crested pterosaur from the Early Cretaceous of Spain: The first European tapejarid (Pterodactyloidea: Azhdarchoidea). PLoS ONE, 7: e38900. 1721 Wang XL, Dong ZM. 2008. Order Pterosauria. In: Li JL, Wu XC and Zhang FC (Eds), The 1722 Chinese fossil reptiles and their kin, 2nd ed., Beijing: Sci Press, p. 215-234. 1723 1724 Wang XL, Zhou ZH. 2003. A new pterosaur (Pterodactyloidea, Tapejaridae) from the Early Cretaceous Jiufotang Formation of Western Liaoning, China and its implications for 1725 biostratigraphy. Chinese Science Bulletin, 48(1): 16-23. 1726 Wang XL, Zhou ZH. 2006. Pterosaur assemblages of the Jehol Biota and their implication for the 1727 1728 Early Cretaceous pterosaur radiation. *Geological Journal*, **41(3–4)**: 405–418. Wang XL, Kellner AWA, Jiang SX, Wang Q, Ma YX, Paidoula Y, Cheng X, Rodrigues T, 1729

Meng X, Zhang JL, Li N, Zhou ZH. 2014. Sexually dimorphic tridimensionally preserved

pterosaurs and their eggs from China. Current Biology, 24(12): 1323-1330.

1730

1731

#### **PeerJ**

- 1732 Wang X, Kellner AW, Jiang S, Cheng X, Wang Q, Ma Y, Paidoula Y, Rodrigues T, Chen H,
- Sayão J, Li N, Zhang J, Bantim RAM, Meng X, Zhang X, Qiu R, Zhou Z. 2017. Egg
- accumulation with 3D embryos provides insight into the life history of a
- 1735 pterosaur. *Science*, **358(6367)**: 1197-1201.
- 1736 Warton DI, Wright IJ, Falster DS, Westoby M. 2006. Bivariate line-fitting methods for
- 1737 allometry. *Biological reviews*, **81(2)**: 259-291.
- 1738 Wellnhofer P, Kellner AWA. 1991. The skull of Tapejara wellnhoferi Kellner (Reptilia,
- 1739 Pterosauria) from the Lower Cretaceous Santana Formation of the Araripe Basin,
- Northeastern Brazil. Mitteilungen der Bayerischen Staatssammlung für Paläontologie und
- 1741 *Historische Geologie*, **31**: 89-106.
- 1742 **Witton MP. 2013.** *Pterosaurs*. Princeton University Press.
- 1743 Wu WH, Zhou CF, Andres B. 2017. The toothless pterosaur Jidapterus edentus
- 1744 (Pterodactyloidea: Azhdarchoidea) from the Early Cretaceous Jehol Biota and its
- paleoecological implications. *PLoS One*, **12(9)**: e0185486.
- 1746 Wu ZJ, Gao FL, Pan YO, Wang X. 2018. Division and correlation of the Jiufotang Formation
- and their rare fossil-bearing beds in western Liaoning, China (in Chinese with English
- abstract). Geoscience, **32(4)**: 758-765.
- 1749 Xi D, Wan X, Li G, Li G. 2019. Cretaceous integrative stratigraphy and timescale of
- 1750 China. Science China Earth Sciences, **62(1)**: 256-286.
- 1751 Yang Z, Benton MJ, Hone DW, Xu X, McNamara ME, Jiang B. 2022. Allometric analysis
- sheds light on the systematics and ontogeny of anurognathid pterosaurs. Journal of
- 1753 *Vertebrate Paleontology*, **41(5)**: e2028796.
- 1754 Zhang L, Yang Y, Zhang L, Guo, S, Wang W, Zheng S. 2007. Precious Fossil-Bearing Beds of
- the Lower Cretaceous Jiufotang Formation in Western Liaoning Province, China. Acta
- 1756 Geologica Sinica-English Edition, **81(3)**: 357-364.
- 1757 Zhang XJ, Jiang SX, Cheng X, Wang XL. 2019. New material of Sinopterus (Pterosauria,
- Tapejaridae) from the Early Cretaceous Jehol Biota of China. *Anais da Academia Brasileira*



1784

1785

20 mm.

de Ciências, 91. 1759 Zhou Z, Barrett PM, Hilton J. 2003. An exceptionally preserved Lower Cretaceous 1760 ecosystem. Nature, 421(6925): 807-814. 1761 1762 Zhou XY, Pêgas RV, Leal MEC, Bonde N. 2019. Nurhachius luei, a new istiodactylid pterosaur (Pterosauria, Pterodactyloidea) from the Early Cretaceous Jiufotang Formation of Chaoyang 1763 City, Liaoning Province (China) and comments on the Istiodactylidae. *PeerJ*, 7: e7688. 1764 1765 Zhou X, Pêgas RV, Ma W, Han G, Jin X, Leal ME, Bonde N, Kobayashi Y, Lautenschlager 1766 S, Wei X, Shen C, Ji S. 2021. A new darwinopteran pterosaur reveals arborealism and an opposed thumb. *Current Biology*, **31(11)**: 2429-2436. 1767 Zhou CF, Niu T, Yu D. 2022a. New data on the postcranial skeleton of the tapejarid Sinopterus 1768 from the Early Cretaceous Jehol Biota. *Historical Biology*, 1-8. 1769 1770 Zhou CF, Yu D, Zhu Z, Andres B. 2022b. A new wing skeleton of the Jehol tapejarid Sinopterus and its implications for ontogeny and paleoecology of the Tapejaridae. Scientific 1771 reports, **12(1)**: 1-10. 1772 1773 1774 **Figures** Figure 1. Stratigraphic chart of the Jiufotang Formation. Columns show the structure, 1775 cyclicity, and basins where known localities outcrop, for each Member of the Jiufotang Formation. 1776 Modified from Wu et al. (2018). 1777 Figure 2. Sinopterus dongi holotype (IVPP V 13363). A, skeleton overview; B, left metacarpus; 1778 C, left foot; D, skull (right lateral view). E-H, respective schematic drawings. Abbreviations: ca, 1779 carpus; co, coracoid; cv, cervical vertebra; d, dentary; d1-d4, digits 1-4; epi, epiphysis; etp, 1780 extensor tendon process; f, frontal; fe, femur; fpc, frontoparietal crest; h, humerus; ios, interorbital 1781 1782 septum; l, left; lpt, lateral proximal tarsal; m, maxilla; mc, metacarpal; mt, metatarsal; n, nasal; naof, nasoantorbital fenestra; pm, premaxilla; ph, phalanx; pt, pteroid; ti, tibia; ul, ulna; r, right; 1783

rad, radius; sca, scapula; st, sternum. Scale bars: A, 50 mm; E, 50 mm; F, 20 mm; G, 10 mm; H,



- 1786 **Figure 3. Sinopterus gui holotype (BPV-077).** A, skeleton overview; B, skull (left lateral view).
- 1787 C–D, respective schematic drawings. Abbreviations: co, coracoid; cv, cervical vertebra; d, dentary;
- dvs, dorsal vertebral series; f, frontal; fe, femur; fi, fibula; fpc, frontoparietal crest; h, humerus; is,
- ischium; j, jugal; l, left; mc, metacarpal; mt, metatarsal; n, nasal; naof, nasoantorbital fenestra; or,
- orbit; pt, pteroid; pu, pubis; prap, preacetabular process; ti, tibia; ul, ulna; r, right; rad, radius; sca,
- scapula. Scale bars: C, 50 mm; D, 50 mm.
- 1792 Figure 4. Huaxiapterus jii holotype (GMN-03-11-001). A, skeleton overview; B, skull (left
- 1793 lateral view, slightly ventrolateral). C–D, respective schematic drawings. Abbreviations: ca,
- carpus; co, coracoid; cv, cervical vertebra; d, dentary; d1–d4, digits 1–4; dv, dorsal vertebra; epi,
- epiphysis; fe, femur; h, humerus; j, jugal; l, left; mc, metacarpal; pm, premaxilla; ph, phalanx; pp,
- prepubis; pt, pteroid; ti, tibia; ul, ulna; r, right; rad, radius; sca, scapula; st, sternum. Scale bars: C,
- 1797 50 mm; D, 20 mm.
- 1798 Figure 5. Huaxiapterus corollatus holotype (ZMNH M813). A, skeleton overview; B, skull
- 1799 (right lateral view); C, left metacarpus. D–F, respective schematic drawings. Abbreviations: ca,
- 1800 carpus; co, coracoid; cv, cervical vertebra; d, dentary; d1-d4, digits 1-4; fe, femur; fpc,
- 1801 frontoparietal crest; h, humerus; l, left; m, maxilla; mand, mandible; mc, metacarpal; mt,
- metatarsal; n, nasal; naof, nasoantorbital fenestra; pm, premaxilla; ph, phalanx; pt, pteroid; ti, tibia;
- ul, ulna; r, right; rad, radius; sca, scapula; sk, skull. Scale bars: A, D, 100 mm; E, F, 10 mm.
- 1804 **Figure 6. Specimen D2525.** A, skeleton overview; B, right foot; C, right metacarpus. D–F,
- respective schematic drawings. Abbreviations: co, coracoid; cv, cervical vertebra; d, dentary; d1–
- 1806 d4, digits 1–4; dsc, distal synpcarpal; etp, extensor tendon process; f, frontal; fe, femur; fpc,
- frontoparietal crest; gas, gastralia; h, humerus; ios, interorbital septum; is, ischium; l, left; lpt,
- lateral proximal tarsal; mc, metacarpal; mt, metatarsal; pc, preaxial carpal; ph, phalanx; poap,
- postacetabular process; pp, prepubis; prap, preacetabular process; psc, proximal syncarpal; pt,
- pteroid; pu, pubis; ti, tibia; ul, ulna; r, right; rad, radius; ri, rib; sca, scapula; st, sternum. Scale bars:
- 1811 D, 50 mm; E, 10 mm; F, 50 mm.
- Figure 7. Huaxiapterus benxiensis holotype (BXGM V0011). A, skeleton overview; B, left



- metacarpus; C, skull (left lateral view). D-F, respective schematic drawings. Abbreviations: cv,
- cervical vertebra; d, dentary; d1-d4, digits 1-4; f, frontal; fe, femur; fpc, frontoparietal crest; h,
- humerus; ios, interorbital septum; j, jugal; l, left; m, maxilla; la, lacrimal; mc, metacarpal; mt,
- metatarsal; naof, nasoantorbital fenestra; np, nasal process; pm, premaxilla; ph, phalanx; pt,
- pteroid; ti, tibia; ul, ulna; r, right; rad, radius. Scale bars: 50 mm.
- 1818 Figure 8. Sinopterus lingyuanensis holotype (JPM-2014-005). A, skeleton overview; B, right
- 1819 foot; C, skull (left lateral view). D–F, respective schematic drawings. Abbreviations: art, articular;
- ca, carpus; cv, cervical vertebra; d, dentary; d1-d4, digits 1-4; fe, femur; fpc, frontoparietal crest;
- 1821 h, humerus; ios, interorbital septum; j, jugal; l, left; lpt, lateral proximal tarsal; mc, metacarpal; mt,
- metatarsal; naof, nasoantorbital fenestra; np, nasal process; pm, premaxilla; ph, phalanx; pt,
- pteroid; pv, pelvis; t, tarsus; ti, tibia; ul, ulna; r, right; rad, radius; sca, scapula; sv, sacral vertebrae.
- 1824 Scale bars: D, 50 mm; E, 10 mm; F, 50 mm.
- Figure 9. *Huaxiapterus atavismus* holotype (XHPM 1009). A, skeleton overview; B, skull (left
- 1826 lateral view). C-D, respective schematic drawings. Abbreviations: ca, carpus; cv, cervical
- vertebra; co, coracoid; d, dentary; d1–d4, digits 1–4; fe, femur; fpc, h, humerus; mand, mandible;
- mc, metacarpal; mt, metatarsal; pmc, premaxillary crest; ph, phalanx; ti, tibia; ul, ulna; r, right;
- rad, radius; sk, skull. Scale bars: 50 mm.
- 1830 **Figure 10. New specimen D4019.** A, skeleton overview; B, skull (left lateral view). C–D,
- respective schematic drawings. Abbreviations: ca, carpus; cv, cervical vertebra; d, dentary; d1–d4,
- digits 1–4; fpc, frontoparietala crest; h, humerus; j, jugal; m, maxilla; mc, metacarpal; mt,
- metatarsal; naof, nasoantorbital fenestra; pm, premaxilla; pmc, premaxillary crest; ph, phalanx; ti,
- tibia; ul, ulna; r, right; rad, radius; ri, rib; sk, skull. Scale bars: 50 mm.
- 1835 **Figure 11. New specimen BPMC 103.** A, skeleton overview; B, skull (left lateral view); C,
- 1836 metacarpus, distal region. D-F, respective schematic drawings. Abbreviations: cv, cervical
- vertebra; d, dentary; d1–d4, digits 1–4; fpc, frontoparietala crest; h, humerus; j, jugal; m, maxilla;
- mc, metacarpal; mt, metatarsal; naof, nasoantorbital fenestra; pm, premaxilla; pmc, premaxillary
- crest; ph, phalanx; ti, tibia; ul, ulna; r, right; rad, radius; ri, rib; sk, skull. Scale bars: D, 50 mm; E,



- 1840 20 mm; F, 10 mm.
- 1841 Figure 12. New specimen BPMC 104. A, skeleton overview; B, skull (left lateral view); C, left
- pelvis; D right femur; E, right metatarsus; F, right pelvis; G, left metacarpus. H–N, respective
- schematic drawings. Abbreviations: cv, cervical vertebra; d, dentary; d1–d4, digits 1–4; etp,
- extensor tendon process; fe, femur; h, humerus; il, illium; is, ischium; m, maxilla; mc, metacarpal;
- mt, metatarsal; naof, nasoantorbital fenestra; pm, premaxilla; ph, phalanx; pp, prepubis; pu, pubis;
- pv, pelvis; ti, tibia; ul, ulna; r, right; sca, scapula; sk, skull; ti, tibia. Scale bars: H, 50 mm; I, 50
- 1847 mm; J–N, 10 mm; G, 50 mm.
- Figure 13. New specimen BPMC 105. A, skeleton overview; B, skull (left lateral view); C, detail
- of right manus. D–F, respective schematic drawings. Abbreviations: ca, carpal; etp, extensor
- tendon process; h, humerus; j, jugal; l, left; mand, mandible; mc, metacarpal; naof, nasoantorbital
- 1851 fenestra; or, orbit; pm, premaxilla; pmc, premaxillary crest; ul, ulna; r, right; ra, radius; rap,
- retroarticular process; sca, scapula; sk, skull; ti, tibia. Scale bars: A, D, 50 mm; B, C, E, F, 20 mm.
- 1853 **Figure 14. New specimen BPMC 106.** A, skeleton overview; B, skull (right lateral view). C–D,
- respective schematic drawings. Abbreviations: art, articular; cv, cervical vertebra; h, humerus; j,
- jugal; mc, metacarpal; np, nasal process; pm, premaxilla; po, postorbital; pt, pteroid; ul, ulna; rad,
- radius; sca, scapula; sk, skull. Scale bars: A, C, 50 mm; B, D, 10 mm.
- Figure 15. New specimen BPMC 107. A, skeleton overview; B, skull (right lateral view); C, left
- 1858 humerus; D, sternum; E, left foot; F, right pelvis. G-L, respective schematic drawings.
- Abbreviations: art, articular; ca, carpus; cv, cervical vertebra; d, dentary; d1–d4, digits 1–4; dpc,
- deltopectoral crest; f, frontal; fe, femur; fpc, frontoparietal crest; h, humerus; il, illium; is, ischium;
- 1861 l, left; mc, metacarpal; mt, metatarsal; naof, nasoantorbital fenestra; pmc, premaxillary crest; ph,
- phalanx; poap, postacetabular process; pt, pteroid; pu, pubis; ti, tibia; ul, ulna; r, right; rad, radius;
- sca, scapula; st, sternum; uc, ulnar crest. Scale bars: A, B, G, H, 50 mm; I–K, 10 mm; L, 30 mm.
- 1864 Figure 16. Resulting dendrogram of the UPGMA analysis. Species names represent their
- 1865 holotypic specimens. Red indicates Morphotype I. Blue indicates Morphotype II.
- 1866 Figure 17. Results of the PCA analyses. A, graph based on components 1 and 2 of the analysis



using mean values imputation for the missing data. B, graph based on components 1 and 2 of the 1867 analysis using iterative imputation for the missing data. Species names represent their holotypic 1868 1869 specimens. Red indicates Morphotype I (polygon represents convex hull; ellipse represents the 1870 95% confidence ellipse). Blue indicates Morphotype II (polygon represents convex hull; ellipse 1871 represents the 95% confidence ellipse). Figure 18. Anatomical variation in the skull and wing in the Sinopterus complex. A, schematic 1872 1873 representation of skull and metacarpus + wing digit of Morphotype I (S. dongi). Based mainly on 1874 the holotype of S. dongi (IVPP V 13363), except for the premaxillary crest (based on the holotype of H. jii; GMN-03-11-001). B, schematic representation of skull and metacarpus + wing digit of 1875 Morphotype II (*H. corollatus*). Based mainly on the holotype of *H. benxiensis* (BXGM V0011). A 1876 1877 and B are not to scale, but are both proportionately scaled to the same metacarpal IV length. 1878 Numbers indicate features that vary between S. dongi and H. corollatus (see text): 1) orbit shape; 2) quadrate reclination; 3) nasal process shape; 4) nasoantorbital fenestra length/height ratio; 5), 1879 premaxillary crest shape; 6) rostrum deflection; 7) metacarpal I length; 8) wing phalanx 4 length. 1880 Figure 19. Eopteranodon lii holotype (BPV 078). A, counterpart; B, main part. C-D, respective 1881 1882 schematic drawings. Abbreviations: cv, cervical vertebra; co, coracoid; d1-d4, digits 1-4; fe, femur; fi, fibula; h, humerus; j, jugal; mand, mandible; mc, metacarpal; pmc, premaxillary crest; 1883 pe, pelvis; ph, phalanx; ti, tibia; ul, ulna; rad, radius. Scale bars: C, 50 mm; D, 10 mm. 1884 1885 Figure 20. Eopteranodon lii holotype (BPV 078) details. A, close-up of the specimen's main 1886 part, and B, schematic drawing. Abbreviations: art, articular; d, dentary; h, humerus; m, maxilla; naof, nasoantorbital fenestra; pmc, premaxillary crest; ppm, posterior premaxillary process. Scale 1887 bars: 50 mm. 1888 1889 **Figure 21. Time-calibrated strict consensus tree.** The two species of the *Sinopterus* complex here regarded as valid are indicated in dark red. 1: Tapejaromorpha. 2: Thalassodromidae. 3: 1890 1891 Tapejaridae. 4: Caupedactylia. 5: Tapejarinae. 6: Sinopterinae. 7: Azhdarchomorpha. 8: Chaoyangopteridae. 9: Alanqidae. 10: Azhdarchidae. 1892

Figure 22. Life reconstruction of the Jiufotang tapejarids. The coexistence between Sinopterus

1893



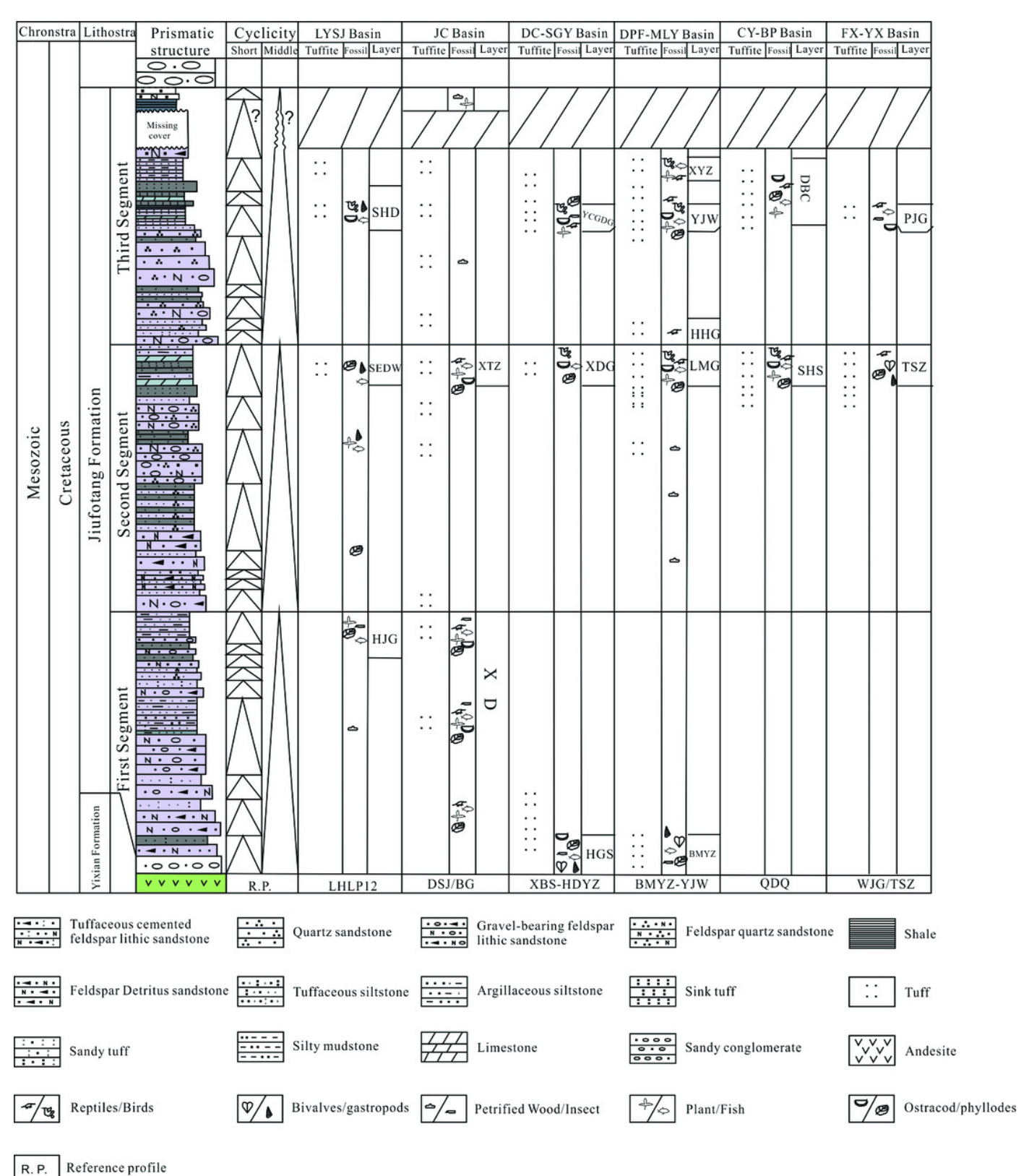
1894	dongi and Huaxiadraco corollatus comb. nov. in the Jiufotang paleoenvironment. Art: courtesy of
1895	Zhao Chuang.
1896	
1897	Tables
1898	Table 1. Systematic nomenclature.
1899	Table 2. Results of the SMA analyses.
1900	Table 3. Summary of main anatomical variations surveyed here in Jehol tapejarids.
1901	Table 4. Summary of taxonomic attributions of Sinopterus complex specimens.
1902	
1903	Supplemental Files
1904	Supplemental File 1. Morphometric dataset. An Excel file with five sheets: (1) skeletal
1905	measurements of the analyzed tapejarid specimens, (2) log-transformed skeletal measurements for
1906	the SMA analyses, (3) morphometric dataset of angles and proportions for the clustering analyses,
1907	(4) rostrum deflection angles in tapejarids, and (5) ontogenetic information for the Jiufotang
1908	tapejarid specimens.
1909	Supplemental File 2. Mesquite file. A nexus-format file for Mesquite, containing the
1910	phylogenetic data matrix.
1911	Supplemental File 3. TNT file for the phylogenetic analysis.



Stratigraphic chart of the Jiufotang Formation.

Columns show the structure, cyclicity, and basins where known localities outcrop, for each Member of the Jiufotang Formation. Modified from Wu *et al.* (2018).





LYSJ Basin represents Lingyuan Sanshijiazi Basin; JC Basin represents Jianchang Basin; DC-SGY Basin represents Dachengzi-Siguanyingzi Basin; DPF-MLY Basin represents Daping fang-Meileyingzi Basin; CY-BP Basin represents Chaoyang-Beipiao Basin; BMYZ represents Baomayingzi layer; FX-YX Basin represents Fuxin-Yixian Basin; XTZ represents Xiaotaizi layer; YCGDG represents Yangcaogoudonggou layer; XDG represents Xidagou layer;

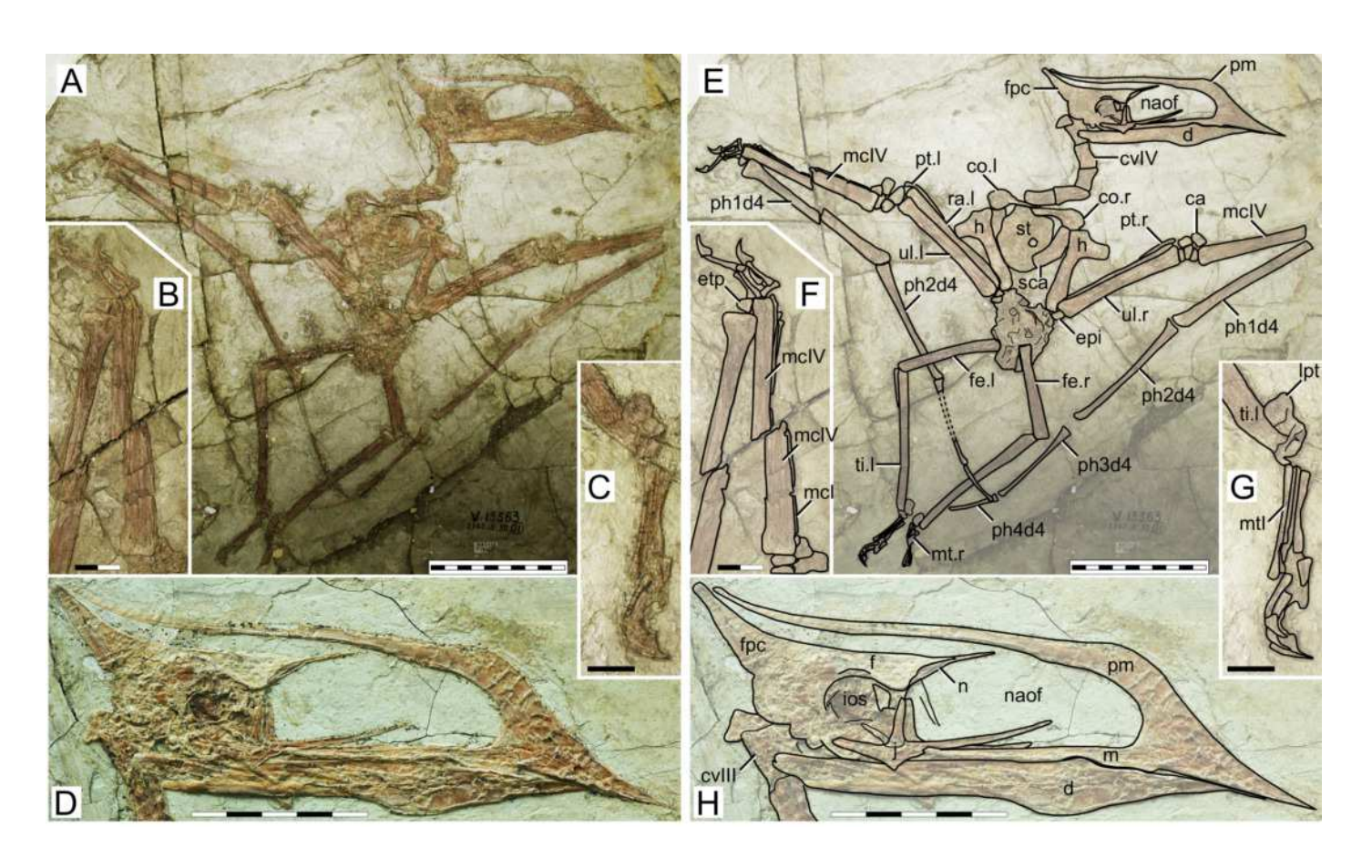
XYZ represents Xiyingzi layer; YJW represents Yuanjiawa layer; HHG represents Huanghuagou layer; LMG represents Lamagou layer; DBC represents Dongbochi layer; SHS represents Shangheshou layer; PJG represents Pijiagou layer; TSZ represents Tuanshanzi layer;

SHD represents Sihedang layer; SEDW represents Saerdaowan layer; HJG represents Hanjiagou layer;

XD represents Xidian layer; HGS represents Huaguoshan layer; DSJ represents Dasanjiazi/Binggou profile; XBS/HDYZ represents Xiaobeishan/Huangdaoyingzi profile BMYZ/YJW represents Baomayingzi/Yuanjiawa profile; QDQ represents Qidaoquan profile; WJG/TSZ represents Wujiagou/Tuanshanzi profile.

Sinopterus dongi holotype (IVPP V 13363).

A, skeleton overview; B, left metacarpus; C, left foot; D, skull (right lateral view). E–H, respective schematic drawings. Abbreviations: ca, carpus; co, coracoid; cv, cervical vertebra; d, dentary; d1–d4, digits 1–4; epi, epiphysis; etp, extensor tendon process; f, frontal; fe, femur; fpc, frontoparietal crest; h, humerus; ios, interorbital septum; I, left; lpt, lateral proximal tarsal; m, maxilla; mc, metacarpal; mt, metatarsal; n, nasal; naof, nasoantorbital fenestra; pm, premaxilla; ph, phalanx; pt, pteroid; ti, tibia; ul, ulna; r, right; rad, radius; sca, scapula; st, sternum. Scale bars: A, 50 mm; E, 50 mm; F, 20 mm; G, 10 mm; H, 20 mm.



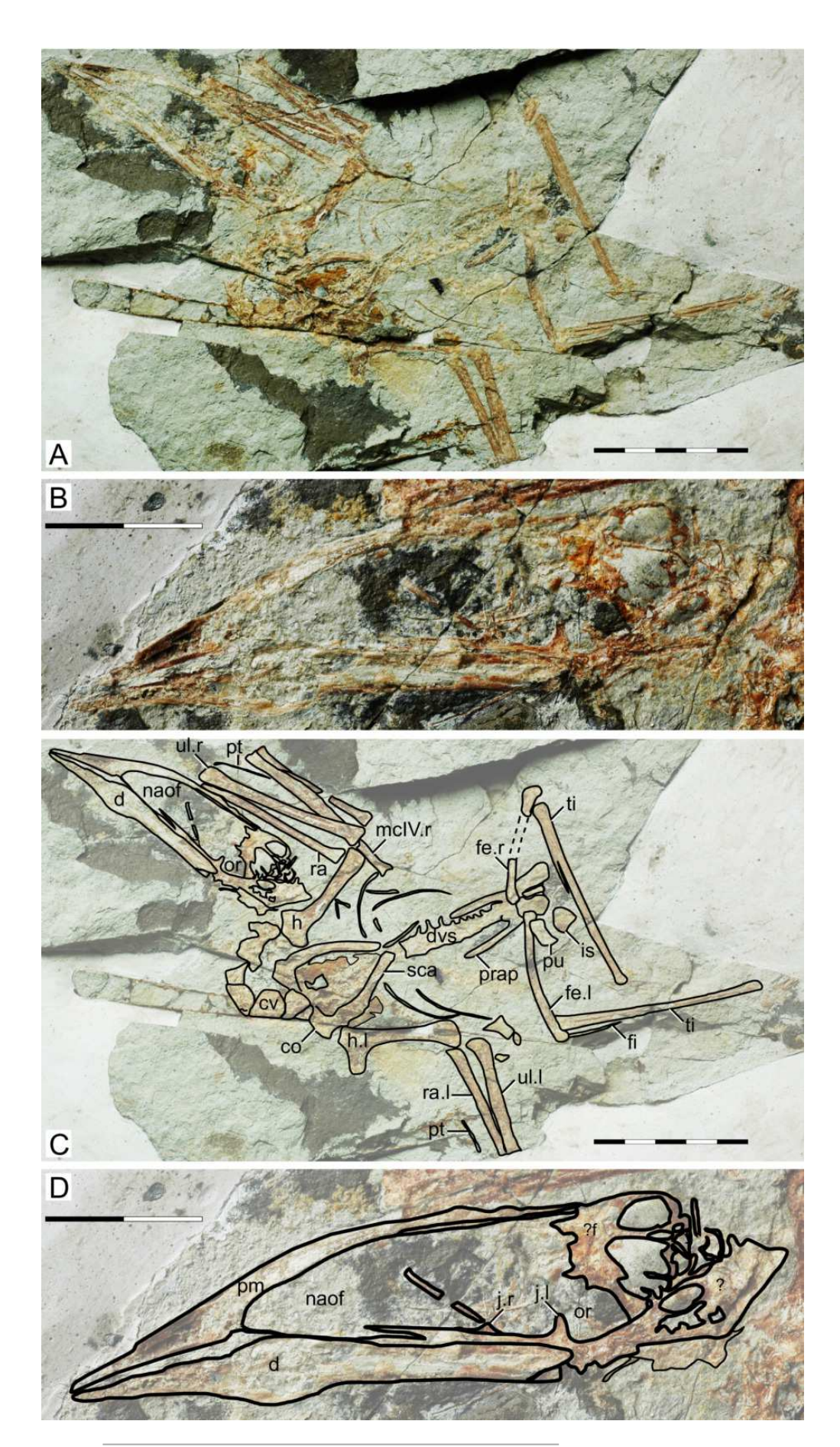


Sinopterus gui holotype (BPV-077).

A, skeleton overview; B, skull (left lateral view). C-D, respective schematic drawings.

Abbreviations: co, coracoid; cv, cervical vertebra; d, dentary; dvs, dorsal vertebral series; f, frontal; fe, femur; fi, fibula; fpc, frontoparietal crest; h, humerus; is, ischium; j, jugal; l, left; mc, metacarpal; mt, metatarsal; n, nasal; naof, nasoantorbital fenestra; or, orbit; pt, pteroid; pu, pubis; prap, preacetabular process; ti, tibia; ul, ulna; r, right; rad, radius; sca, scapula.

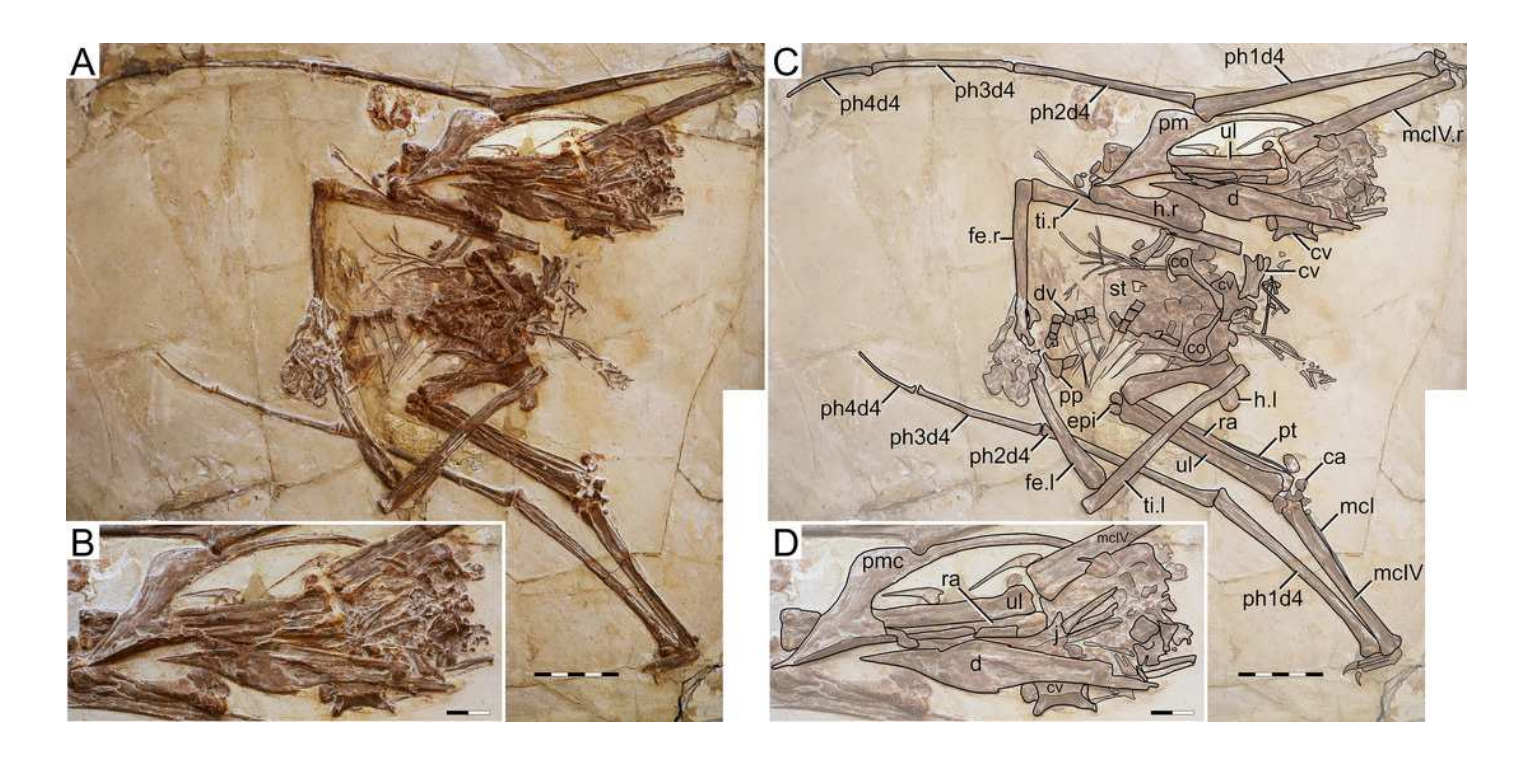
Scale bars: C, 50 mm; D, 50 mm.



PeerJ reviewing PDF | (2022:10:78770:0:1:NEW 3 Nov 2022)

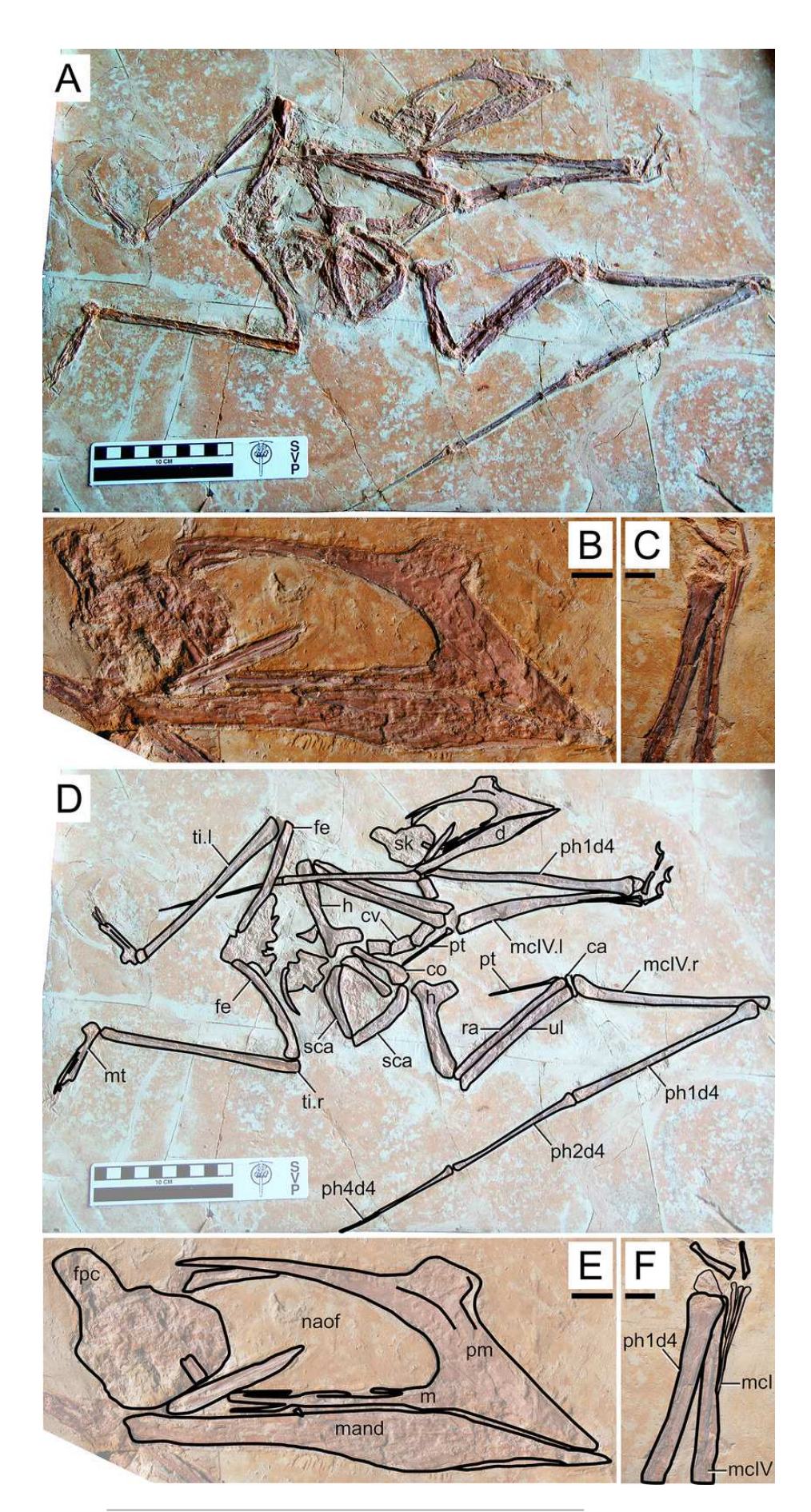
Huaxiapterus jii holotype (GMN-03-11-001).

A, skeleton overview; B, skull (left lateral view, slightly ventrolateral). C–D, respective schematic drawings. Abbreviations: ca, carpus; co, coracoid; cv, cervical vertebra; d, dentary; d1–d4, digits 1–4; dv, dorsal vertebra; epi, epiphysis; fe, femur; h, humerus; j, jugal; l, left; mc, metacarpal; pm, premaxilla; ph, phalanx; pp, prepubis; pt, pteroid; ti, tibia; ul, ulna; r, right; rad, radius; sca, scapula; st, sternum. Scale bars: C, 50 mm; D, 20 mm.



Huaxiapterus corollatus holotype (ZMNH M813).

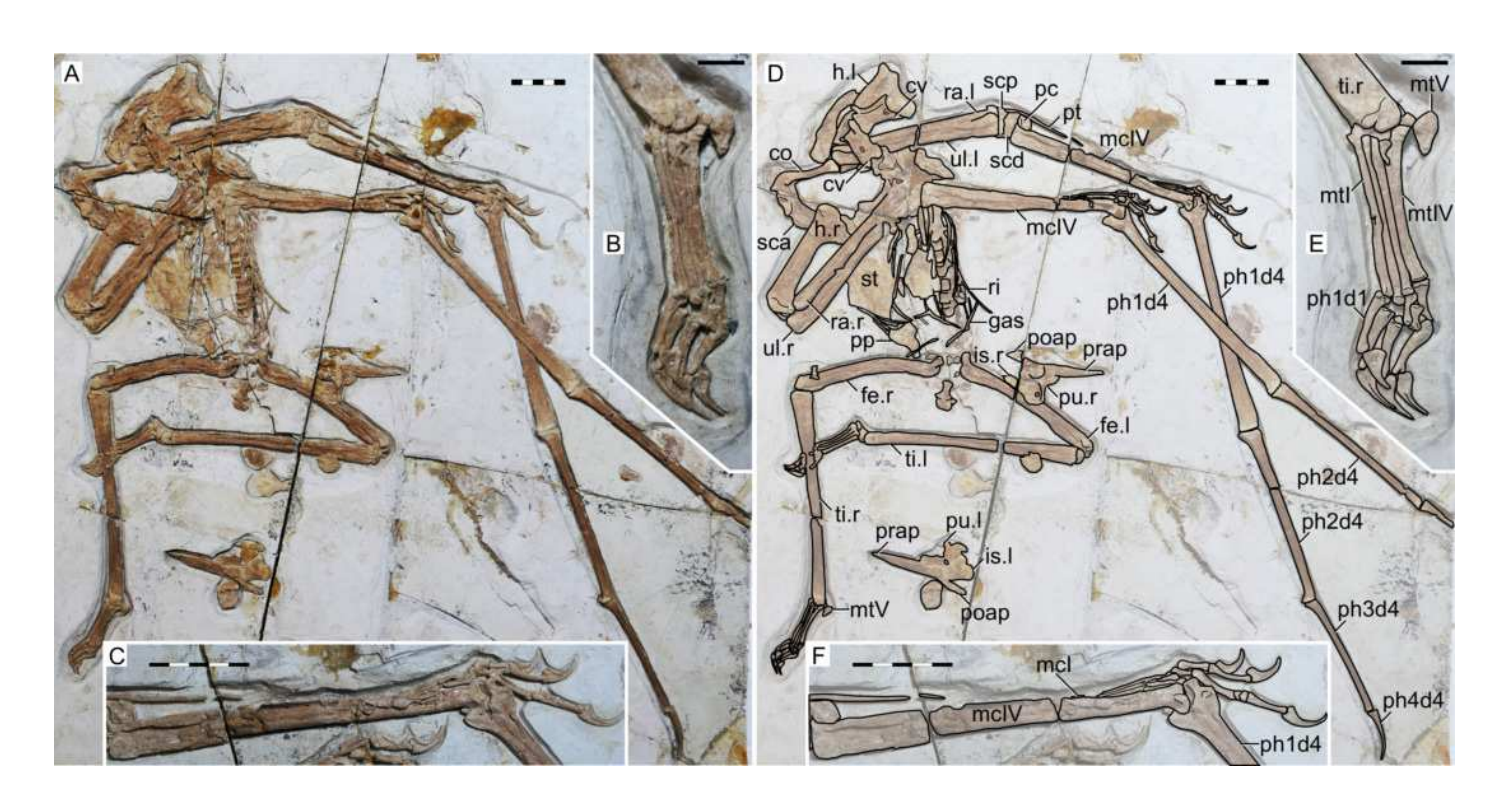
A, skeleton overview; B, skull (right lateral view); C, left metacarpus. D–F, respective schematic drawings. Abbreviations: ca, carpus; co, coracoid; cv, cervical vertebra; d, dentary; d1–d4, digits 1–4; fe, femur; fpc, frontoparietal crest; h, humerus; l, left; m, maxilla; mand, mandible; mc, metacarpal; mt, metatarsal; n, nasal; naof, nasoantorbital fenestra; pm, premaxilla; ph, phalanx; pt, pteroid; ti, tibia; ul, ulna; r, right; rad, radius; sca, scapula; sk, skull. Scale bars: A, D, 100 mm; E, F, 10 mm.



PeerJ reviewing PDF | (2022:10:78770:0:1:NEW 3 Nov 2022)

#### Specimen D2525.

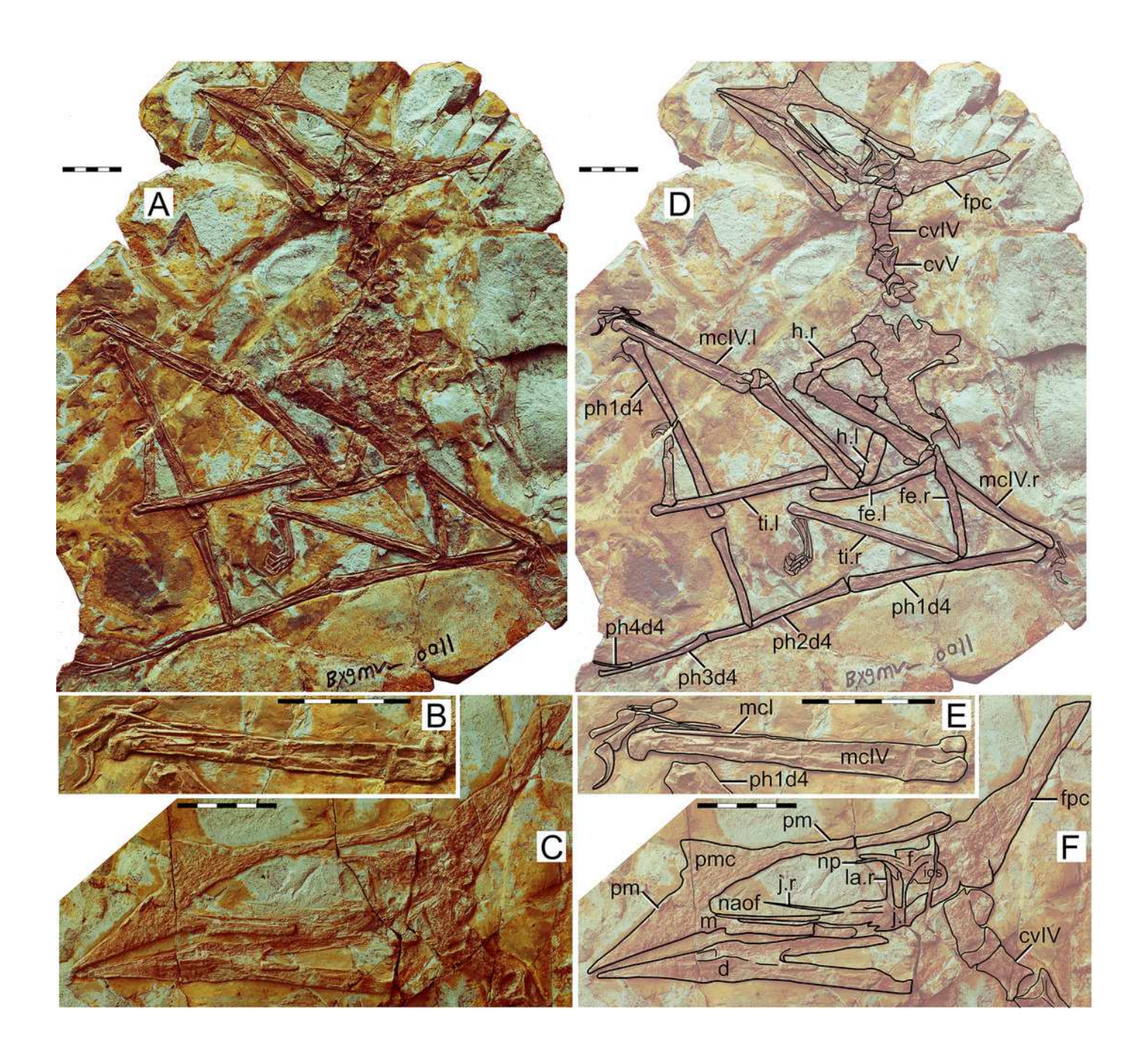
A, skeleton overview; B, right foot; C, right metacarpus. D-F, respective schematic drawings. Abbreviations: co, coracoid; cv, cervical vertebra; d, dentary; d1-d4, digits 1-4; dsc, distal synpcarpal; etp, extensor tendon process; f, frontal; fe, femur; fpc, frontoparietal crest; gas, gastralia; h, humerus; ios, interorbital septum; is, ischium; l, left; lpt, lateral proximal tarsal; mc, metacarpal; mt, metatarsal; pc, preaxial carpal; ph, phalanx; poap, postacetabular process; pp, prepubis; prap, preacetabular process; psc, proximal syncarpal; pt, pteroid; pu, pubis; ti, tibia; ul, ulna; r, right; rad, radius; ri, rib; sca, scapula; st, sternum. Scale bars: D, 50 mm; E, 10 mm; F, 50 mm.





Huaxiapterus benxiensis holotype (BXGM V0011).

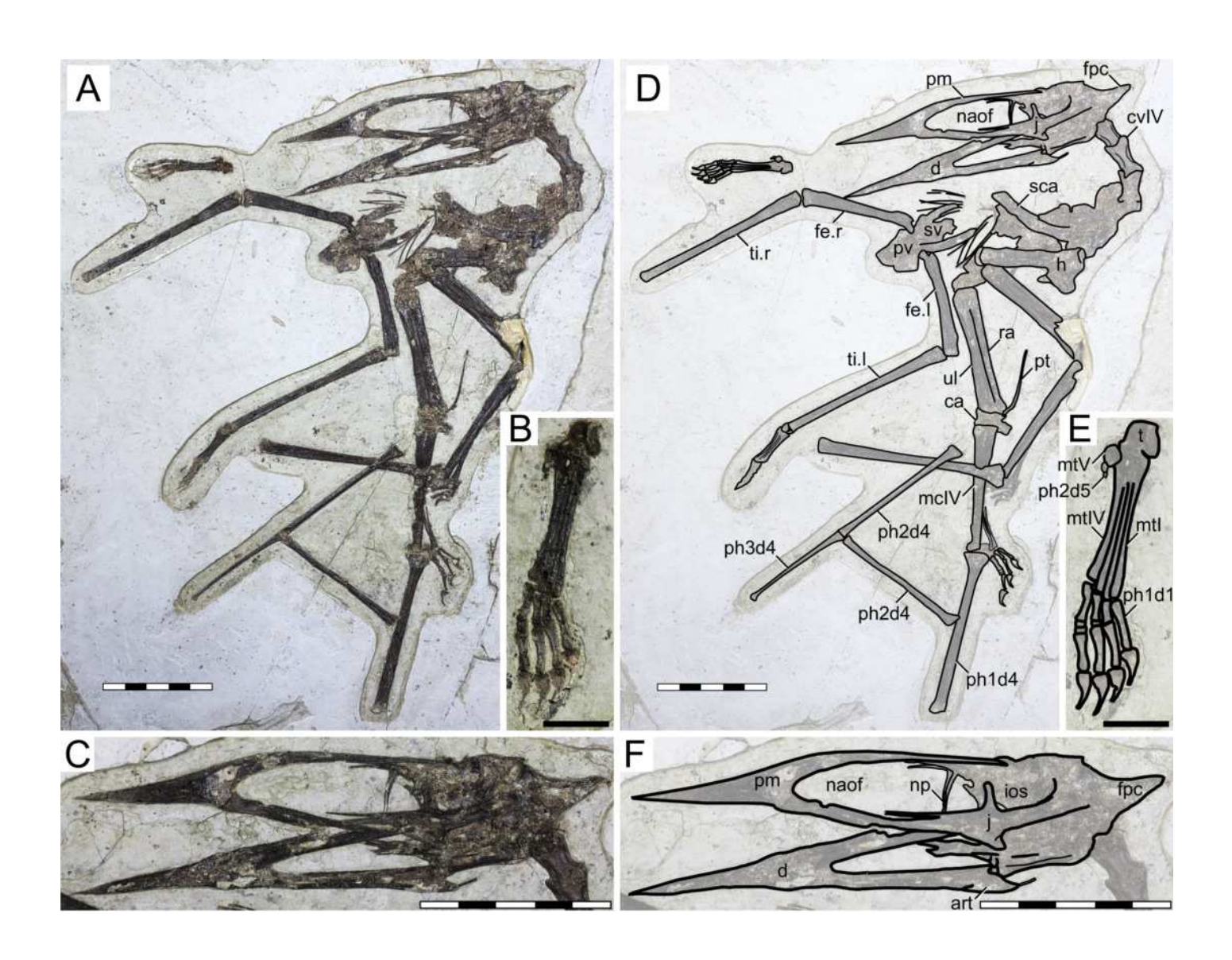
A, skeleton overview; B, left metacarpus; C, skull (left lateral view). D-F, respective schematic drawings. Abbreviations: cv, cervical vertebra; d, dentary; d1–d4, digits 1–4; f, frontal; fe, femur; fpc, frontoparietal crest; h, humerus; ios, interorbital septum; j, jugal; l, left; m, maxilla; la, lacrimal; mc, metacarpal; mt, metatarsal; naof, nasoantorbital fenestra; np, nasal process; pm, premaxilla; ph, phalanx; pt, pteroid; ti, tibia; ul, ulna; r, right; rad, radius. Scale bars: 50 mm.





Sinopterus lingyuanensis holotype (JPM-2014-005).

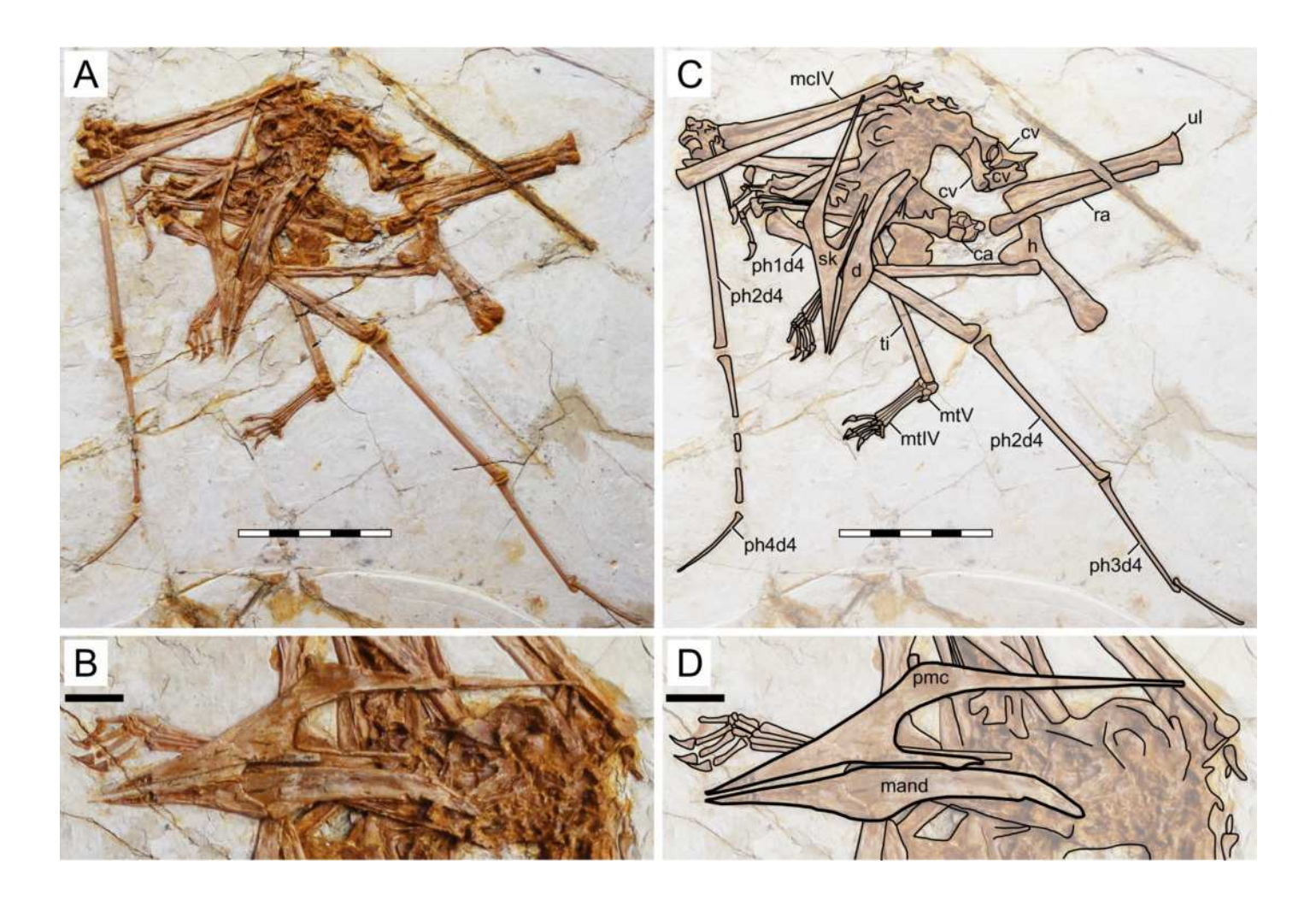
A, skeleton overview; B, right foot; C, skull (left lateral view). D–F, respective schematic drawings. Abbreviations: art, articular; ca, carpus; cv, cervical vertebra; d, dentary; d1–d4, digits 1–4; fe, femur; fpc, frontoparietal crest; h, humerus; ios, interorbital septum; j, jugal; l, left; lpt, lateral proximal tarsal; mc, metacarpal; mt, metatarsal; naof, nasoantorbital fenestra; np, nasal process; pm, premaxilla; ph, phalanx; pt, pteroid; pv, pelvis; t, tarsus; ti, tibia; ul, ulna; r, right; rad, radius; sca, scapula; sv, sacral vertebrae. Scale bars: D, 50 mm; E, 10 mm; F, 50 mm.



Huaxiapterus atavismus holotype (XHPM 1009).

A, skeleton overview; B, skull (left lateral view). C-D, respective schematic drawings.

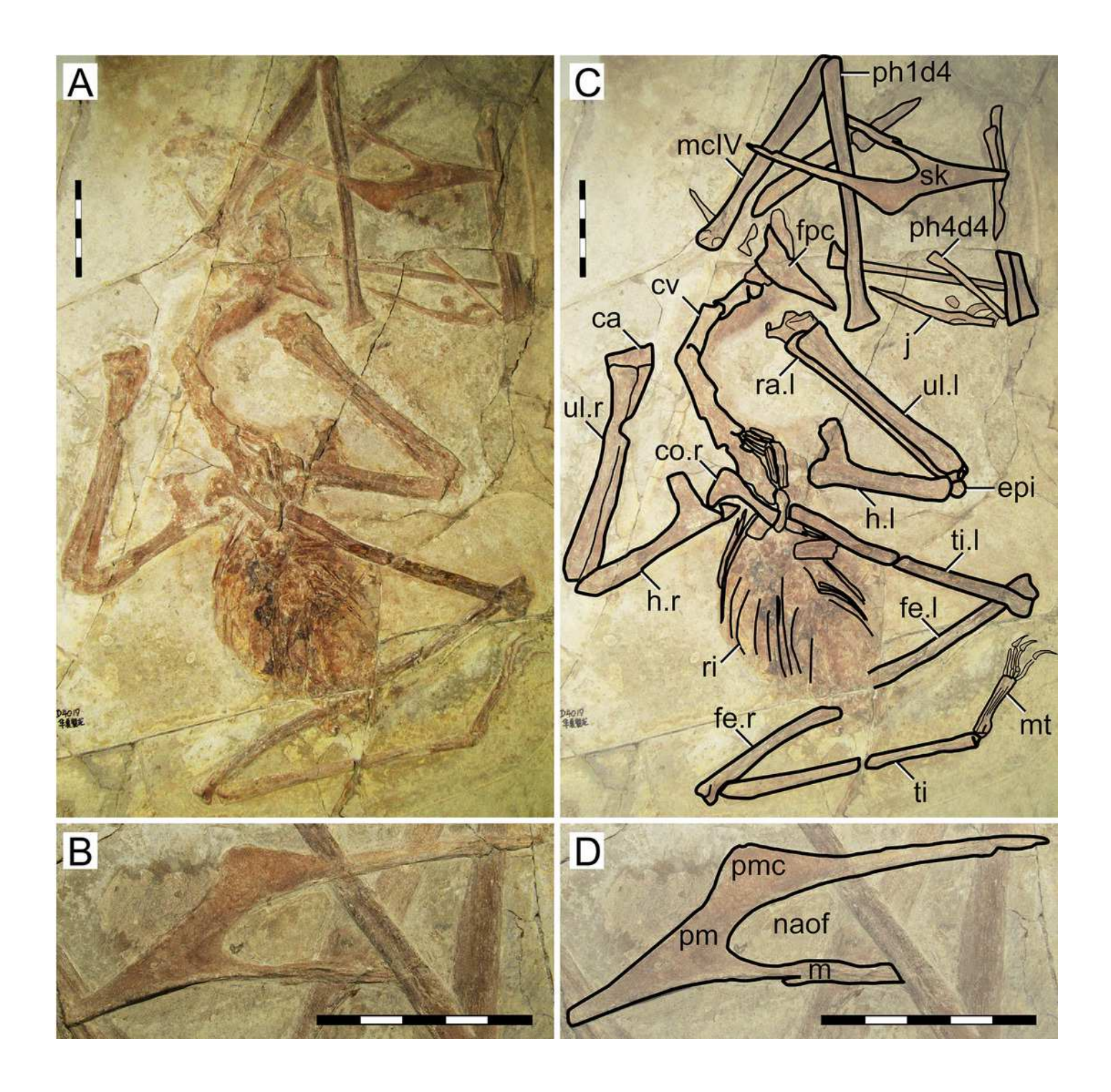
Abbreviations: ca, carpus; cv, cervical vertebra; co, coracoid; d, dentary; d1-d4, digits 1-4; fe, femur; fpc, h, humerus; mand, mandible; mc, metacarpal; mt, metatarsal; pmc, premaxillary crest; ph, phalanx; ti, tibia; ul, ulna; r, right; rad, radius; sk, skull. Scale bars: 50 mm.





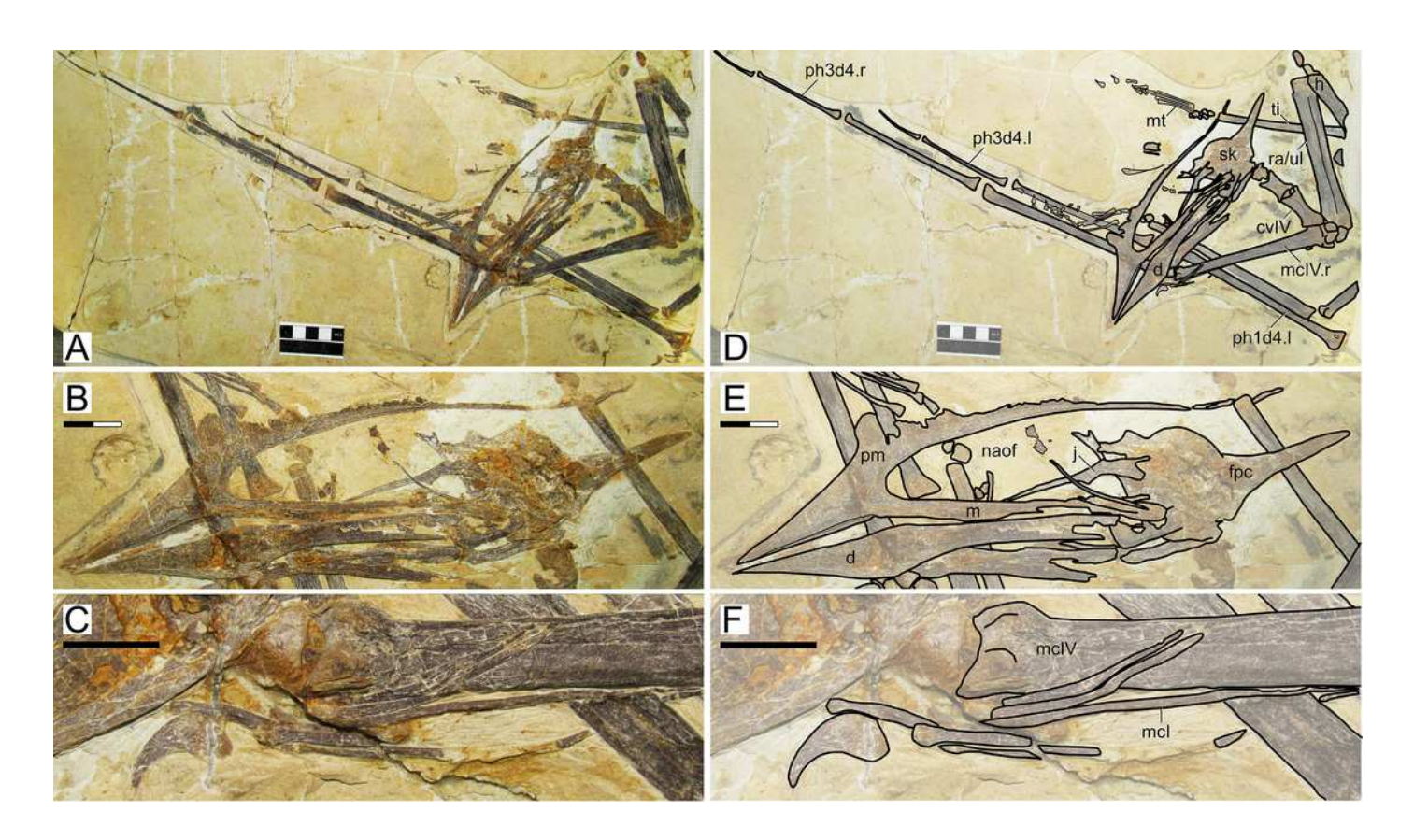
New specimen D4019.

A, skeleton overview; B, skull (left lateral view). C-D, respective schematic drawings. Abbreviations: ca, carpus; cv, cervical vertebra; d, dentary; d1-d4, digits 1-4; fpc, frontoparietala crest; h, humerus; j, jugal; m, maxilla; mc, metacarpal; mt, metatarsal; naof, nasoantorbital fenestra; pm, premaxilla; pmc, premaxillary crest; ph, phalanx; ti, tibia; ul, ulna; r, right; rad, radius; ri, rib; sk, skull. Scale bars: 50 mm.



New specimen BPMC 103.

A, skeleton overview; B, skull (left lateral view); C, metacarpus, distal region. D–F, respective schematic drawings. Abbreviations: cv, cervical vertebra; d, dentary; d1–d4, digits 1–4; fpc, frontoparietala crest; h, humerus; j, jugal; m, maxilla; mc, metacarpal; mt, metatarsal; naof, nasoantorbital fenestra; pm, premaxilla; pmc, premaxillary crest; ph, phalanx; ti, tibia; ul, ulna; r, right; rad, radius; ri, rib; sk, skull. Scale bars: D, 50 mm; E, 20 mm; F, 10 mm.





New specimen BPMC 104.

A, skeleton overview; B, skull (left lateral view); C, left pelvis; D right femur; E, right metatarsus; F, right pelvis; G, left metacarpus. H–N, respective schematic drawings.

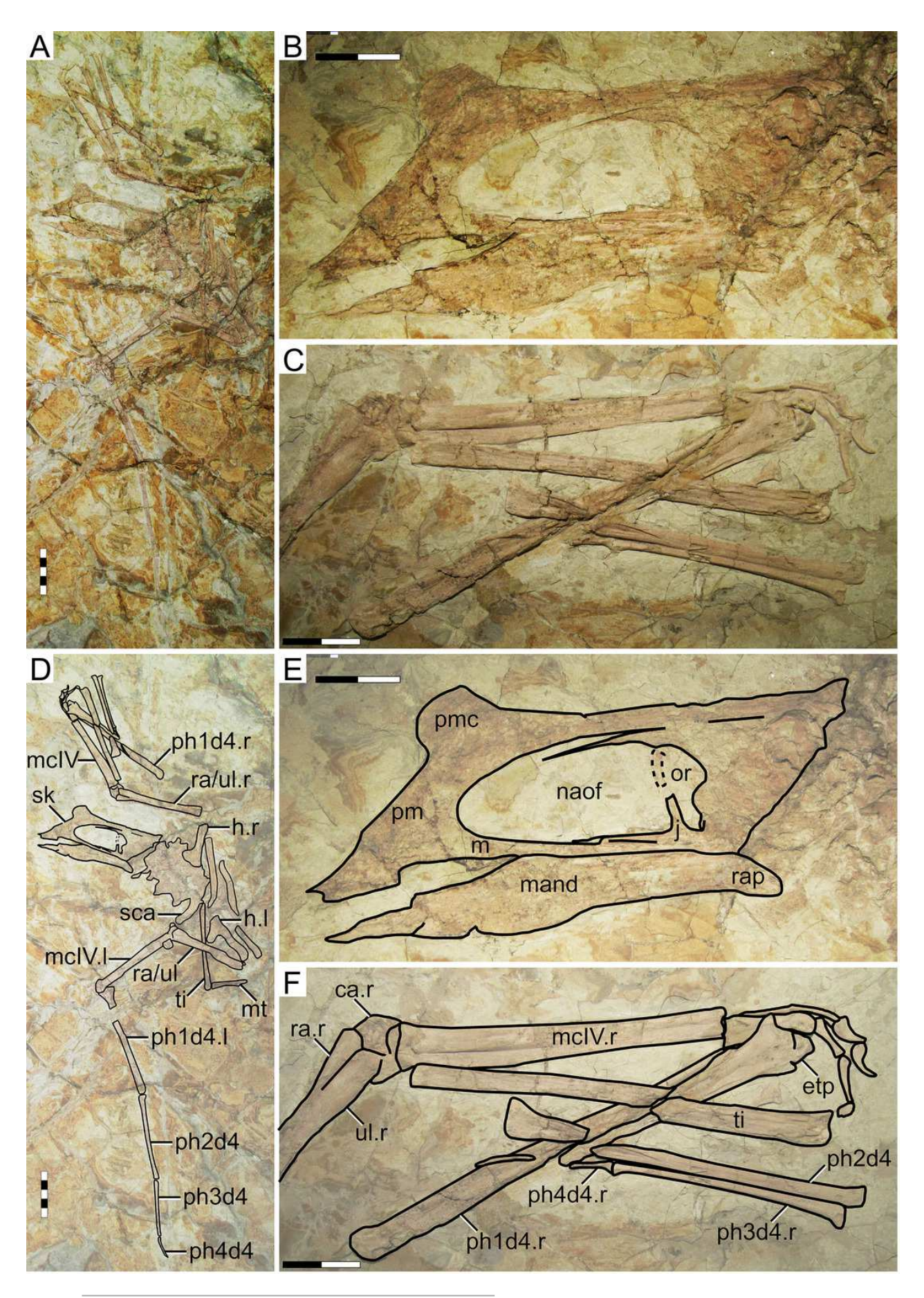
Abbreviations: cv, cervical vertebra; d, dentary; d1–d4, digits 1–4; etp, extensor tendon process; fe, femur; h, humerus; il, illium; is, ischium; m, maxilla; mc, metacarpal; mt, metatarsal; naof, nasoantorbital fenestra; pm, premaxilla; ph, phalanx; pp, prepubis; pu, pubis; pv, pelvis; ti, tibia; ul, ulna; r, right; sca, scapula; sk, skull; ti, tibia. Scale bars: H, 50 mm; J–N, 10 mm; G, 50 mm.





New specimen BPMC 105.

A, skeleton overview; B, skull (left lateral view); C, detail of right manus. D–F, respective schematic drawings. Abbreviations: ca, carpal; etp, extensor tendon process; h, humerus; j, jugal; l, left; mand, mandible; mc, metacarpal; naof, nasoantorbital fenestra; or, orbit; pm, premaxilla; pmc, premaxillary crest; ul, ulna; r, right; ra, radius; rap, retroarticular process; sca, scapula; sk, skull; ti, tibia. Scale bars: A, D, 50 mm; B, C, E, F, 20 mm.



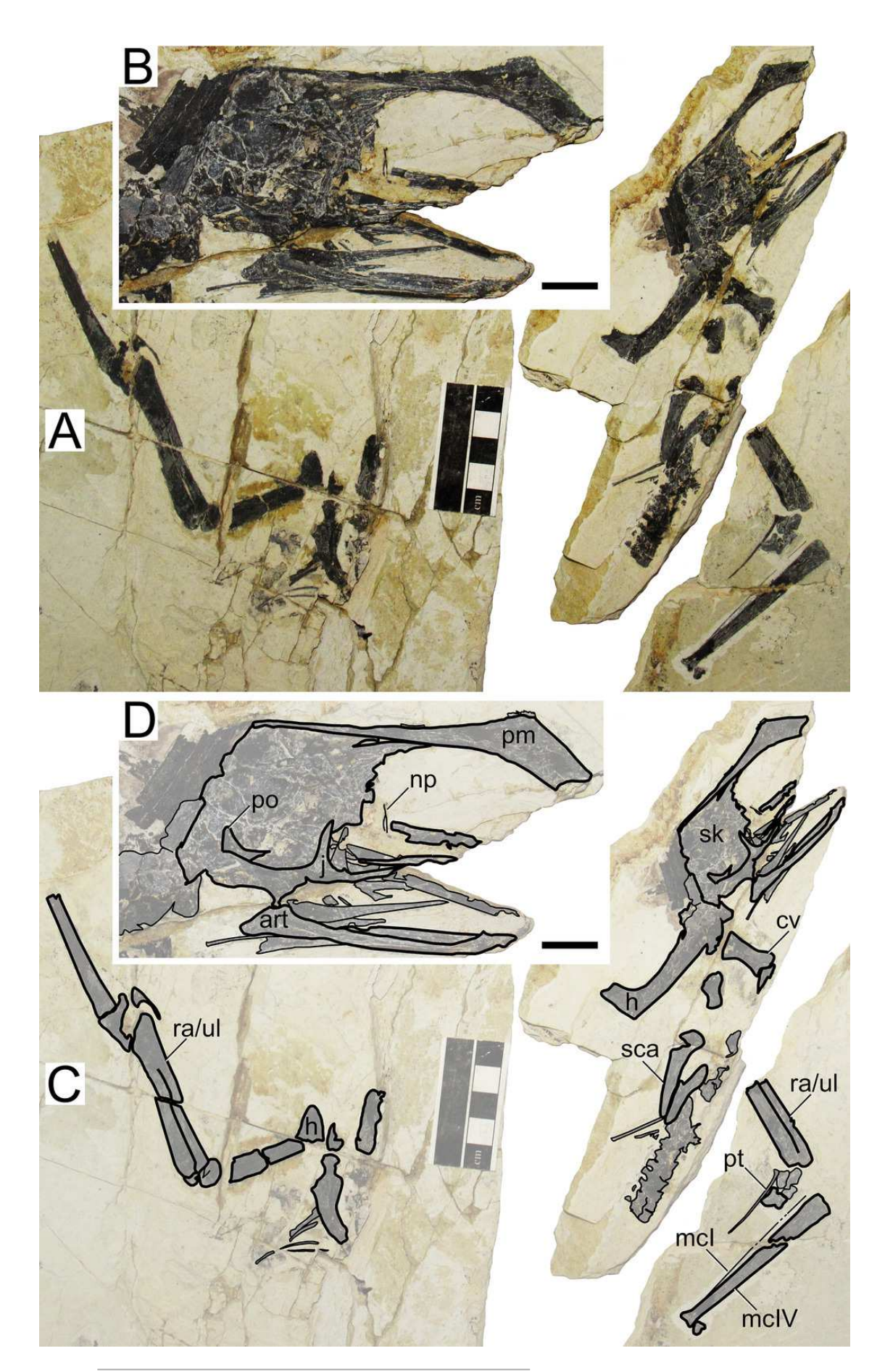
PeerJ reviewing PDF | (2022:10:78770:0:1:NEW 3 Nov 2022)



New specimen BPMC 106.

A, skeleton overview; B, skull (right lateral view). C-D, respective schematic drawings.

Abbreviations: art, articular; cv, cervical vertebra; h, humerus; j, jugal; mc, metacarpal; np, nasal process; pm, premaxilla; po, postorbital; pt, pteroid; ul, ulna; rad, radius; sca, scapula; sk, skull. Scale bars: A, C, 50 mm; B, D, 10 mm.

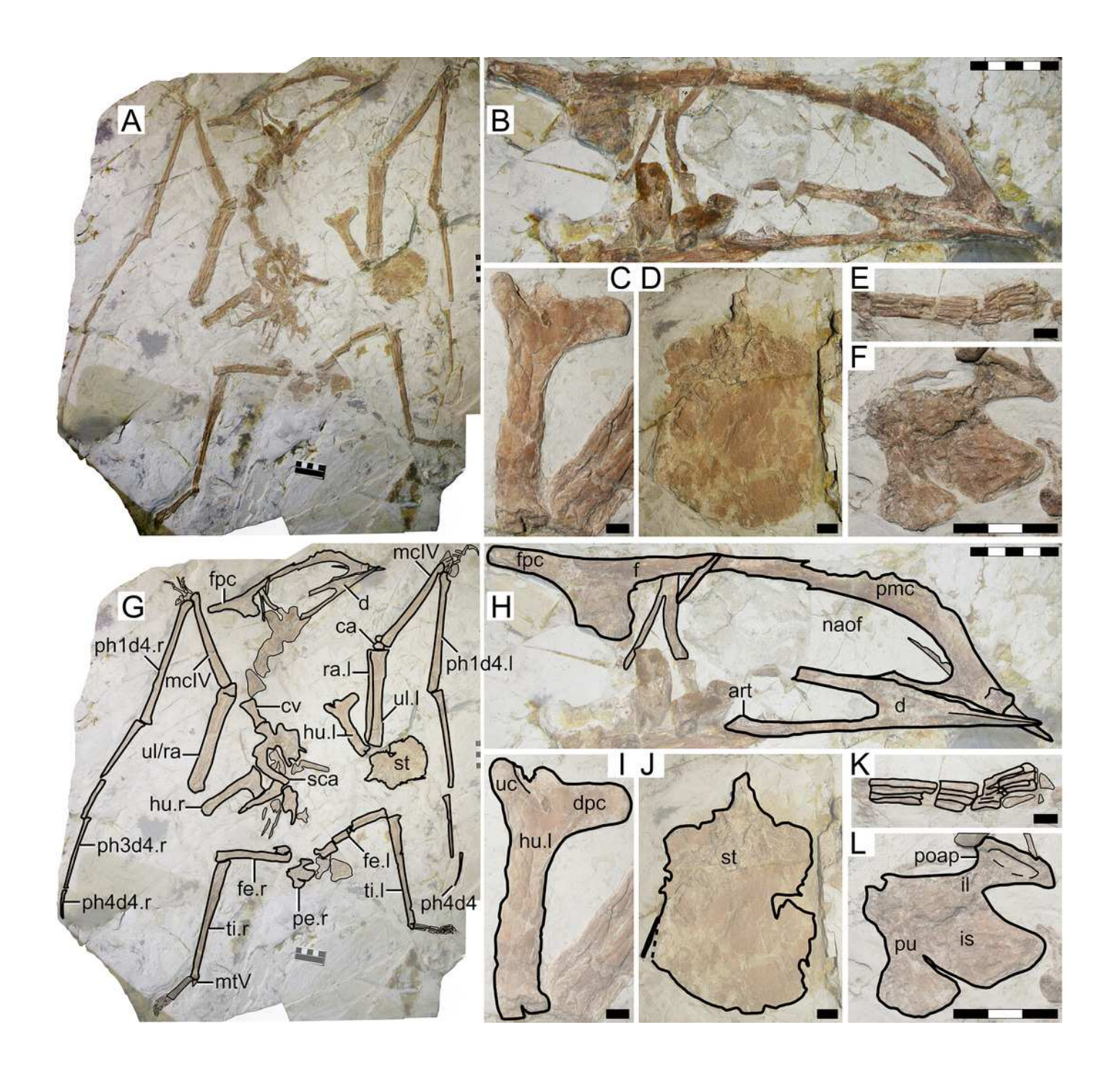


PeerJ reviewing PDF | (2022:10:78770:0:1:NEW 3 Nov 2022)



New specimen BPMC 107.

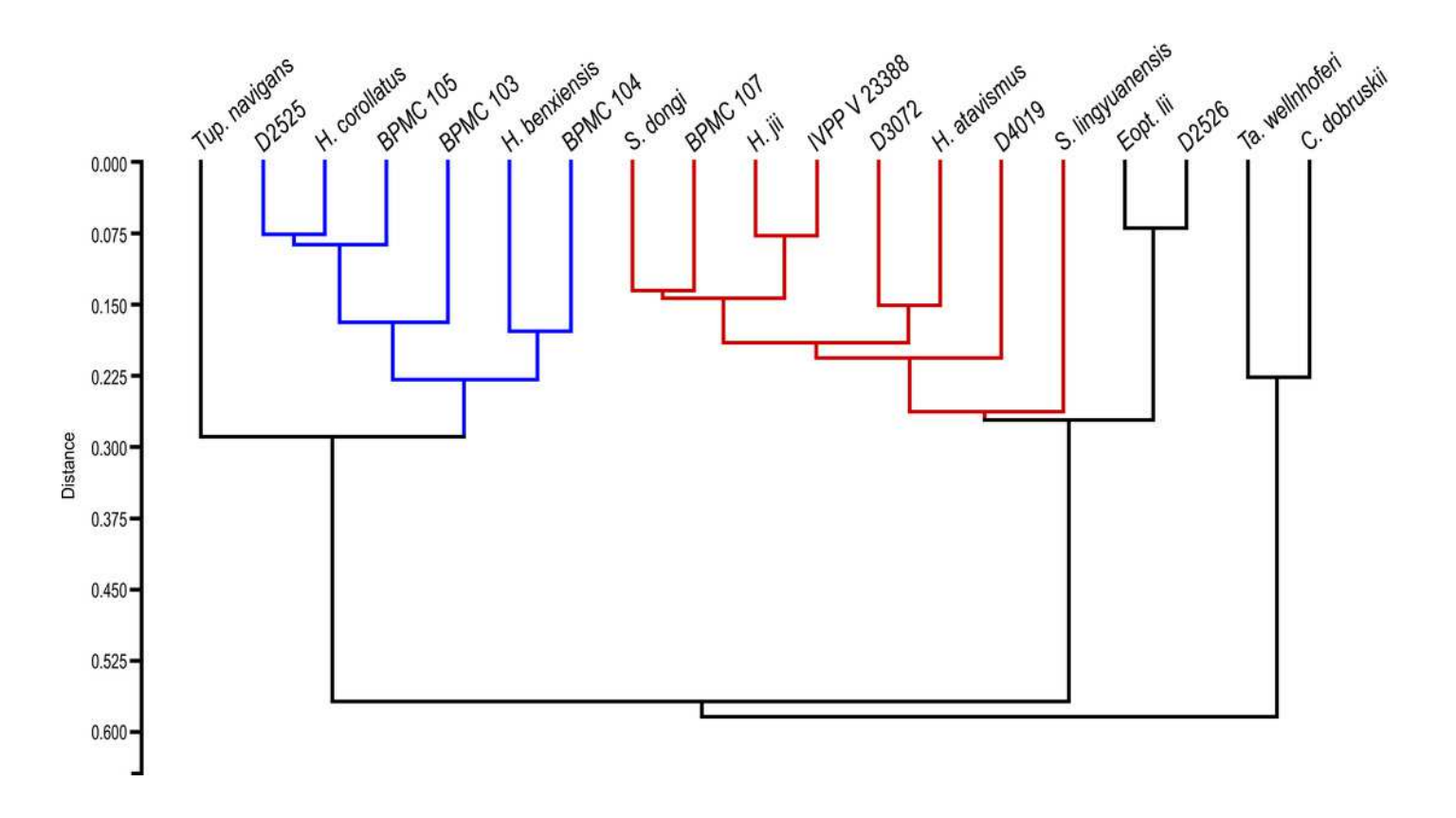
A, skeleton overview; B, skull (right lateral view); C, left humerus; D, sternum; E, left foot; F, right pelvis. G–L, respective schematic drawings. Abbreviations: art, articular; ca, carpus; cv, cervical vertebra; d, dentary; d1–d4, digits 1–4; dpc, deltopectoral crest; f, frontal; fe, femur; fpc, frontoparietal crest; h, humerus; il, illium; is, ischium; l, left; mc, metacarpal; mt, metatarsal; naof, nasoantorbital fenestra; pmc, premaxillary crest; ph, phalanx; poap, postacetabular process; pt, pteroid; pu, pubis; ti, tibia; ul, ulna; r, right; rad, radius; sca, scapula; st, sternum; uc, ulnar crest. Scale bars: A, B, G, H, 50 mm; l–K, 10 mm; L, 30 mm.





Resulting dendrogram of the UPGMA analysis.

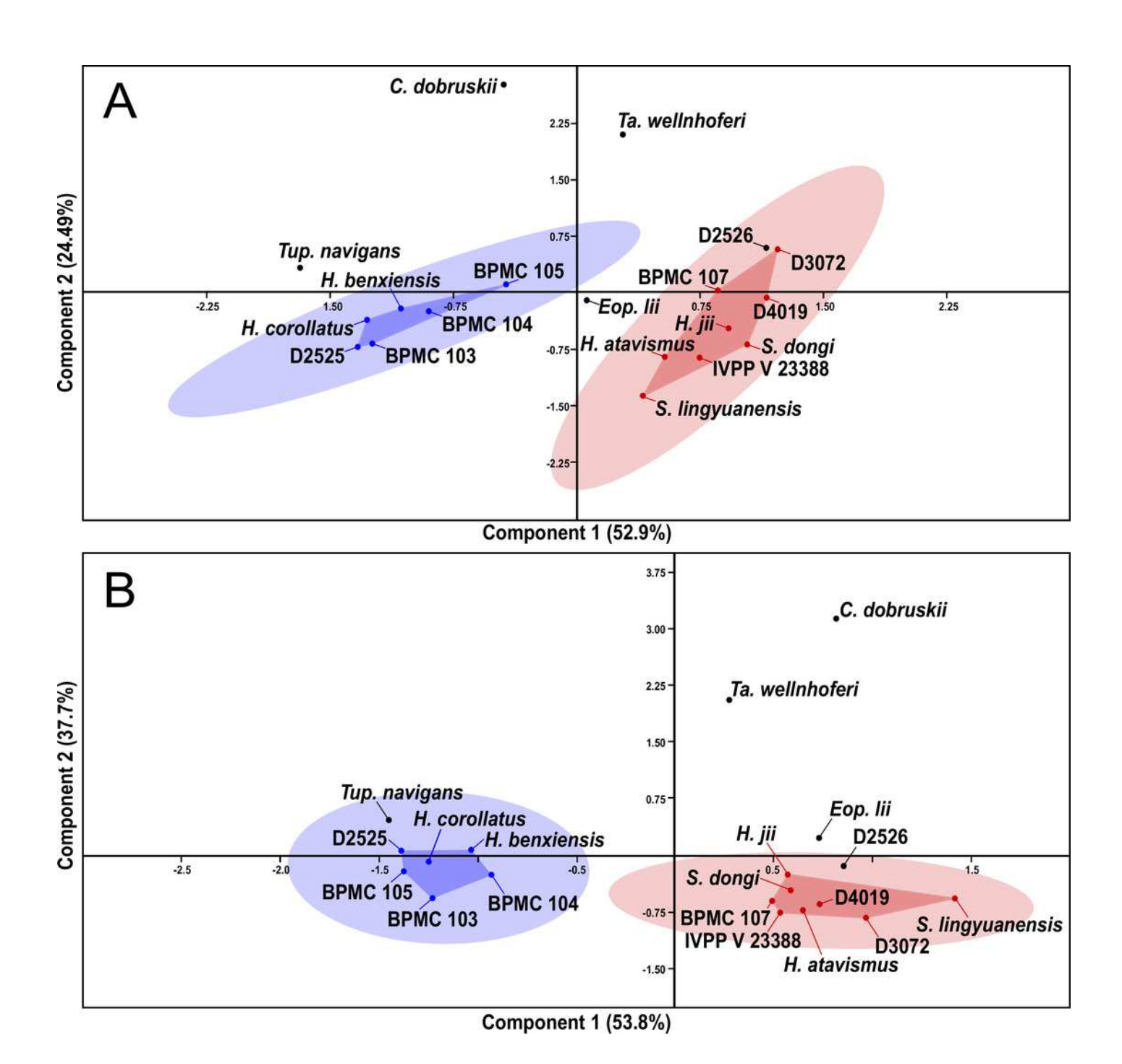
Species names represent their holotypic specimens. Red indicates Morphotype I. Blue indicates Morphotype II.





Results of the PCA analyses.

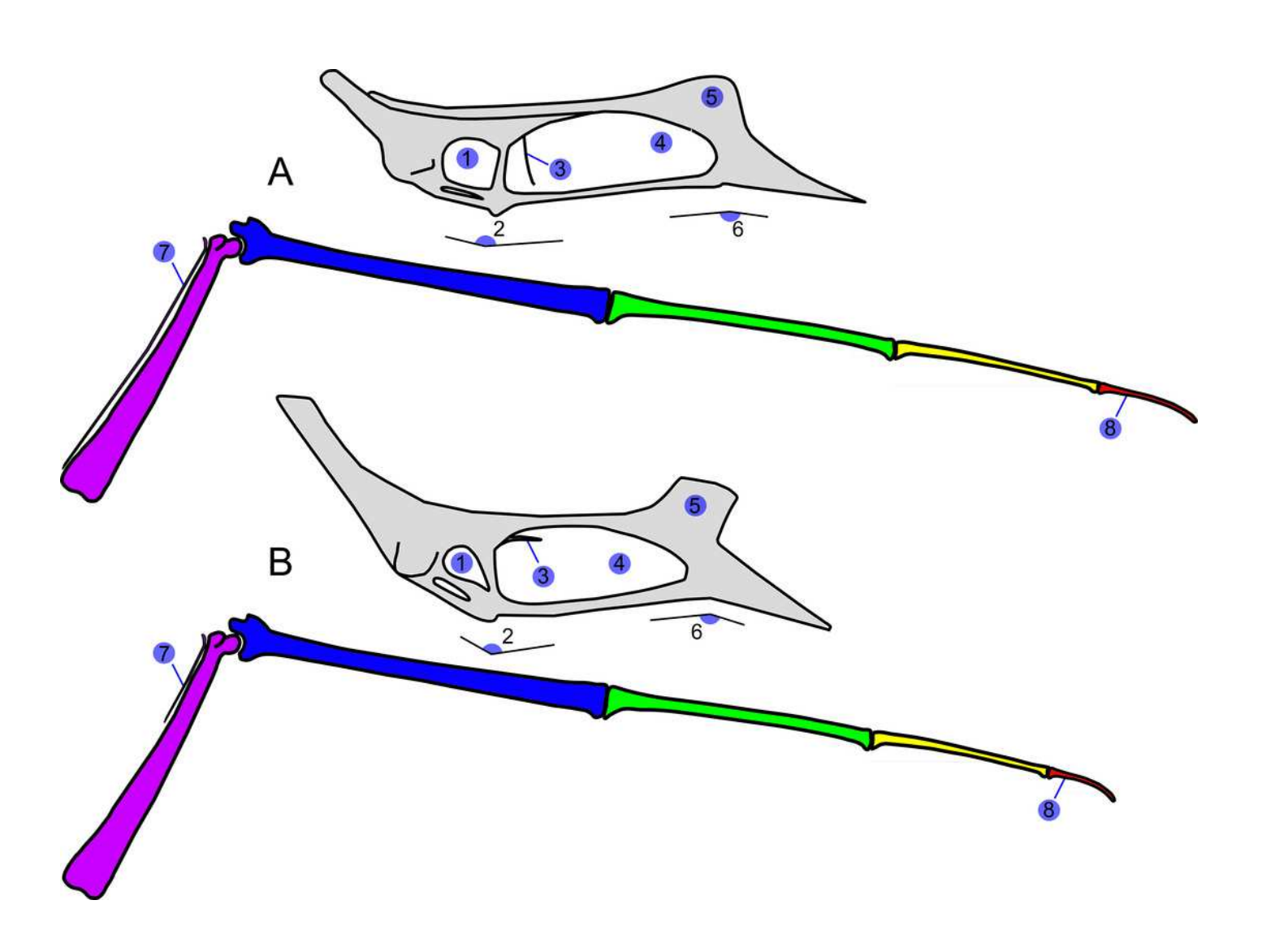
A, graph based on components 1 and 2 of the analysis using mean values imputation for the missing data. B, graph based on components 1 and 2 of the analysis using iterative imputation for the missing data. Species names represent their holotypic specimens. Red indicates Morphotype I (polygon represents convex hull; ellipse represents the 95% confidence ellipse). Blue indicates Morphotype II (polygon represents convex hull; ellipse represents the 95% confidence ellipse).





Anatomical variation in the skull and wing in the Sinopterus complex.

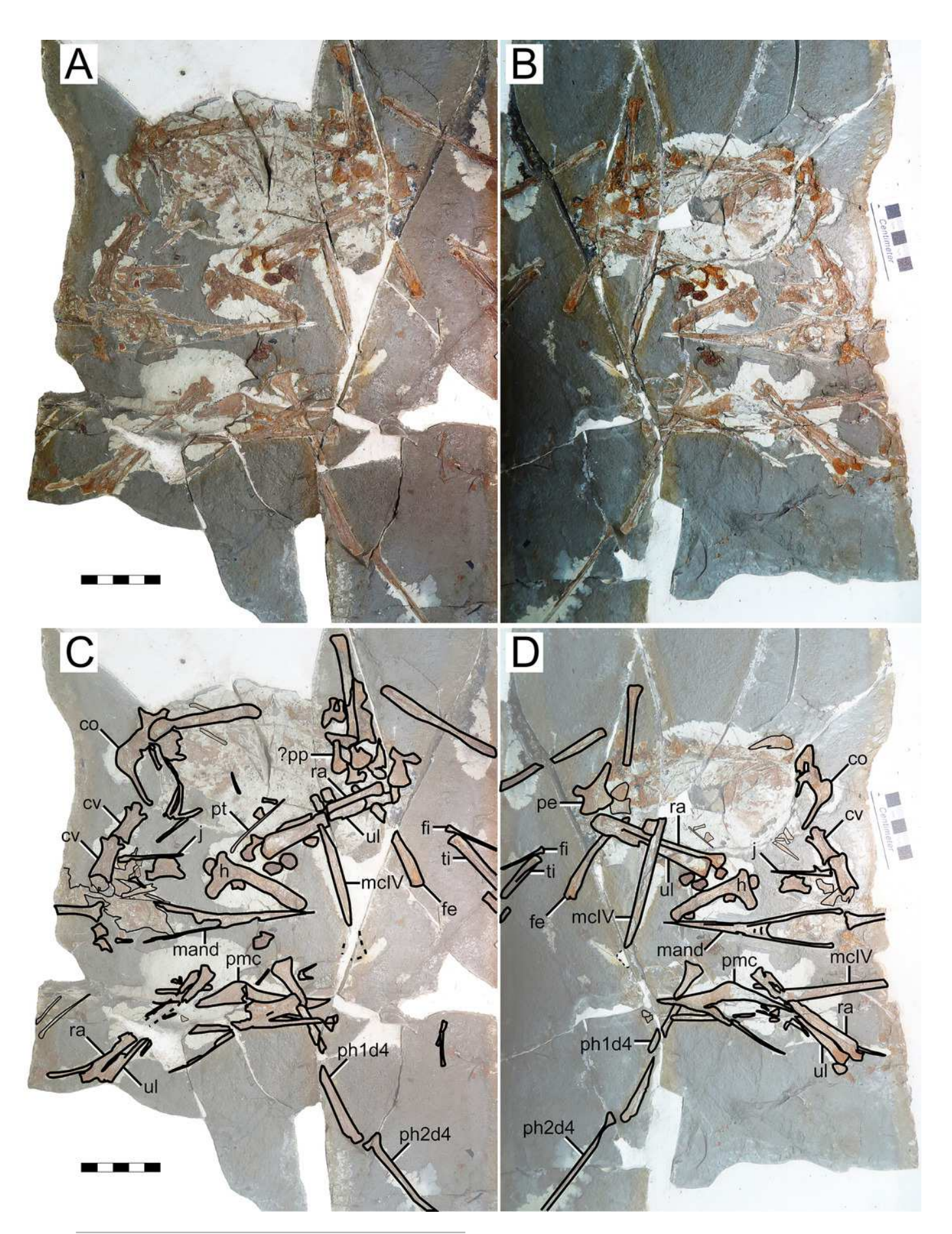
A, schematic representation of skull and metacarpus + wing digit of Morphotype I (*S. dongi*). Based mainly on the holotype of *S. dongi* ( IVPP V 13363 ), except for the premaxillary crest (based on the holotype of *H. jii*; GMN-03-11-001 ). B, schematic representation of skull and metacarpus + wing digit of Morphotype II (*H. corollatus*). Based mainly on the holotype of *H. benxiensis* (BXGM V0011). A and B are not to scale, but are both proportionately scaled to the same metacarpal IV length. Numbers indicate features that vary between *S. dongi* and *H. corollatus* (see text): 1) orbit shape; 2) quadrate reclination; 3) nasal process shape; 4) nasoantorbital fenestra length/height ratio; 5), premaxillary crest shape; 6) rostrum deflection; 7) metacarpal I length; 8) wing phalanx 4 length.





Eopteranodon lii holotype (BPV 078).

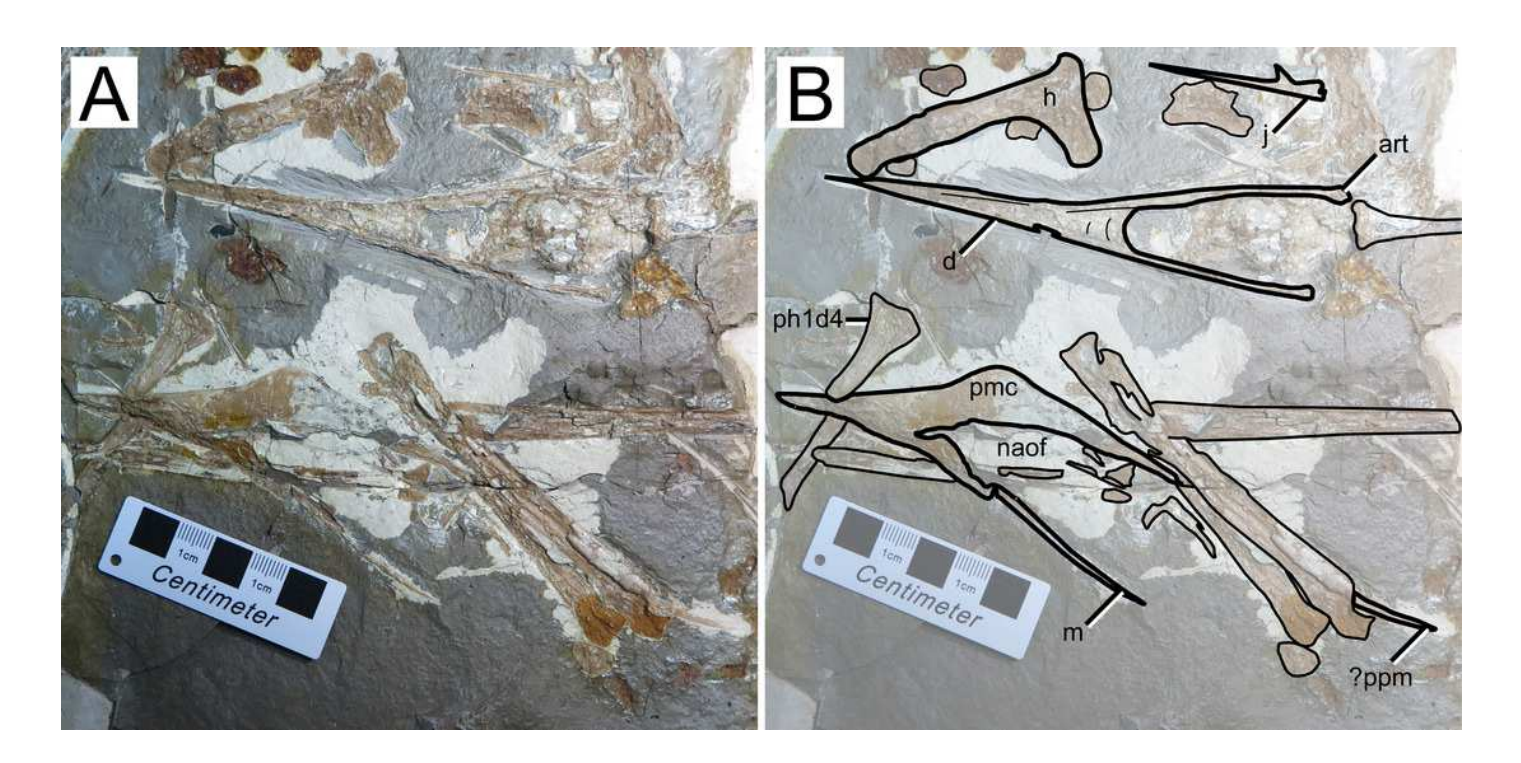
A, counterpart; B, main part. C-D, respective schematic drawings. Abbreviations: cv, cervical vertebra; co, coracoid; d1-d4, digits 1-4; fe, femur; fi, fibula; h, humerus; j, jugal; mand, mandible; mc, metacarpal; pmc, premaxillary crest; pe, pelvis; ph, phalanx; ti, tibia; ul, ulna; rad, radius. Scale bars: C, 50 mm; D, 10 mm.



PeerJ reviewing PDF | (2022:10:78770:0:1:NEW 3 Nov 2022)

Eopteranodon lii holotype (BPV 078) details.

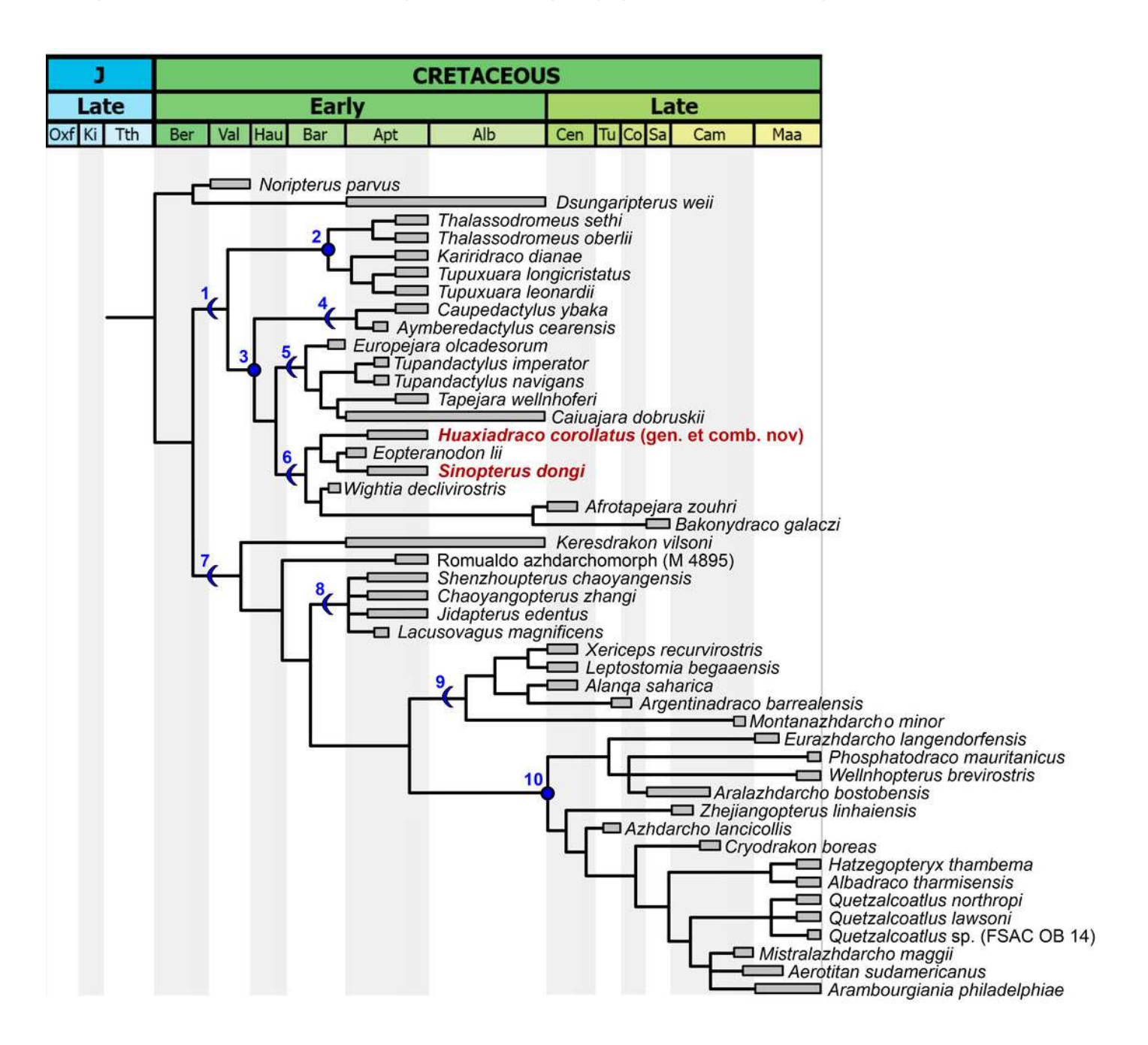
A, close-up of the specimen's main part, and B, schematic drawing. Abbreviations: art, articular; d, dentary; h, humerus; m, maxilla; naof, nasoantorbital fenestra; pmc, premaxillary crest; ppm, posterior premaxillary process. Scale bars: 50 mm.



Time-calibrated strict consensus tree.

The two species of the *Sinopterus* complex here regarded as valid are indicated in dark red.

1: Tapejaromorpha. 2: Thalassodromidae. 3: Tapejaridae. 4: Caupedactylia. 5: Tapejarinae. 6: Sinopterinae. 7: Azhdarchomorpha. 8: Chaoyangopteridae. 9: Alanqidae. 10: Azhdarchidae.



Life reconstruction of the Jiufotang tapejarids.

The coexistence between *Sinopterus dongi* and *Huaxiadraco corollatus* comb. nov. in the Jiufotang paleoenvironment. Art: courtesy of Zhao Chuang.





Table 1(on next page)

Systematic nomenclature.

Clade	Nominal author	Definition	Composition and remarks	ICPN conversion and Regnum code
Tapejaroidea	Kellner (2003)	The least inclusive clade containing <i>Tapejara</i> wellnhoferi Kellner 1989, <i>Quetzalcoatlus</i> northropi Lawson 1975, and <i>Dsungaripterus</i> weii Young 1964.	Includes the sister-taxa Dsungaripteridae and Azhdarchoidea.	This work [820].
Azhdarchoidea	Unwin (1995)	The least inclusive clade containing <i>Tapejara</i> wellnhoferi Kellner 1989 and <i>Quetzalcoatlus</i> northropi Lawson 1975.	Includes the sister-taxa Tapejaromorpha and Azhdarchomorpha.	Andres (2021), [355].
Tapejaromorpha	Andres <i>et al.</i> (2014)	The most inclusive clade containing <i>Tapejara</i> wellnhoferi Kellner 1989 but not <i>Azhdarcho</i> lancicollis Nessov 1984.	Includes the sister-taxa Tapejaridae and Thalassodromidae.	Andres (2021), [356].
Thalassodromidae	Witton (2008)	The least inclusive clade containing Thalassodromeus sethi Kellner & Campos 2002 and Tupuxuara longicristatus Kellner & Campos 1988.	Includes <i>Thalassodromeus</i> , <i>Tupuxuara</i> , and <i>Kariridraco</i> .	Andres (2021), [770].
Tapejaridae	Kellner (1989)	The least inclusive clade containing <i>Tapejara</i> wellnhoferi Kellner 1989, <i>Sinopterus dongi</i> Wang & Zhou 2003, and <i>Caupedactylus ybaka</i> Kellner 2013.	The first registered definition (Andres, 2021) is (unrestrictedly) emended here (by the addition of <i>Caupedactylus</i> as an internal specifier) in order to stabilize the clade's diagnosis, usage, and content, under the context of the present reference phylogeny. Characterized mainly by downturned rostra and tall rostral crests, it contains Caupedactylia and Eutapejaria.	Andres (2021), [357], unrestrictedly emended here.
Caupedactylia	This work.	The most inclusive clade containing Caupedactylus ybaka Kellner 2013 but not Tapejara wellnhoferi Kellner 1989.	Includes <i>Caupedactylus</i> and <i>Aymberedactylus</i> . This clade englobes tapejarids which share a symphyseal shelf dorsoventrally steep and deep, and a flat dentary fossa.	This work, [821].
Eutapejaria	This work.	The most inclusive clade containing <i>Tapejara</i> wellnhoferi Kellner 1989 but not <i>Caupedactylus</i> ybaka Kellner 2013.	This clade englobes tapejarids which share a dorsal dentary eminence, and contains Tapejarinae and Sinopterinae ( <i>sensu</i> Andres, 2021).	This work, [822].
Azhdarchomorpha	Pêgas <i>et</i> al. (2021)	The most inclusive clade containing <i>Azhdarcho lancicollis</i> Nessov 1984 but not <i>Thalassodromeus sethi</i> Kellner & Campos 2002 or <i>Tapejara wellnhoferi</i> Kellner 1989.	Includes <i>Keresdrakon</i> , Chaoyangopteridae, Alanqidae, and Azhdarchidae.	Pêgas <i>et al.</i> (2021), [574].

Chaoyangopteridae	Lü <i>et al</i> . 2008	The most inclusive clade containing Chaoyangopterus zhangi Wang & Zhou 2003 but not Quetzalcoatlus northropi Lawson 1975.	Includes Chaoyangopterus, Jidapterus, Shenzhoupterus, and Lacusovagus.	Andres (2021), [368].
Azhdarchiformes	Andres (2021)	The most inclusive clade containing Quetzalcoatlus northropi Lawson 1975 but not Chaoyangopterus zhangi Wang & Zhou 2003.	Under the present reference phylogeny, the Azhdarchiformes include Alanqidae and Azhdarchidae.	Andres (2021), [771].
Alanqidae	Pêgas <i>et al.</i> 2021	The most inclusive clade containing <i>Alanqa</i> saharica Ibrahim et al. 2010 but not <i>Chaoyangopterus zhangi</i> Wang & Zhou 2003 or <i>Azhdarcho lancicollis</i> Nessov 1984.	Includes <i>Alanqa</i> , <i>Argentinadraco</i> , <i>Xericeps</i> , <i>Leptostomia</i> , and <i>Montanazhdarcho</i> . Characterized by bowed-out lateral jaw margins in cross-section, and possibly by a pair of dentary occlusal ridges.	Pêgas <i>et al.</i> (2021), [576].
Azhdarchidae	Padian 1986	The least inclusive clade containing <i>Azhdarcho lancicollis</i> Nessov 1984, <i>Phosphatodraco mauritanicus</i> Pereda-Suberbiola <i>et al.</i> 2003, and <i>Quetzalcoatlus northropi</i> Lawson 1975.	Includes Eurazhdarcho, Aralazhdarcho, Phosphatodraco, Wellnhopterus, Zhejiangopterus, Azhdarcho, and Quetzalcoatlinae. Characterized by a vestigial cervical neural spine.	Andres (2021), [371]. Emended by Pêgas <i>et al</i> . (2021).

2 Table 1. Systematic nomenclature.



Table 2(on next page)

Results of the SMA analyses.



					Intercep	SMA lower	SMA upper	Correlatio	
X	y	p	$\mathbb{R}^2$	Slope	t	CI	CI	n	n
	rostru								
humeru s	m index	0.037	0.399	-1,103	3,87	-3,683	-0,55	-	11
	rostral value	0.017	0.484	-0,703	1,988	-1,078	-0,36	-	11
	rostru m def.	0.079	0.253	-0,13	0.722	0.22	1.09	N/C	13
	naof h/l	0.172	0.195	-0,577	1,472	-2,299	-0,184	N/C	11
	orbit°	0.392	0.248	-0,715	3,202	-3,437	0,146	N/C	5
	Q°	0.231	0.591	-0,194	2,543	-0,514	0,003	N/C	4
	cv IV	0.0056	0.746	0,872	-0,19	0,605	1,324	N/C	8
	cv V	< 0.001	0.855	1,047	-0,555	0,668	1,471	=	8
	ul	< 0.001	0.961	1,106	-0,029	0,957	1,238	=	16
	pt	< 0.001	0.864	1,122	-0,396	0,738	1,394	=	11
	mcI	0.837	0.004	-1,89	5,479	-6,655	-0,905	N/C	12
	mcIV	< 0.001	0.922	1,1562	-0,08	0,933	1,372	=	16
	ph1	< 0.001	0.971	1,083	0,15	0,939	1,197	=	15
	ph2	< 0.001	0.965	1,081	0,034	0,947	1,201	=	15
	ph3	< 0.001	0.901	0,986	0,047	0,827	1,111	=	13
	ph4	0.122	0.202	1,0535	-0,367	0,379	3,381	N/C	13
	fe	< 0.001	0.957	1,144	-0,179	1,00	1,262	≅ (+)	13
	ti	< 0.001	0.943	1,1811	-0,084	1,008	1,305	$\cong$ (+)	15
	mtI	< 0.001	0.94	0,921	-0,249	0,701	1,131	=	11
	mtII	< 0.001	0.936	0,889	-0,174	0,616	1,081	=	12

<sup>1</sup> 

6 tíbia; ul, ulna.

<sup>2</sup> Table 2. Results of the SMA analyses. Abbreviations: CI, one-tailed 95% confidence interval;

<sup>3</sup> N/C, non-correlated; -, negative allometry; =, isometry;  $\cong$ , near-isometry; +, positive allometry.

<sup>4</sup> Anatomical abbreviations: cv, cervical vertebra; def., deflection; fe, femur; h, height/ l, length;

<sup>5</sup> mc, metacarpal; mt, metatarsal; naof, nasoantorbital fenestra; ph, wing phalanx; pt, pteroid; ti,



## Table 3(on next page)

Summary of main anatomical variations surveyed here in Jehol tapejarids.



Species	Pmc shape	Rostrum def.	Naof h/l	Nasal process	Orbit shape	Q°	<b>Longest</b> cervical	Pt/ul	McI/ McIV	Ph4d4/ ph1d4
Sinopterus dongi	Heaped	12°–15°	>3	Subv.	Subq.	~160°	cv IV	< 0.50	>0.90	0.30– 0.40
Eopteranodon lii	Heaped	~15°	?	Subv.	Subq.	~160°	cv IV	>0.50	>0.90	~0.45
Huaxiadraco corollatus	Subq.	~20°	2.2– 2.5	Ant.	Pirif.	~150°	cv V	~0.50	0.30– 0.40	~0.20

#### 2 Table 3. Summary of main anatomical variations surveyed here in Jehol tapejarids.

- 3 Abbreviations: ant., anteriorly directed; cv, cervical; d, digit; def., deflection; h, height; l, length;
- 4 mc, metacarpal; ph, phalanx; pirif., piriform; pmc, premaxillary crest; pt, pteroid; Q°, quadrate
- 5 inclination; ul, ulna; subq., subquadrangular; subv., subvertical.

6

1



## Table 4(on next page)

Summary of taxonomic attributions of *Sinopterus* complex specimens.



Specimen	Original attribution	Reference	Present attribution (this work)
Sinopterus dongi holotype	Sinopterus dongi	Wang & Zhou (2003)	Sinopterus dongi
Sinopterus gui holotype	Sinopterus gui	Li <i>et al.</i> (2003)	Sinopterus dongi
Huaxiapterus jii holotype	Huaxiapterus jii	Lü <i>et al.</i> (2005)	Sinopterus dongi
Huaxiapterus corollatus holotype	Huaxiapterus corollatus	Lü et al. (2006a)	Huaxiadraco corollatus
D2525	Sinopterus dongi	Lü <i>et al.</i> (2006b)	Huaxiadraco corollatus
Huaxiapterus benxiensis holotype	Huaxiapterus benxiensis	Lü <i>et al.</i> (2007)	Huaxiadraco corollatus
Nemicolopterus crypticus holotype	Nemicolopterus crypticus	Wang <i>et al.</i> (2008)	Sinopterinae indet.
PMOL-AP00030	Tapejaridae indet.	Liu <i>et al.</i> (2015)	Sinopterinae indet.
Sinopterus lingyuanensis holotype	Sinopterus lingyuanensis	Lü <i>et al</i> . (2016)	Sinopterus dongi
Huaxiapterus atavismus holotype	Huaxiapterus atavismus	Lü <i>et al</i> . (2016)	Sinopterus dongi
IVPP V 23388	Sinopterus atavismus	Zhang <i>et al</i> . (2019)	Sinopterus dongi
D3072	Sinopterus dongi	Shen <i>et al.</i> (2021)	Sinopterus dongi
SDUST-V1012	Sinopterus sp.	Zhou <i>et al.</i> (2022a)	Sinopterinae indet.
SDUST-V1014	Sinopterus sp.	Zhou <i>et al.</i> (2022b)	cf. Sinopterus dongi
D4019	-	_	Sinopterus dongi
BPMC 103	_	_	Huaxiadraco corollatus
BPMC 104	-	-	Huaxiadraco corollatus
BPMC 105	_	_	Huaxiadraco corollatus
BPMC 106	-	-	Sinopterus dongi
BPMC 107	_	_	Sinopterus dongi

2 Table 4. Summary of taxonomic attributions of Sinopterus complex specimens.